



HAL
open science

Innovative composite polymer materials for CO₂ separation

Di Wang

► **To cite this version:**

Di Wang. Innovative composite polymer materials for CO₂ separation. Material chemistry. Normandie Université, 2024. English. NNT : 2024NORMIR09 . tel-04812230

HAL Id: tel-04812230

<https://theses.hal.science/tel-04812230v1>

Submitted on 30 Nov 2024

HAL is a multi-disciplinary open access archive for the deposit and dissemination of scientific research documents, whether they are published or not. The documents may come from teaching and research institutions in France or abroad, or from public or private research centers.

L'archive ouverte pluridisciplinaire **HAL**, est destinée au dépôt et à la diffusion de documents scientifiques de niveau recherche, publiés ou non, émanant des établissements d'enseignement et de recherche français ou étrangers, des laboratoires publics ou privés.



Normandie Université

THÈSE

Pour obtenir le diplôme de doctorat

Spécialité **CHIMIE**

Préparée au sein de l'**INSA Rouen Normandie**

Innovative composite polymer materials for CO2 separation

Présentée et soutenue par

DI WANG

Thèse soutenue le 29/05/2024

devant le jury composé de :

M. NICOLAS DESILLES	MAITRE DE CONFERENCES DES UNIVERSITES HDR - INSA Rouen Normandie	Directeur de thèse
MME KATERYNA FATYEYEVA	MAITRE DE CONFERENCES DES UNIVERSITES HDR - Université de Rouen Normandie	Co-directeur de thèse
M. CÉDRIC PLESSE	PROFESSEUR DES UNIVERSITÉS - CY Cergy Paris Université	Président du jury
MME. GERALDINE GOUHIER	PROFESSEUR DES UNIVERSITÉS - Université de Rouen Normandie	Membre
M. FABRICE GOUANVE	MAITRE DE CONFERENCES DES UNIVERSITES HDR - Université Claude Bernard Lyon 1	Rapporteur
M. ANTHONY SZYMCZYK	PROFESSEUR DES UNIVERSITÉS - Université de Rennes	Rapporteur

Thèse dirigée par **NICOLAS DESILLES** (LABORATOIRE POLYMERES BIOPOLYMERES SURFACES)
et **KATERYNA FATYEYEVA** (LABORATOIRE POLYMERES BIOPOLYMERES SURFACES)

THÈSE

Pour obtenir le diplôme de doctorat

Spécialité CHIMIE

Préparée au sein de l'INSA Rouen Normandie

Innovative composite polymer materials for CO₂ separation

Présentée et soutenue par

Di WANG

Soutenance prévue le 29/05/2024

devant le jury composé de

M. FABRICE GOUANVE	MAITRE DE CONFERENCES HDR, Université Claude Bernard Lyon 1	Rapporteur du jury
M. ANTHONY SZYMCZYK	PROFESSEUR DES UNIVERSITES, Université de Rennes	Rapporteur du jury
MME GERALDINE GOUHIER	PROFESSEUR DES UNIVERSITES, Université de Rouen Normandie	Membre du jury
M. CEDRIC PLESSE	PROFESSEUR DES UNIVERSITES, CY Cergy Paris Université	Membre du jury
M. NICOLAS DESILLES	MAITRE DE CONFERENCES HDR, Institut National des Sciences Appliquées Rouen Normandie	Directeur de thèse
MME KATERYNA FATYEYEVA	MAITRE DE CONFERENCES HDR, Université de Rouen Normandie	Co-directeur de thèse

Thèse dirigée par NICOLAS DESILLES et KATERYNA FATYEYEVA (Polymères, Biopolymères, Surfaces)

Acknowledgements

First of all, I would like to express my sincere thanks to the China Scholarship Council (CSC) for its financial support to my life in France.

It's my honor to invite Mr Anthony SZYMCZYK (professor, University of Rennes), Mr Fabrice GOUANVE (assistant professor, University of Claude Bernard Lyon 1), Ms Géraldine GOUHIER (professor, University of Rouen Normandie) and Mr Cédric PLESSE (professor, CY Cergy-Paris University) to review my work of PhD, thanking for their precious time and valuable advice.

I would like to express gratitude from the bottom of my heart to my supervisors Mr Nicolas DESILLES (assistant professor, INSA Rouen Normandie) and Ms Kateryna FATYEYEVA (assistant professor, University of Rouen Normandie) for their enlightenment, patience, encouragement and guidance. It's my honor to finish my PhD project under their supervision. During the 42 months of my PhD, they taught me how to face difficulties and how to solve them both in work and life. Without their support, I couldn't have improved my professional skills, finished my project or have earned my PhD. I will never forget the precious time I spent working with them in France.

My appreciation would be expressed to Corinne CHAPPEY for gas permeation test. I also would like to express my appreciation to Catherine LEGRAND, Jeremy DESHAIS, Fabien BOUST and Murielle HIBLOT for their help in the lab. In particular, Catherine LEGRAND patiently taught me to speak French and tests.

I extend my sincere appreciation to the faculty and staff of PBS laboratory, especially those from MM and MPBM teams, as well as those who supported me in completing my PhD work: Fabrice BUREL, Gaëlle MORANDI, Daniela VULUGA-LEGROS, Nasreddine KÉBIR, Laurence LECAMP.

It's my pleasure to thank all my colleagues for their help, support and encouragement in PBS, especially MM and MPBM: Yuzhen LOU, Xuelian LIU, Yaroslav KOBZAR, Olivier HINTIROGLOU, Aurelie DESTEPHEN, Vincent VALETTE, Vincent GONNOT, Klara JASTAK, Guillaume Le CRAS, Bao DING, Luis NUNEZ, Souraya ALAMEDDINE, Patricia Batista PEGUERO, Ludvina CHAILLY, Mohammad EBRAHIMI. They have brought a lot of help and happiness to my work life and my daily life, and I am so happy to spend my time with them in France. Particularly, Yuzhen LOU, Xuelian LIU,

Acknowledgements

Klara JASTAK and Vincent VALETTE who helped me get through the tough times, taught me to speak French and helped adapt to life in France.

I truly appreciate the company and joy of my friends from China: Bo JIANG, Jing ZHANG, Jie XU, Xuefei WANG, Xiaojing HAN, Ce ZHANG and Yudong MENG. Especially the support and help of my close friends: Jiang JING, Xingguo WANG and Minghang WANG.

My gratitude is also extended to my master supervisor Mr Hongfei LI and my teachers Mr Sheng ZHANG, Ms Xiaoyu GU, Mr Jun SUN, Mr Zhiyuan ZHANG for their support and enlightenment. All of them are from CFSM (Beijing University of Chemical Technology).

I would like to express my heartfelt gratitude to my girlfriend Malak, for her unwavering support, encouragement, and understanding throughout my doctoral journey. Her love, patience, and belief in me have been constant sources of strength and motivation. I am truly blessed to have her by my side.

Finally, I would like to express my deepest gratitude to my family specially my parents, for their unwavering love, encouragement, and support throughout my doctoral journey. Their sacrifices, understanding, and belief in me have been the driving force behind my accomplishments. I am profoundly grateful for their unconditional love and endless encouragement.

With deepest appreciation, Di WANG

Oral Communications

C1 Polysulfone-based composite membranes: elaboration and characterization

Di WANG, Nicolas DESILLES, Kateryna FATYEYEVA

Journée de l'Ecole Doctorale Normande de Chimie, Caen, France, 23-24 May, 2022

C2 Composite membrane with high CO₂ selectivity and separation ability

Di WANG, Nicolas DESILLES, Kateryna FATYEYEVA

JNOEJC 2022, Caen, France, 9-10 June, 2022

C3 Preparation and characterization of polysulfone-based composite membranes

Di WANG, Nicolas DESILLES, Kateryna FATYEYEVA

42^{èmes} journées du GFP Grand Ouest, Rennes, France, 5-6 July, 2022

C4 Influence of the composition of polysulfone-based dense composite membranes on the CO₂ gas separation performance

Di WANG, Corinne CHAPPEY, Nicolas DESILLES, Kateryna FATYEYEVA

XIV Scientific Conference "Membranes and Membrane Processes in Environmental Protection", Zakopane/Kościelisko, Poland, 21-24 June, 2023

Table of Contents

Abbreviations	I
List of Figures.....	V
List of Tables.....	VIII
General Introduction	1
Chapter 1 Composite membranes based on ionic liquids for CO₂ separation	5
1.1 CO ₂ separation technology	4
1.1.1 Absorption technology.....	5
1.1.2 Adsorption technology.....	6
1.1.3 Cryogenic distillation.....	6
1.1.4 Hydrate technology	6
1.1.5 Membrane technology	7
1.2 Membrane classification	8
1.2.1 General classification.....	8
1.2.2 Ionic liquids-based membranes.....	11
1.3 Gas permeation mechanism through a membrane	15
1.3.1 Solution-diffusion mechanism	16
1.3.2 Facilitated transport mechanism	16
1.3.3 Molecular sieving mechanism	17
1.3.4 Preferential adsorption-monomolecular surface diffusion mechanism	18
1.4 Factors influencing gas permeation properties	19
1.4.1 Nature of polymer matrix.....	19
1.4.2 Additives	21
1.4.2.1 Zeolites.....	21
1.4.2.2 Organic frameworks (MOFs).....	22
1.4.2.3 Oxide nanoparticles	23
1.4.2.4 Nano-carbon.....	24
1.4.2.5 Ionic liquids (ILs)	26

Table of contents

1.4.3	Gas properties	32
1.4.4	Operation parameters	33
1.4.4.1	Temperature	33
1.4.4.2	Pressure	33
1.4.4.3	Humidity	34
1.5	Summary and outlook	35
	References.....	38
Chapter 2 Synthesis and characterization of ionic liquids		54
2.1	Synthesis of ionic liquids	53
2.1.1	[Meim][TFSO ₃] and [Vim][TFSO ₃]	53
2.1.2	[Meim][Tf ₂ N] and [Vim][Tf ₂ N].....	54
2.1.3	Li(DOBA)[Tf ₂ N] and Li(HDA)[Tf ₂ N]	54
2.2	Characterization of ILs	55
2.2.1	Structural characterization	55
2.2.1.1	FT-IR analysis	55
2.2.1.2	¹ H NMR spectroscopy	57
2.2.2	Thermal characterization	63
2.2.2.1	Thermal stability	63
2.2.2.2	Differential scanning calorimetry (DSC).....	66
2.3	Conclusion	68
	References.....	69
Chapter 3 Preparation and characterization of PSF-based dense composite membranes		71
3.1	Introduction.....	71
3.2	Membrane preparation.....	71
3.2.1	Solvent selection	72
3.2.2	Polymer concentration	73
3.2.3	Supporting material.....	73
3.2.4	Solvent evaporation conditions.....	74

Table of contents

3.2.5	Optimized membrane preparation procedure.....	75
3.3	Membrane Characterization.....	75
3.3.1	Transparency of membrane.....	75
3.3.2	FT-IR spectroscopy and SEM-mapping.....	76
3.3.3	Thermal characterization	85
3.3.3.1	Thermal degradation	85
3.3.3.2	Differential scanning calorimetry (DSC).....	88
3.3.4	Surface energy	91
3.3.5	Mechanical properties.....	94
3.3.6	Gas separation.....	95
3.4	Conclusion	102
	References.....	103
 Chapter 4 Preparation and characterization of PES-based composite membranes.....		105
4.1	Introduction.....	105
4.2	Membrane preparation	106
4.2.1	PES-based composite membranes	106
4.3	Membrane Characterization.....	106
4.3.1	Transparency	106
4.3.2	Chemical structure and microstructure of membranes	107
4.3.3	Thermal characterization	112
4.3.3.1	Thermal stability	112
4.3.3.2	Differential scanning calorimetry (DSC).....	114
4.3.4	Surface energy	116
4.3.5	Mechanical properties.....	117
4.3.6	Gas separation.....	119
4.4	Conclusion	122
	References.....	123
 General Conclusion and Prospects.....		125

Table of contents

Annex.....	126
Annex 1 Reagents.....	126
Annex 2 Characterizations.....	129
Annex 3 ¹ H NMR analysis	131
Annex 4 DSC thermograms.....	132

Abbreviations

ABS: Acrylonitrile-butadiene-styrene

AC: Activated carbon

AMP: 2-amino-2-methyl-1-propanol

APTMS: 3-aminopropyltrimethoxysilane

AFSNP: APTMS functionalized silica nanoparticle

CA: Cellulose acetate

CMS: Carbon molecular sieve membrane

CNT: Carbon nanotubes

DE: Diethyl ether

DEA: Diethanolamine

DMF: Dimethylformamide

DOBA: 2,2'-(ethylenedioxy)bis(ethylamine)

DSC: Differential scanning calorimetry

FFV: Fractional free volume

FT-IR: Fourier transform infrared

FTM: Facilitated transport membrane

GC: Glycerol

GO: Graphene oxide

GQD: Graphene oxide quantum dots

H[Tf₂N]: Bis(trifluoromethanesulfonyl)imide

H[TFSO₃]: Trifluoromethanesulfonic acid

HDA: 2-(2-aminoethoxy) ethanol

IL: Ionic liquid

ILGMs: Ionic liquid gel membranes

ILMCs: Ionic liquid membrane contactors

ILMMMs: Ionic liquid composite mixed matrix membranes

ILPMs: Ionic liquid composite polymer membranes

IPCC: Intergovernmental Panel on Climate Change

Li(DOBA)[Tf₂N]: Lithium bis(trifluoromethylsulfonyl)imide-
salt-2,2'-(ethylenedioxy)bis(ethylamine)

Li(HDA)[Tf₂N]: Lithium bis(trifluoromethylsulfonyl)imide-
salt-2-hydroxyethylenediamine

Li[Tf₂N]: Bis(trifluoromethane)sulfonimide lithium salt

[Meim][Tf₂N]: Methyl imidazolium bis(trifluoromethylsulfonyl)imide

[Meim][TFSO₃]: Methyl imidazolium trifluoromethane sulfonate

MDEA: Methyldiethanolamine

MEA: Monoethanolamine

Meim: 1-methylimidazole

MMMs: Mixed matrix membranes

MOFs: Metal organic frameworks

MWCNTs: Functionalized carbon nanotubes

NMP: *N*-methyl-2-pyrrolidone

NMR: Nuclear magnetic resonance

PA: Polyamide

PC: Polycarbonate

PDA: Polydopamine

PDLA: Poly-D-lactic acid
PDMS: Polydimethylsiloxane
PEBA: Polyether-block-amide copolymer
PE: Polyethylene
PEO: Polyether
PES: Polyethersulfone
PEG: Polyethylene glycol
PEGDE: Polyethylene glycol diglycidyl ether
PI: Polyimide
PILMs: Poly(ionic liquid)s membranes
PILs: Poly(ionic liquid)s
PLA: Poly(lactic acid)
PLLA: Poly-L-lactic acid
PPO: Poly(phenylene oxide)
PQD: Polymer-like quantum dot
PSF: Polysulfone
PTFE: Polytetrafluoroethylene
PVA: Poly(vinyl alcohol)
PVAm: Poly(vinyl amine)
PVC: Poly(vinyl chloride)
PVDF: Poly(vinylidene fluoride)

RH: Relative humidity

SEM: Scanning electron microscopy
SILMs: Supported ionic liquid membranes

TB: Träger-base polymer
TETA: Triethylenetetramine

Abbreviations

TGA: Thermogravimetric analysis

THF: Tetrahydrofuran

Vim: *N*-vinyl imidazole

[Vim][Tf₂N]: Vinyl imidazolium bis(trifluoromethylsulfonyl)imide

[Vim][TFSO₃]: Vinyl imidazolium trifluoromethane sulfonate

ZIF-C: Zeolitic imidazolate framework cuboid

List of Figures

Figure 1-1 Classification of membranes	8
Figure 1-2 Robeson's upper bound of CO ₂ /N ₂ (a) and O ₂ /N ₂ (b)	10
Figure 1-3 Synthesis of crosslinked PILs membranes	14
Figure 1-4 Possible gas separation mechanisms through a membrane	15
Figure 1-5 Commonly used IL cations	26
Figure 1-6 Commonly used IL anions	27
Figure 1-7 Chemical structure of PSF	36
Figure 1-8 Chemical structure of PES	37
Figure 2-1 Synthetic route of [Meim][TFSO ₃] and [Vim][TFSO ₃] preparation	54
Figure 2-2 Synthetic route of [Vim][Tf ₂ N] and [Meim][Tf ₂ N] preparation	54
Figure 2-3 Synthetic route of Li(DOBA)[Tf ₂ N] and Li(HDA)[Tf ₂ N] preparation	55
Figure 2-4 FT-IR spectra of synthesized ILs	56
Figure 2-5 ¹ H NMR spectra of [Meim][TFSO ₃] (a), 1-methylimidazole (b), and trifluoromethanesulfonic acid (c)	59
Figure 2-6 ¹ H NMR spectra of Li(DOBA)[Tf ₂ N]	60
Figure 2-7 ¹ H NMR spectra of [Vim][TFSO ₃]	61
Figure 2-8 ¹ H NMR spectra of [Meim][Tf ₂ N]	61
Figure 2-9 ¹ H NMR spectra of [Vim][Tf ₂ N]	62
Figure 2-10 ¹ H NMR spectra of Li(HDA)[Tf ₂ N]	62
Figure 2-11 TGA and DTG curves of ILs	64
Figure 2-12 TGA isothermal curves of ILs at 150°C	65
Figure 2-13 DSC curves of ILs	67
Figure 3-1 Cross-section SEM images of PSF/10[Meim][TFSO ₃] membranes prepared from THF (a), DMF (b), and NMP (c) solutions	75
Figure 3-2 Optical images of PSF/ILs-based membranes	77
Figure 3-3 FT-IR spectra of PSF/ILs composite membranes	78
Figure 3-4 SEM images and F-mapping of PSF/[Meim][TFSO ₃] membranes	80

List of Figures

Figure 3-5 SEM images and F-mapping of PSF/[Vim][TFSO ₃] membranes	81
Figure 3-6 SEM images and F-mapping of PSF/[Meim][Tf ₂ N] membranes	83
Figure 3-7 SEM images and F-mapping of PSF/[Vim][Tf ₂ N] membranes	84
Figure 3-8 SEM images and F-mapping of PSF/Li(DOBA) [Tf ₂ N] and PSF/Li(HDA) [Tf ₂ N] membranes	85
Figure 3-9 TGA curves of PSF/IL composite membranes.....	87
Figure 3-10 Linear fit of T _g by Gordon-Taylor equation (Equation 3-3).....	90
Figure 3-11 Permeability coefficients of PSF/IL-based membranes	98
Figure 3-12 Diffusion coefficients of PSF/IL-based membranes	100
Figure 3-13 Solubility coefficients of PSF/IL-based membranes.....	101
Figure 4-1 Optical photos of PES and PES/ILs membranes.....	107
Figure 4-2 FT-IR spectra of PES and PES/ILs membranes	109
Figure 4-3 SEM images and F-mappings of PES, PES/[Meim][TFSO ₃] and PES/[Vim][TFSO ₃] membranes	110
Figure 4-4 SEM images and F-mappings of PES, PES/[Meim][Tf ₂ N] and PES/[Vim][Tf ₂ N] membranes	111
Figure 4-5 SEM images and F-mappings of PES, PES/Li(DOBA)[Tf ₂ N] and PES/Li(HDA)[Tf ₂ N] membranes	112
Figure 4-6 TGA curves of PES and PES/ILs membranes.....	113
Figure 4-7 T _g linear fits by Gordon-Taylor equation (Equation 3-3) for PES/IL composite membranes	115
Figure 4-8 Stress - strain curves of PES and PES/ILs composite membranes	117
Figure 4-9 Permeability coefficients of PES/IL-based membranes.....	119
Figure 4-10 Diffusion coefficients of PES/IL-based membranes.....	121
Figure 4-11 Solubility coefficients of PES/IL-based membranes.....	121
Figure A2-1 Set up for gas separation.....	113
Figure A3-1 ¹ H NMR spectrum of <i>N</i> -vinylimidazole (Vim)	113
Figure A3-2 ¹ H NMR spectrum of bis(trifluoromethanesulfonyl)imide (Tf ₂ N).....	113

List of Figures

Figure A4-1 DSC curves of PSF, PSF/[Meim][TFSO ₃] and PSF/[Vim][TFSO ₃] membranes ..	113
Figure A4-2 DSC curves of PSF, PSF/[Meim][Tf ₂ N] and PSF/[Vim][Tf ₂ N] membranes	113
Figure A4-3 DSC curves of PSF, PSF/Li(DOBA)[Tf ₂ N] and PSF/Li(HDA)[Tf ₂ N] membranes	133
Figure A4-4 DSC curves of PES, PES/[Meim][TFSO ₃] and PES/[Vim][TFSO ₃] membranes .	133
Figure A4-5 DSC curves of PES, PES/[Meim][Tf ₂ N] and PES/[Vim][Tf ₂ N] membranes	134
Figure A4-6 DSC curves of PES, PES/Li(DOBA)[Tf ₂ N] and PES/Li(HDA)[Tf ₂ N] membranes	134

List of Tables

Table 1-1 Advantages and disadvantages of different separation technologies.....	5
Table 1-2 Advantages and disadvantages of different types of membranes	9
Table 1-3 Different types of ILs-based membranes.....	12
Table 1-4 Diffusion and solubility coefficients of SILMs with different ILs	13
Table 1-5 Properties of some gas molecules.....	16
Table 1-6 Gas permeability and selectivity of several polymer matrices	20
Table 1-7 Gas permeability of PLA with different crystallinities	21
Table 1-8 Diffusion and solubility coefficients of PE and PLA	32
Table 2-1 ¹ H NMR chemical shifts of synthesized ILs.....	57
Table 2-2 TGA data (T _{5%} , T _{max} and isothermal weight loss at 150°C) of ILs.....	64
Table 2-3 DSC data of ILs	66
Table 3-1 Properties of solvents.....	72
Table 3-2 Tested supporting materials to obtain PSF/[Meim][TFSO ₃] composite membranes ..	74
Table 3-3 T _g value of PSF/IL composite membranes	89
Table 3-4 Solvent contact angles and surface energy of PSF-based membranes (air-contacting surface).....	92
Table 3-5 Solvent contact angles and surface energy of PSF-based membranes (PVA-contacting surface).....	93
Table 3-6 Mechanical properties of PSF and PSF/ILs membranes	95
Table 3-7 Gas selectivity of PSF/IL-based membranes	99
Table 4-1 T _g of PES/ILs membranes.....	114
Table 4-2 Solvent contact angles and surface energy of PES and PES/ILs membranes	116
Table 4-3 Mechanical data of PES and PES/ILs membranes	118
Table 4-4 Gas selectivity data of PES and PES/ILs membranes	120
Table A1-1 Short name, chemical structure and CAS number of chemicals.....	127

General Introduction

Since the onset of the Industrial Revolution in the mid-19th century, there has been a notable surge in greenhouse gas concentration in the atmosphere, especially of CO₂ primarily driven by the combustion of fossil fuels. These greenhouse gases cause global warming and bring about many serious problems, such as the rise of sea level, the return of climate, and the increase of diseases. Additionally, CO₂ as an acidic gas is often found in energy gases (natural gas, biogas), and the presence of CO₂ reduces the calorific value and damage gas transportation pipelines. Therefore, the CO₂ separation technologies are highly desirable and have attracted great interest.

In general, the traditional CO₂ separation technology including absorption, adsorption, cryogenic distillation and hydrate, have the disadvantages of high energy consumption, high cost and environmental pollution. Compared to traditional CO₂ separation techniques, membrane technology offers the ease of operation, simple maintenance, stability and low cost. Therefore, the membrane separation technology has been studied by many researchers with high expectations during the last decades.

In the 1980s, the first generation of polymer membranes for gas mixtures separation was developed. The fast growth of the polymer membrane application is driven by its low production cost and ease of upscaling. The ease of fabrication, involving various polymer materials and tunable membrane configurations, further promotes the utilization of polymer membranes for the CO₂ removal. In general, there are three types of polymer materials for membranes: rubbery and glassy polymers, and copolymers. Rubbery polymers (including poly(dimethylsiloxane) (PDMS), poly(acrylonitrile-*co*-butadiene-*co*-styrene) (ABS), poly(ethylene oxide) (PEO), polyurethane (PU)), have flexible structures due to the high intersegmental mobility. They operate above their glass transition temperature (T_g) and have high gas permeability but low selectivity. By contrast, glassy polymers have a rigid structure and are used below their T_g . The examples of common glassy polymers for gas separation are polysulfone (PSF), polyethersulfone (PES), polycarbonate (PC), polyimide (PI), and polyetherimide (PEI). Compared to rubbery polymers, glassy polymers have been frequently chosen to elaborate gas separation membranes owing to their good mechanical properties and high selectivity. Copolymers combine glassy and rubbery features in their structures. For example, polyether block amide (PEBA) has been also applied to improve the gas separation properties. This polymer comprises hard (glassy) polyamide segments that provide mechanical strength, while the flexible component

(polyether) plays an important role in the CO₂ transport. Owing to its promising properties, PEBA has been widely selected as a polymer matrix to fabricate membranes for CO₂/N₂ and CO₂/CH₄ separation. Among all studied polymers, the excellent mechanical properties and high gas selectivity of PSF and PES are rather attractive for gas separation membranes.

It is widely known that most polymer membranes face limitations in terms of the trade-off between selectivity and permeability, which is represented by Robeson's upper bound. Therefore, it is not possible to achieve high gas permeability and selectivity with a single polymer. According to previous works, CO₂ permselectivity of polymer membranes were enhanced with different fillers: zeolite, graphene oxide, organic frameworks, metal oxides, silica and ionic liquids (ILs). In recent years, ILs have attracted more and more attention in the field of gas separation due to their outstanding properties: negligible vapor pressure, high thermal stability, excellent CO₂ absorption capacity and adjustable properties, making them promising candidates for CO₂ separation. Also, the incorporation of ILs can provide an efficient pathway to enhance the CO₂ permeability and selectivity of polymer membranes.

In this thesis, six ILs are synthesized and introduced into glassy polymers (PSF and PES) to prepare dense composite membranes with high CO₂ permeability and selectivity.

Four chapters are orderly organized.

Chapter 1 gives an overview of composite membranes based on ionic liquids for CO₂ separation.

Chapter 2 details the synthesis and characterization of six ILs with different cations and anions. Their chemical structures are confirmed by FT-IR and ¹H NMR analysis, and the effect of cations and anions on their thermal behavior (TGA and DSC) is studied.

Chapter 3 presents the optimization of the dense membrane preparation procedure. PSF-based dense composite membranes with different ILs as well as different ILs loadings are prepared. Their thermal behavior, mechanical property, surface energy, microstructure and gas permeation are investigated and discussed.

PES-based composite membranes containing ILs are presented and characterized in Chapter 4. Their thermal and mechanical properties are correlated with their microstructure and gas permeation performance.

Finally, a general conclusion and prospects are given prior to the Annexes.

This work was made possible thanks to the cooperation between the MM and MPBM teams of PBS laboratory, and funding from CSC.

Chapter 1
Composite membranes based on ionic liquids
for CO₂ separation

Introduction

The development of modern industry has led to an important increase in global energy consumption, particularly owing to the combustion of fossil fuels, resulting in a significant rise of atmospheric CO₂ concentration [1,2]. CO₂ is the primary driver of global warming and has the most significant negative effect, contributing to approximately 55% of the observed increase in global temperature [3]. According to the report from the Intergovernmental Panel on Climate Change (IPCC), it will be impossible to achieve the goal of limiting global warming to approximately 1.5°C or even 2°C unless there are immediate, quick, and substantial reductions in greenhouse gas emission [4,5]. IPCC predicted the CO₂ concentration might reach 570 ppmv by 2100 in the atmosphere, which would result in an average global temperature increase of approximately 1.9°C and a rise of sea levels of 3.8 meters [6]. On the other hand, in the case of energy gas resources, such as natural gas, shale gas, biogas, syngas, a certain amount of CO₂ as impurity can decrease the heating values and gas quality [7] (thus demanding higher energy consumption for conversion and transport) and cause corrosion of pipelines and equipment [8]. Therefore, CO₂ separation is essential for controlling greenhouse gases emission and energy gases purification.

This Chapter is divided into four parts. Firstly, five CO₂ separation technologies are introduced. Secondly, different types of membranes are listed and compared, with an emphasis on ionic liquid-based composite membranes. Thirdly, the mechanisms involved during gas separation through a membrane are detailed. And finally, the factors (nature of polymer matrix, additives, gas properties and test conditions) influencing gas permeation properties are gathered and explained. To conclude, a summary and an outlook of CO₂ separation composite membranes containing ILs are presented.

1.1 CO₂ separation technology

In order to separate CO₂ from gas mixtures, several technologies are available: absorption, adsorption, cryogenic distillation, hydrate and membrane technology [9]. The advantages and disadvantages of each method are presented in Table 1-1.

Table 1-1 Advantages and disadvantages of different separation technologies [6,10]

Method	Advantages	Disadvantages
Absorption	Suitable for industrial application Operating at low CO ₂ feed concentration	High energy consumption Corrosion caused by amines degradation Emission of harmful by-products Expensive for regeneration
Adsorption	High capacity of CO ₂ adsorption High pressure operation High selectivity over other gases	High energy consumption Difficulty of regeneration Not suitable for cyclic operation
Cryogenic distillation	High product purity	High energy consumption Only suitable for high CO ₂ feed concentration (50%) Need pre-processing step to remove humidity from mixed feed steam
Hydrate	High product purity	High pressure and low temperature Secondary pollution High capital cost
Membrane technology	High energy efficiency Low operation cost Small footprint Simplicity in operation and installation	Limited by Robeson's upper bound

1.1.1 Absorption technology

The CO₂ absorption consists in preferential physical or chemical interaction of CO₂ and liquid absorbers, thus achieving CO₂ separation from the gases mixture [11]. Due to the chemical reactivity of CO₂ with amines, the amines absorption technology is widely used in industrial production, especially in post-combustion systems. Primary amines (monoethanolamine (MEA), 2-amino-2-methyl-1-propanol (AMP)), secondary amines (diethanolamine (DEA)) and tertiary amines (methyldiethanolamine (MDEA)) are usually used [12]. However, such absorption technology has many harmful to the environment drawbacks, such as corrosive by-products formation, high energy consumption and use of volatile amines. In order to overcome such limitations, environmentally friendly CO₂ absorbers were developed [13]. Currently, ILs are used for CO₂ separation due to the

strong physical or chemical interactions between ILs and CO₂. Besides, ILs are environmentally friendly owing to negligible vapor pressure [14–16]. To enhance the CO₂ absorption capacity of ILs, different functionalized ILs have been designed, for example amino-functionalized ILs [17].

1.1.2 Adsorption technology

Adsorption process using porous solid sorbents is an advantageous method as compared with solvent-based absorption, owing to easy operation, rapid reaction, low corrosion, and low energy consumption for regeneration [18]. Vacuum, pressure, temperature, and electric swing adsorption can renew solid adsorbents following CO₂ capture. Pressure and temperature swing adsorption techniques are commercially accessible for CO₂ removal from natural gas, and in pre-combustion systems for hydrogen generation [19]. Solid sorbents are efficient at elevated temperatures and their properties are comparable with the properties of the solvents used in pre-combustion processes.

A wide variety of materials are used as sorbents, among them zeolites (aluminosilicates and titanosilicates), molecular sieves and activated carbons [20,21]. In addition, metal organic frameworks (MOFs) are proposed to serve as novel sorbents owing to their controllable pore size and surface chemistry [22–24]. Despite the significant progress in this field, the stability and regeneration of sorbent material should be improved and controlled.

1.1.3 Cryogenic distillation

Cryogenic distillation is based on the physical low-temperature condensation using different gas liquefaction temperatures [25]. This technology is extensively used for the separation of nitrogen from air, but the separation of CO₂ is still under investigation [26]. The main advantage is the high purity of obtained CO₂. However, CO₂ can be separated from other light gases only below its liquefaction temperature of ~ -130°C. Moreover, the cooling devices and their significant energy consumption during the process significantly limit this technology.

1.1.4 Hydrate technology

CO₂ separation *via* hydrate-based methods is based on the remarkable properties of hydrates [27].

CO₂ hydrates are solid crystalline compounds formed by the sequestration of CO₂ molecules within a lattice composed of water molecules under specific temperature and pressure conditions. After the hydrate's formation, a process of selective separation from the gas mixture can be applied. The dissociation and subsequent release of collected CO₂ from hydrates can be accomplished by either pressure decreasing or temperature rising. The captured CO₂ can be subsequently gathered and subjected to additional treatment for storage or further use. Hydrate-based CO₂ separation technique attracts considerable interest, due to its high selectivity, low energy consumption, and the possibility to be used at ambient temperature [28]. However, the hydrate-based separation is still a subject of continuous investigation as numerous limitations should be overcome prior to its implementation on a commercial level (Table 1-1).

1.1.5 Membrane technology

Membranes may separate gases by sieving and/or sorption-diffusion process (depending on the membrane structure, i.e. porous or dense) thus allowing for one or more components to pass preferentially through the membrane [29,30]. The inherent membranes simplicity has many benefits as compared to other separation technologies, namely the use of small-scale equipment, reduced environmental impact, simple incorporation into the existing processes, and low energy consumption and operating costs [31–33].

In the past few years, great efforts have been made for the design of efficient and cost-effective membrane materials for emerging and potential applications [34]. Rapid progress in membrane technology enabled the current commercial use of membrane-based systems on an industrial scale for different gas separation processes, namely CO₂ removal from natural gas, vapor/gas separation, nitrogen separation from air, and hydrogen recovery [35]. CO₂ separation application includes separating CO₂ from post-combustion (CO₂/N₂ mixture), pre-combustion (CO₂/H₂ or H₂/CO₂ mixture), and from biomethane (CO₂/CH₄ mixture). In order to develop advanced membranes with high permeability and selectivity to specific gases, good thermal/chemical resistance and sufficient mechanical stability towards the harsh environments of gas separation processes are required.

1.2 Membrane classification

1.2.1 General classification

Numerous research articles dealing with CO₂ separation membranes can be found illustrating the rapid development of CO₂ separation membranes over the past decade [36]. From structure and material point of view, the classification shown in Figure 1-1 can be established. The advantages and disadvantages of the different types of membranes are presented in Table 1-2.

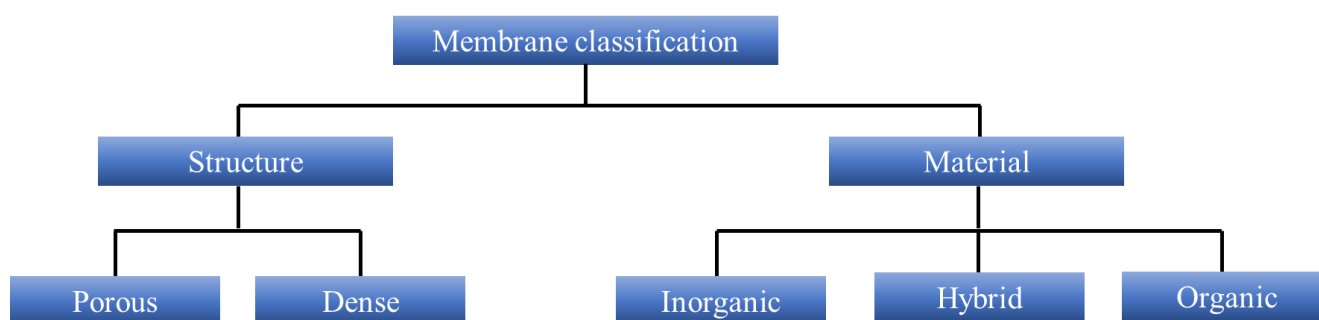


Figure 1-1 Classification of membranes

According to membrane material, composite membranes are usually divided into inorganic (ceramic, metallic, carbon molecular sieves, silica, zeolites, and metalorganic frameworks (MOFs)), organic (polymer membranes), and hybrid composite membranes (mixed matrix membranes). Typical inorganic membranes, such as zeolite and carbon membranes, have been widely studied for CO₂ separation [37,38]. Usually, they have pores of appropriate size, which can serve as molecular sieves to separate gas molecules [39]. Moreover, inorganic membranes exhibit excellent CO₂ selectivity due to their good CO₂ affinity against CH₄ or N₂. For example, the mixed linker tetrahedral imidazolate framework-4 (TIF-4) MOF membrane, fabricated by Xia *et al* [40], revealed to be highly CO₂ selective with CO₂/N₂ separation factor of 27 due to the effective pore size of TIF-4, that lies between the kinetic diameters of CO₂ (3.3 Å) and N₂ (3.64 Å). However, although inorganic membranes have interesting CO₂ separation properties, such as high selectivity and great thermal and chemical stability, they are rather brittle and their fabrication is very complex and expensive.

Table 1-2 Advantages and disadvantages of different types of membranes [41]

Properties	Polymer membranes	Inorganic membranes	Hybrid membranes
Fabrication cost	Low	High	Moderate
Chemical and thermal stability	Moderate	High	High
Synthesis and processability	Easy	Difficult	Easy
Plasticization	Susceptible	Insusceptible	Insusceptible
Surface roughness	Low	High	Moderate
Fouling resistance	Low	Moderate	Moderate
Cleaning after fouling	Difficult	Easy	Easy
Swelling	Frequently occurs	Swelling-free	Limited-swelling
Resistant to pressure	Moderate	High	High
Mechanical strength	Good	Poor	Excellent
Gas separation performance	Below the Robeson's upper bound	Above the Robeson's upper bound	Above the Robeson's upper bound

Many studies have been conducted on polymer membranes for selective separation of CO₂ [42]. In 1991, Robeson pointed out the trade-off between gas selectivity and gas permeability of polymer membranes, which was updated in 2008 (Figure 1-2) [43–46]. Robeson plotted this trade-off by analyzing a substantial amount of permeation data for different polymers gathered from literature, including multiple polymer-gas combinations. The graphical representation referred to as the "Robeson's plot" is a logarithmic plot of selectivity vs permeability for the gas with the higher permeability, as shown in Figure 1-2a (CO₂/N₂) and Figure 1-2b (O₂/N₂). The lines represent the maximum possible combinations of permeability and selectivity for CO₂/N₂ and O₂/N₂ gas pairs among various polymers. Materials with high gas separation efficiency would be positioned to the right and above the upper-bound. The advantages of polymer membranes, namely good mechanical properties, low cost, synthetic feasibility, and largescale production, make them very attractive for gas separation processes.

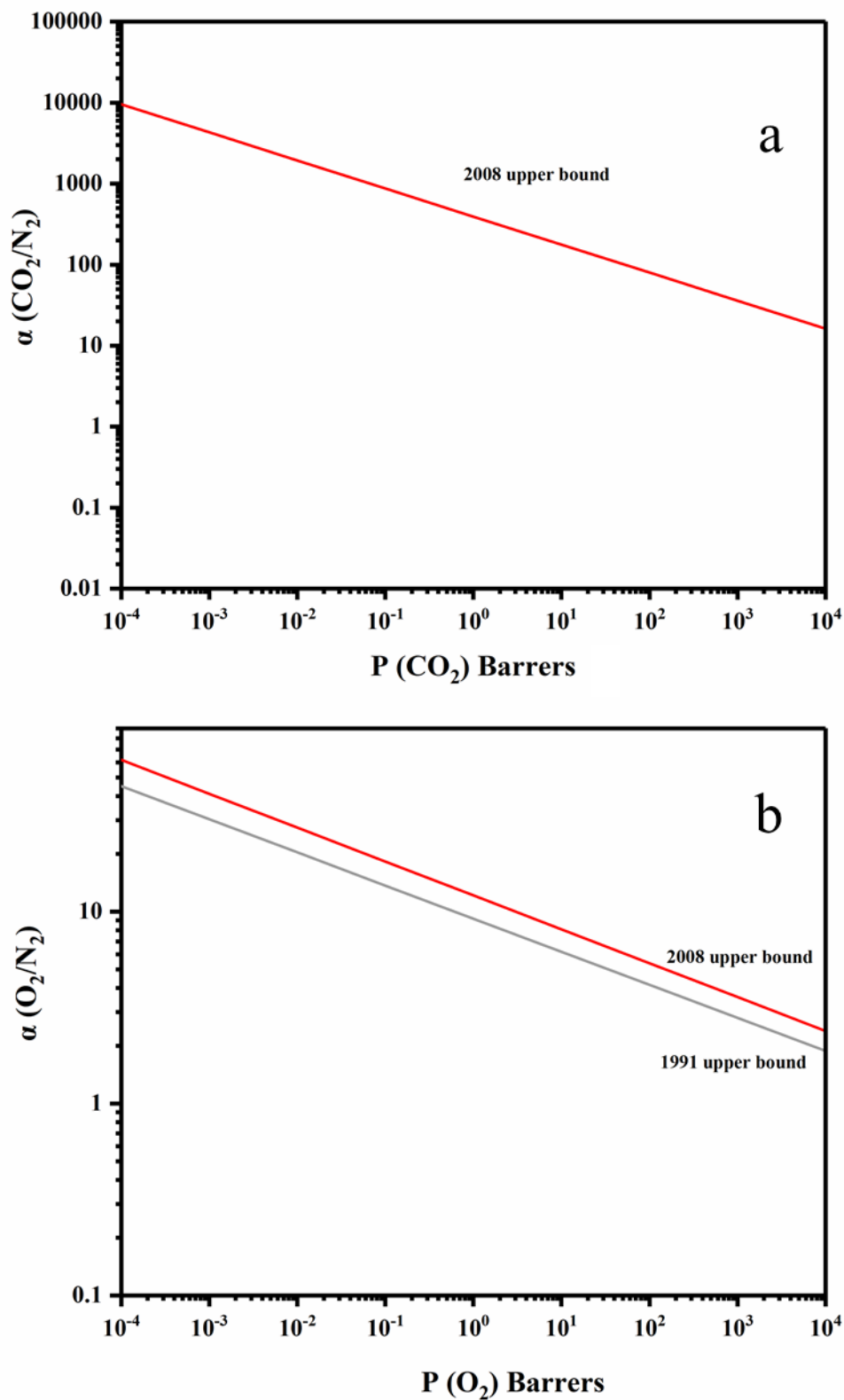


Figure 1-2 Robeson's upper bound of CO₂/N₂ (a) and O₂/N₂ (b)

Mixed matrix membranes are composed of a polymer material mixed with dispersed inorganic fillers [47]. As a continuous phase, polymers should have easy processability. On the other hand, solid inorganic filler particles serve as dispersed phase to provide gas selectivity and/or improve physical and thermal properties. A high affinity between phases is necessary. Otherwise, there will be voids at the interface between polymer and fillers, resulting in a decrease of the membrane gas selectivity. Gas separation through mixed matrix membranes also follows the Robeson's upper bound trend.

In recent years, many studies have focused on the use of ILs in CO₂ separation membranes. Therefore, different types of membrane containing ILs are listed, discussed and compared in section 1.2.2

1.2.2 Ionic liquids-based membranes

The use of polymer/IL membranes has gained tremendous popularity in the field of CO₂ separation due to their strong separation efficiency. An ionic liquid-based membranes classification was reported by Yan *et al* [48], dividing membranes into six categories (Table 1-3).

Swati *et al* [49] used four ILs, namely 1-butylsulfonate-3-methylimidazolium *p*-toluene sulfonate ([BSmim][tos]), 1-butylsulfonate pyridine *p*-toluene sulfonate ([BSmpy][tos]), 1-butyl-3-methylimidazolium chloride ([Bmim][Cl]) and 1-butylpyridine chloride ([Bpy][Cl]), with porous polyvinylidene fluoride (PVDF) support to fabricate SILMs for CO₂ separation. The SILMs were stable up to 0.6 MPa at room temperature without IL leaching. PVDF/[BSmim][tos] showed the best CO₂/N₂ and CO₂/CH₄ selectivities of 56.2 and 47.5 at 0.5 MPa, respectively. This can be explained by the [BSmim][tos] highest CO₂ solubility coefficient and permeability among the four studied ILs (Table 1-4).

Table 1-3 Different types of ILs-based membranes [48]

Membrane type	Advantages	Disadvantages
Supported Ionic Liquids Membranes (SILMs) A class of composite membranes consisting of an IL immobilized or supported within a porous material	<ul style="list-style-type: none"> ◇ High interfacial area per unit volume for mass transfer ◇ More efficient in application over other liquid membrane processes 	<ul style="list-style-type: none"> ◇ In over-time operation, the ionic liquid is pushed out from the membrane pores, resulting in a non-selective transport ◇ Thick membranes will exhibit improved stability and reasonable lifetimes but lower gas flux ◇ Regeneration is complicated and difficult
Ionic Liquids composite Polymer Membranes (ILPMs) A combination of ILs with polymer matrix, ILs are entrapped between polymer chains or clusters	<ul style="list-style-type: none"> ● Prevent the membrane from excessive swelling and maintain the gas separation performances even at increased temperature and pressure conditions 	<ul style="list-style-type: none"> ● Gas permeability and diffusivity are hindered through the solid polymer matrix ● Possible plasticization ● Limited by Robeson's upper bound line
Ionic Liquids composite Mixed Matrix Membranes (ILMMMs) A combination of inorganic fillers, ILs and polymers	<ul style="list-style-type: none"> ◇ Membrane performances including permeability and selectivity are enhanced due to the synergetic effect between ILs and fillers ◇ Added inorganic fillers increase the sorption/diffusion ◇ ILs help to fill the interfacial voids thus ensuring higher thermal and mechanical properties than other membrane types 	<ul style="list-style-type: none"> ◇ ILs could cause pore blockage in porous matrices ◇ Surface voids and filler agglomeration affect the gas separation and structure of membranes ◇ Poor compatibility between polymers and inorganic fillers
Poly(Ionic Liquids) Membranes (PILMs) A class of polymer materials that are derived from polymerizable ILs	<ul style="list-style-type: none"> ● Tunable charge and wettability ● Improved mechanical properties thus promoting both gas permeability and ideal selectivity ● Room temperature ionic liquids (RTILs) with polymerizable groups can be converted into composite dense membranes resulting in a friendly process 	<ul style="list-style-type: none"> ● Separation performances of PILMs mainly depend on monomer and polymerization methods ● The stability of membrane needs to be improved by adding plasticizers
Ionic Liquids Gel Membranes (ILGMs) Composite materials consisting of ILs and a gel matrix	<ul style="list-style-type: none"> ◇ Liquid-like gas transport properties in a solid state, so easier to handle and to prepare membrane modules for industrial applications 	<ul style="list-style-type: none"> ◇ Thermal and mechanical stability is limited ◇ Gas permeability and ideal selectivity are low ◇ Nature of gelators is limited ◇ High packing density is required ◇ Suffering the trade-off effect between CO₂ permeability and selectivity of gas pair
Ionic Liquids Membrane Contactors (ILMCs) ILs as the liquid phase within a membrane-based system to facilitate mass transfer or chemical reactions between two immiscible phases, typically a gas and a liquid	<ul style="list-style-type: none"> ● Long-time operation ● Higher active surface area to volume ratio ● Low resistance to gas flow ● Self-supporting structure ● Ability to be used at high pressure 	<ul style="list-style-type: none"> ● Poor stability and processability ● Selection of materials is limited ● Some ILs can dissolve the polymer or polymer-based sealing membrane ● Low surface tension of ILs

Table 1-4 Diffusion and solubility coefficients of SILMs with different ILs [49]

IL	Diffusion coefficient (10 ⁻⁸ cm ² s ⁻¹)			Solubility coefficient (10 ⁻² cm ³ (STP)cm ⁻³ cmHg ⁻¹)		
	CO ₂	N ₂	CH ₄	CO ₂	N ₂	CH ₄
[BSmim][tos]	3.04	2.21	2.40	9.06	0.22	0.24
[BSmpy][tos]	3.79	2.32	2.45	7.29	0.22	0.25
[Bmim][Cl]	5.43	4.50	4.70	5.07	0.21	0.20
[Bpy][Cl]	5.89	4.80	4.90	4.68	0.17	0.21

Li *et al* [50] designed a series of ILs with 1-alkyl-3-methylimidazolium cation ([C_nMIM]⁺) and tetrafluoroborate ([BF₄]⁻), acetate ([Ac]⁻) or glycine ([Gly]⁻) anions. These ILs were introduced into Pebax[®] to investigate the CO₂ permeability and selectivity of ILPMs. Among all composite membranes, Pebax[®]/[C₆MIM][Gly] (20 wt%) exhibited a notable level of CO₂ permeability (1490 Barrer) and CO₂/N₂ selectivity (93) as compared to pure Pebax[®] with CO₂ permeability of 350 Barrer and CO₂/N₂ selectivity of 30. This fact can be explained by the microstructure of the Pebax[®]/[C₆MIM][Gly] (20 wt%) membrane, characterized by free volume cavities with a certain radius (0.338 nm), which enhance the selective transport of CO₂ molecules and exhibit precise molecular sieving capability. Furthermore, such polymer composite membranes contain amino and carboxyl groups within the free amino acid anions of IL. These groups play a crucial role in enabling the mobility of CO₂, hence facilitating the CO₂ transport with remarkable efficiency.

Estahbanati *et al* [51] introduced 1-butyl-3-methylimidazolium tetrafluoroborate ([Bmim][BF₄]) ionic liquid and silver nanoparticles to Pebax[®]1657 in order to improve gas separation properties. Pebax[®]/Ag (0.5 wt%)/IL (50 wt%) ILMMMs exhibited the highest CO₂ permeability (180 Barrer) and selectivity (CO₂/CH₄ = 61.0 and CO₂/N₂ = 187.5) at 35°C and 10 bar in comparison with pure Pebax[®]1657. The electro-positive part of the silver nanoparticles interacts with electron rich oxygen atoms such as ether segment of Pebax1657 and form stable MMMs in order to enhance gas transport properties. And IL can improve the permeability to CO₂ and form a selective layer around the nanoparticles, thus providing a better interfacial adhesion between polymer and filler.

Two kinds of poly(ionic liquid) (PILs) were synthesised (Figure 1-3) and used to fabricate PILMs

for CO₂ separation [52]. PILs(2) membrane exhibited an excellent CO₂ permeability of 170 Barrer and a CO₂/N₂ permselectivity of 36 due to the CO₂ affinity of ether groups of PILs(2).

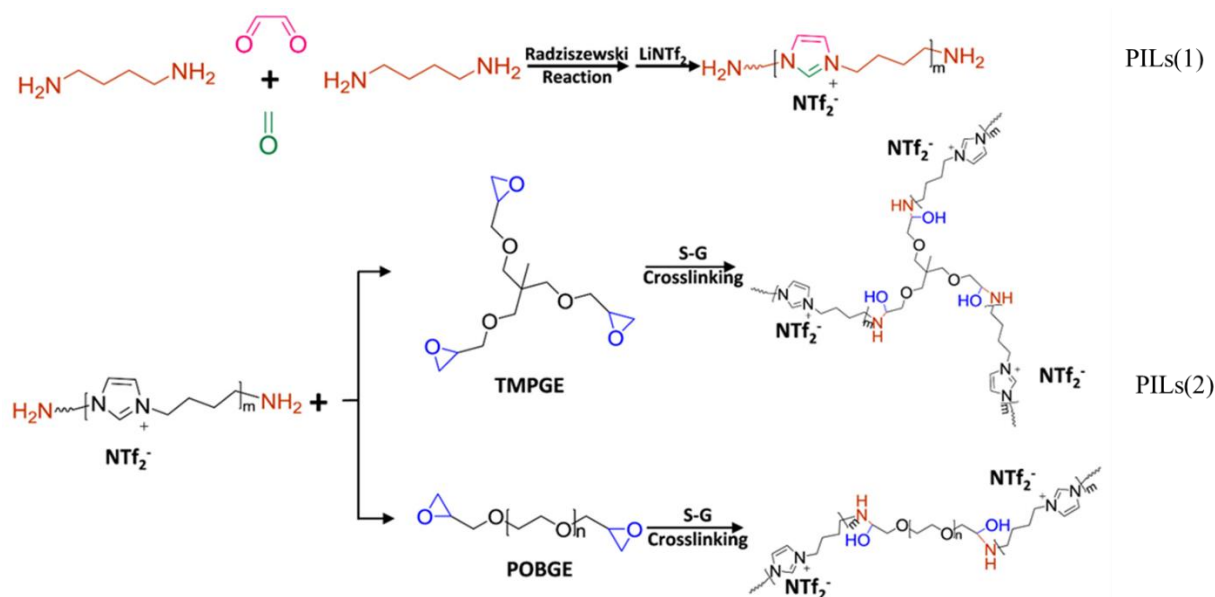


Figure 1-3 Synthesis of crosslinked PILs membranes [52]

Tetrabutylphosphonium prolineate ([P₄₄₄₄][Pro])⁻-based tough gel membrane was fabricated for CO₂ separation under humid conditions [53]. At room temperature, the membrane exhibited good stability at 70% relative humidity (RH). More importantly, at 30°C and 70% of RH, and a CO₂ partial pressure of 0.1 kPa, the membrane showed high CO₂ permeability (around 50 000 Barrer) and CO₂/N₂ selectivity (up to 8 100), because the presence of water promoted the absorption of CO₂ by the NH₂ groups of ILGMs.

Martins *et al* [54] removed CO₂ from xenon anaesthesia circuits using an 50 wt% amino-acid ionic liquid solution (cholinium lysinate [Cho⁺][Lys⁻]) in a membrane contactor (polytetrafluoroethylene (PTFE)). The ILMCs showed a CO₂ capture capacity of 3.50 mol/kg IL, due to the CO₂ affinity of [Cho⁺][Lys⁻] and a reaction between -NH₂ and CO₂.

The industrialization of ILs-based membranes depends on their stability and gas separation performance. Among all ILs-based membranes, ILPMs exhibit superior stability and gas separation performance. Therefore, ILPMs are the most suitable membrane type for high-efficiency CO₂ separation.

1.3 Gas permeation mechanism through a membrane

There are four main mechanisms: solution-diffusion mechanism [55], facilitated transport mechanism [56], molecular sieving mechanism [57] and preferential adsorption-monomolecular surface diffusion mechanism [58] (Figure 1-4). In general, the permeation mechanism depends strongly on the properties of gas molecules (Table 1-5).

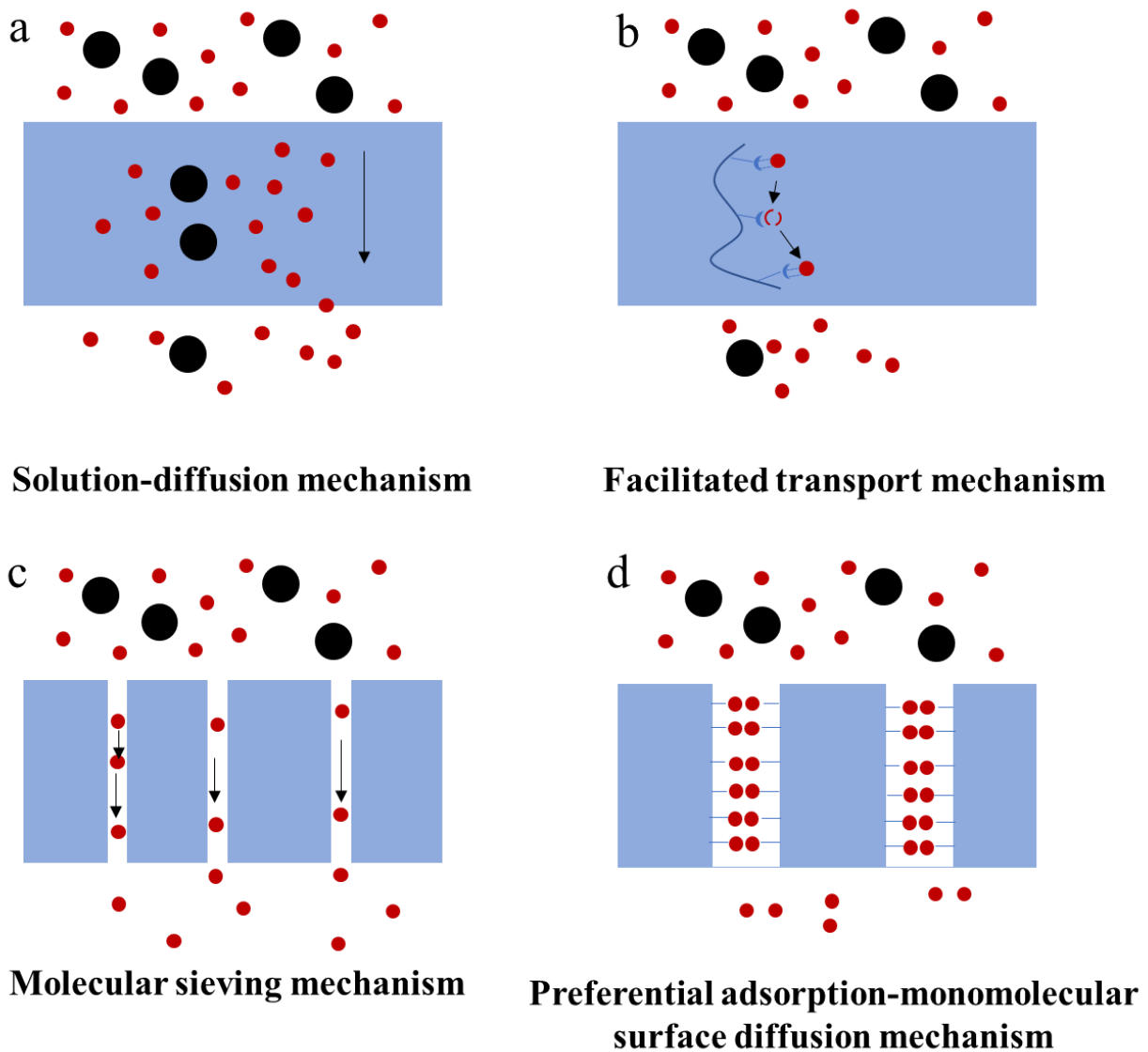


Figure 1-4 Possible gas separation mechanisms through a membrane [59]

Table 1-5 Properties of some gas molecules [41,60]

Parameter (unit)	CO ₂	N ₂	O ₂	CH ₄
Molecular weight (g/mol)	44.01	28.01	31.99	16.04
Kinetic diameter (Å)	3.30	3.64	3.46	3.82
Density, at 0°C and 1 atm (g/L)	1.98	1.25	1.43	0.72
Quadrupole moment (Å)	4.30	1.52	0.39	0
Critical temperature (°C)	31.1	-147.0	-118.6	-82.1

1.3.1 Solution-diffusion mechanism

The solution-diffusion mechanism has proven to be effective in elucidating gases transport within dense membranes (Figure 1-4a) [61]. The solution-diffusion mechanism includes 3 steps: absorption, diffusion and desorption [62]. At first, the gas absorbs on the membrane surface, and this step corresponds to the solubility coefficient S . Then, gas molecules diffuse across the membrane thickness. Diffusion takes place due to the concentration gradient, which provokes molecules to be transported from the membrane surface with the highest concentration (outside the membrane) to the side of the membrane with the lowest concentration (the permeate side). This step is characterized by the diffusion coefficient D . Finally, the gas is desorbed on the permeate side and the whole permeation process is completed, thus giving the permeability coefficient P [63]:

$$P = D \times S \quad (\text{Equation 1-1})$$

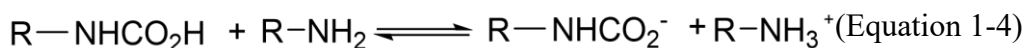
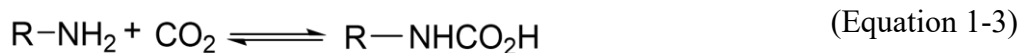
$$\text{Selectivity can be determined as follows: } \alpha_{i/j} = \frac{P_i}{P_j}, \quad (\text{Equation 1-2})$$

where P_i and P_j denote the permeability of gas species i and j within the membrane, respectively.

1.3.2 Facilitated transport mechanism

Facilitated transport mechanism refers to the phenomenon observed in membrane-dependent separation process, in which the transport of certain molecules across the membrane is promoted by carrier molecules, resulting in improved transport (Figure 1-4b) [64]. Facilitated transport mechanism depends on reversible interactions between molecules and carriers present within the membrane. Such mechanism allows molecules to be transported across the membrane against the concentration gradient

and more efficiently. For CO₂ separation, amino groups are the most common carriers that facilitate the CO₂ transport. The reactions between amino groups and CO₂ are following [65–67]:



where R is equivalent to alkyl.

Chen *et al* [68] reported that amino acid functionalized graphene oxide (arg@GO) nanosheets were synthesized and incorporated into Pebax[®] membranes for CO₂ separation. Pebax[®]/arg@GO (0.4 wt%) nanosheets presented promising CO₂ permeation (169 Barrer) and CO₂/N₂ selectivity (70), and surpassed the 2008 upper bound (Figure 1-2): the amino and carboxylic groups in amino acids improved the CO₂ facilitated transport mechanism. Mubashir *et al* [69] introduced ZIF-62 to cellulose acetate (CA) to obtain composite membranes for CO₂ separation. The CA/ZIF-62 (8 wt%) showed the highest CO₂ permeability (84.8 Barrer) and a CO₂/CH₄ ideal selectivity of 35.3, which were 436.7% and 189.3%, respectively, higher than those of pristine CA membrane. This result can be explained by the high CO₂ adsorption on ZIF-62, due to the organic ligands attached to the unsaturated Zn²⁺ metal of ZIF-62, which improve affinity towards CO₂ *via* electrostatic interactions and π - π interactions.

1.3.3 Molecular sieving mechanism

The molecular sieving mechanism refers to a phenomenon observed in separation procedures when the molecules are selectively separated by the membrane according to their size and shape (Figure 1-4c) [70]. This mechanism is based on the fact that the membrane possesses distinct holes or cavities at the molecular scale, which facilitate the passage of smaller molecules but block the transfer of the largest ones. In gas separation, porous membranes can be used to separate gases with different kinetic diameters. The accurate regulation of pore size is necessary because of the tiny difference in molecule size between CO₂ and other gases such as H₂, N₂, and CH₄ (Table 1-5). Microporous membranes with small pore size and narrow pore size distribution typically demonstrate exceptional selectivity during gas separation. Hou *et al* [71] fabricated a novel carbon molecular sieve membrane

(CMS) using pyrolysis of a hydroxyl-containing polyetherimide (BAHPPF-6FDA type HPEI) precursor for CO₂ separation. The CO₂ permeability of CMS pyrolyzed at 700°C is 3200 Barrer and CO₂/N₂ (and CH₄) selectivity is 43.8 (and 72.7). These values are higher than those obtained for membranes pyrolyzed at 500°C and 600°C, owing to the pore distribution: CMS-700°C has more pores in the 3–4 Å range, but fewer in the 4–7 Å and 7–15 Å ranges, as compared to CMS-500°C and CMS-600°C. The pore size of CMS-700°C is more appropriated for the separation of gas molecules (CO₂, N₂ and CH₄) according to their dynamic diameter (Table 1-5).

1.3.4 Preferential adsorption-monomolecular surface diffusion mechanism

The notion of preferential adsorption-monomolecular surface diffusion mechanism is frequently used in separation or transportation of certain molecules across a membrane or adsorbent material (Figure 1-4d) [72,73]. Preferential adsorption-monomolecular surface diffusion mechanism is based on two fundamental processes: preferential adsorption and monomolecular diffusion. The preferential adsorption involves the selective adsorption of CO₂ from gases mixture onto the membrane surface. The adsorption is rather selective as some molecules display a greater affinity towards the membrane surface owing to chemical interactions (adsorption sites, hydrogen bonding, and other intermolecular forces). Monomolecular diffusion refers to the migration of CO₂ when it diffuses inside the membrane. Also, CO₂ molecules can pass through the membrane micropores easier than other gases due to its smaller kinetic diameter (Table 1-5). Preferential adsorption-monomolecular surface diffusion mechanism is a combination of facilitated transport mechanism (Figure 1-4b) and molecular sieving mechanism (Figure 1-4c). Yuan *et al* [74] introduced a novel type of Cr³⁺-induced microporous (HMMP-1) filler with amine-rich nanochannels into polyvinyl amine (PVAm) to prepare facilitated transport mixed matrix membranes for CO₂ separation. The PVAm/HMMP-1 (44.4 wt%) mixed matrix membrane exhibits the maximum CO₂ permeance of 1544 GPU and CO₂/N₂ selectivity of 252 at a feed gas pressure of 0.2 MPa from a CO₂/N₂ mixture (15/85 vol%). The amine-rich micropore gas transport channels enable CO₂ to be easily adsorbed and transported through the membrane.

1.4 Factors influencing gas permeation properties

In order to prepare polymer-based membranes with high gas permeability and selectivity, it is important to study the factors affecting the gas permeation. Among these factors are the nature of polymer matrix, additives, gas properties and test conditions (temperature, pressure and humidity).

1.4.1 Nature of polymer matrix

The key element of membrane CO₂ separation technology is the choice of a suitable polymer matrix, whose physical and chemical properties determine the separation efficiency. To date, many polymer matrices have been investigated for CO₂ separation. According to their chemical structure, they are classified into three types: glassy polymers [75], rubbery polymers [76] and copolymers [77]. The gas permeability through the polymer membranes depends mainly on the polymer nature (glassy, rubbery and copolymer) and crystallinity. Glassy polymers possess low gas permeability but high selectivity. Among them are polycarbonate (PC) [78–80], CA [81–84], polyimides (PI) [85–87], polyether sulfone (PES) [88–90], polysulfone (PSF) [91–93] and poly(phenylene oxide) (PPO) [94]. Rubbery polymers have high gas permeability and low selectivity, as the separation takes place above their glass transition temperature. It is the case of poly(acrylonitrile-butadiene-styrene) (ABS) [95], poly(dimethylsiloxane) (PDMS) [96–98], poly(ethylene glycol) (PEG) [99,100], polyurethane (PU) [101]. Copolymers (for example: PEBA [102]) have gas permeability and selectivity between glassy and rubbery polymers. Polymer membranes, both glassy and rubbery ones, have the limitation of trade-off between their permeability and selectivity (Figure 1-2) [103]. And in general, a single polymer is not efficient for gas separation. The gas permeation properties of some polymers used for CO₂ separation are presented in Table 1-6. Usually, glassy polymers should be chosen for high CO₂ selectivity.

Table 1-6 Gas permeability and selectivity of several polymer matrices

Polymer	Type/grade	Testing conditions			Performance	Selectivity		Ref
		T/°C	P/bar	Gas Pair	P _{CO2} /Barrer	CO ₂ /N ₂	CO ₂ /H ₂	
PDMS	PDMS41	35	4	Single gas	166	13.8	2.35	[104]
PBI	N/A	25	20	Single gas	0.025	3.57	N/A	[105]
PEO	DM14	25	0.98	Single gas	45	68	N/A	[106]
PPO	BPPO _{dp}	25	0.69	Single gas	78	30	N/A	[107]
PU	N/A	25	3	Single gas	167	N/A	N/A	[108]
PVA	Mowiol®8-88	25	2	Single gas	0.027	N/A	0.47	[109]
PSF	N/A	25	3	Single gas	3.65	N/A	N/A	[93]
PES	ULTRASON® E-6020 P	25	5	Single gas	2.86	N/A	N/A	[88]
CA	N/A	35	2.6	Single gas	5.96	25.8	N/A	[110]
PI	6FDA-DAM	25	2	CO ₂ /CH ₄ 50/50	390	N/A	N/A	[111]
PEBA	Pebax®1657	35	10	Single gas	110	78.6	N/A	[112]
Teflon	Teflon AF2400	35	N/A	Single gas	2200	4.58	1.05	[113]

Furthermore, gas permeability is generally lower for polymers with high crystallinity, as the gas can diffuse only through amorphous regions [114]. Guinault *et al* [115] performed gas barrier tests on poly(lactic acid) (PLA) obtained with different crystallinity degrees by heating and recrystallisation (Table 1-7). As one can see, He and O₂ permeability decreased when the polymer crystallinity increased.

Table 1-7 Gas permeability of PLA with different crystallinities [115]

Polymer	P_{He}	P_{O_2}	Crystallinity degree
	(10^{10} Barrer)	(10^{10} Barrer)	X_c (%)
Poly-L-lactic acid	95	2.1	2.5
Poly-L-lactic acid	38	1.2	58
Poly-D-lactic acid	202	2.1	2
Poly-D-lactic acid	50	0.8	37

1.4.2 Additives

In order to increase its performance, the membrane can be composed of one or more polymers with different additives. Each component can have a certain influence on the CO₂ separation. Extensive studies have been conducted to enhance the efficiency of gas separation by using different kinds of fillers: zeolites [116–118], MOFs [119–123], oxide nanoparticles (TiO₂, SiO₂, MgO, ZnO) [124,125], nanocarbon (carbon nanotubes, carbon fibers, graphene, graphene oxide carbon molecular sieves and activated carbons) [126], and ILs [127–129]. Some obtained results are discussed below.

1.4.2.1 Zeolites

Zeolites are a class of natural or synthetically produced crystalline aluminosilicate minerals, which are characterized by a porous and framework-like structure. Zeolites exhibit significant potential for molecular sieving membranes due to their homogeneous pore system with dimensions at the molecular scale, high porosity, and exceptional thermal and chemical durability. These characteristics make zeolites particularly appropriate for the gas separation in industrial conditions.

Zeolites belong to the most advanced molecular sieve family, and they have been widely used in both rubbery and glassy polymers as gas separation membranes [130]. The utilization of carbon-modified zeolites as additives in polysulfone membranes were investigated to enhance the gas separation performance [131]. The addition of carbon-modified zeolites at 0.25 wt% to the PSF matrix significantly enhanced the selectivity for CO₂/CH₄ (107.66%), O₂/N₂ (24.79%), CO₂/N₂ (18.55%), and H₂/CH₄ (140.56%) separation. Such improved gas selectivity can be attributed to the high

microporosity of carbon-modified zeolites obtained by chemical vapor deposition (BET surface area $\sim 2939 \text{ m}^2/\text{g}$, total pore volume $\sim 1.929 \text{ cm}^3/\text{g}$, micropore volume using t-plot $\sim 1.90 \text{ cm}^3/\text{g}$, mean pore width size $\sim 12.2 \text{ \AA}$). The presence of carbon-modified zeolite particles with a high degree of microporosity has important influence on the diffusion of gases with low kinetic diameters (such as H₂, CO₂, O₂, and N₂) (Table 1-5). On the contrary, the diffusion of gases with high kinetic diameters (such as CH₄) (Table 1-5) is hindered by this type of zeolite. The increased gas permeance observed in case of composite membranes containing zeolite-templated carbons can be due to the specific surface area of zeolite-templated carbons that consequently enhances the membrane gas adsorption capability. Furthermore, the observed increase in permeance might be attributed to the larger pore volume and favorable pore size distribution of zeolite-templated carbons, which facilitates efficient molecular transmission. Pure silica Si-CHA zeolite was synthesized and introduced into Pebax[®]-1657 for CO₂ separation from CH₄ [132]. Pebax[®]-1657/silica Si-CHA zeolite (10 wt%) is characterized by the CO₂ permeability of 116.11 Barrer and a CO₂/CH₄ selectivity of 23.28 at a feed pressure of 4 bar and room temperature due to favorable diffusion of gases with small kinetic diameter (Table 1-5) [133].

1.4.2.2 Organic frameworks (MOFs)

MOFs are a kind of nano porous materials that consist of the assembly of metal ions (Co²⁺, Ni²⁺, Al³⁺, Fe²⁺, etc.) with organic linkers. MOFs exhibit a unique property owing to their organic and inorganic constituents. Due to their exceptional high porosity, extensive surface area, well defined open channels, diverse structural characteristics, and abundant functions, MOFs have been widely utilized in several domains, such as gas storage and separation, catalysis, and sensing [134]. MOFs-based composite membranes show great potential for gas separation. For instance, the amino-functionalized MOFs like amino-functionalized UiO-66 [23-27], ZIF-7 [28-31] and zeolitic imidazole framework (ZIF-8) [32-34] were used to enhance the selective transport of CO₂ through facilitated transport or selective adsorption.

PES-based composite membranes modified with 3-aminopropyltriethoxysilane (APTES) functionalized NH₂-MIL-101(Al) were studied by Ahmadipouya *et al* [135]. With the increased APTES functionalized NH₂-MIL-101(Al) loading, an increase of CO₂ permeability and CO₂/CH₄

selectivity is noticed by about 50% and 80%, respectively, as compared with pure PES. The increase in permeability could be attributed to the highly porous structure of APTES functionalized NH₂-MIL-101(Al) nanoparticles. These nanoparticles facilitate rapid gas transport through intra-particle channels within the composite membrane and enhance the free volume at the APTES functionalized MOF/PES interface by disrupting the packing of polymer chains. Meanwhile, APTES enhance the strong interactions between the MOF surface and polar CO₂ molecules, as well as the interfacial interactions between PES and MOFs without any non-selective voids, thus CO₂/CH₄ selectivity was increased.

The OH-functionalized mixed-linker-ZIF-7 was synthesized and incorporated into Pebax[®]2533 for CO₂/N₂ separation [136]. The CO₂ adsorption of the functionalized linker was higher than that of pure ZIF due to the affinity of -OH and CO₂, indicating the benefit of such functionalization on CO₂ adsorption. Hence, the Pebax[®]/ZIF-7-OH (14 wt%) membrane demonstrated a CO₂ permeability performance of 273 Barrer and a CO₂/N₂ separation factor of 38. These values were increased by 60% and 145%, respectively, as compared with the neat Pebax[®] membrane.

1.4.2.3 Oxide nanoparticles

There exist numerous types of oxide nanoparticles, such as TiO₂, SiO₂, Al₂O₃, ZrO₂, etc., which are frequently employed as membrane fillers due to their ability to alter the characteristics of adjacent polymers and the interface between fillers and polymers. The presence of oxide nanoparticles can result in an increase or decrease of the gas permeation path, ultimately leading to enhanced permeability. In addition, many oxide nanoparticles exhibit a pronounced affinity towards CO₂, making them promising in CO₂ capture and separation from other gases, such as N₂.

Ahmad *et al* [137] incorporated TiO₂ nanoparticles in polyvinyl alcohol (PVA) in order to improve the gas separation efficiency of PVA. The results indicated that the incorporation of TiO₂ at a concentration of up to 10 wt% results in the enhancement of both permeability and selectivity of the composite membrane. Hydrogen bonding between PVA and TiO₂ alter the overall crystallinity, thus disturbing the organized arrangement of PVA molecules and enhancing the available free space. The presence of hydrogen bonds also causes the formation of voids that could facilitate non-selective fluid flow. Therefore, the permeability of O₂, CO₂, and H₂ increased to 95%, 79%, and 62%, respectively,

and the selectivity of O₂/N₂, H₂/N₂, and CO₂/N₂ increased to 38%, 26.5%, and 14%, respectively.

Ariazadeh *et al* [138] functionalized SiO₂ nanoparticles by APTES. These particles were introduced into Pebax[®] 1074 to enhance gas permeability and selectivity. The results of the permeation testing demonstrated that the addition of 12.5 wt% of SiO₂ or amine-functionalized SiO₂ nanoparticles to Pebax[®] matrix resulted in a significant increase of CO₂ permeability and ideal CO₂/CH₄ selectivity. Besides, Pebax[®]/amine functionalized SiO₂ membranes were characterized by higher CO₂ permeability (128.9 Barrer) and ideal CO₂/CH₄ selectivity (27.3) than Pebax[®]/SiO₂ (CO₂ permeability: 126.4 Barrer, CO₂/CH₄ selectivity: 23.3) and pure Pebax[®] (CO₂ permeability: 64.5 Barrer, CO₂/CH₄ selectivity: 20.8). The strong CO₂ adsorption capacity of SiO₂ nanoparticles along with the selective voids' formation at the SiO₂-Pebax[®] interface ensure a positive impact of SiO₂ on the enhanced gas separation efficiency. The gas permeation experiments also demonstrated that amine modification of SiO₂ particles prior to their incorporation into the Pebax[®] matrix increased the CO₂ permeability due to the affinity of amine groups and CO₂, thus also improving the CO₂/CH₄ selectivity.

1.4.2.4 Nano-carbon

Nano carbon typically refers to carbon materials or structures that have nanoscale dimension. Carbon in various forms includes zero-dimensional (0-D) carbon quantum dots (QDs), one-dimensional (1-D) carbon nanotubes (CNT) and carbon fibers, two-dimensional (2-D) graphene and graphene oxide (GO), and three-dimensional (3-D) carbon molecular sieves and activated carbons [139]. Nano carbon possesses unique properties and performance, such as specific surface area with different sizes and shapes that can be efficiently used in gas separation.

Two kinds of QDs (namely, graphene oxide QDs (GQD) and polymer-like QDs (PQD)) were used to disrupt the intrinsic crystal arrangement of Pebax[®] in order to enhance the gas permeability and selectivity [140]. It was found that primary interactions occur between GQD and the PA6 segments, whereas PQD interacts with both PEO and PA6 segments simultaneously, thus directly changing gas selectivity. The CO₂/N₂ selectivity of Pebax[®]/PQD membranes was characterized by a constant rise with the PQD content increasing. However, 0.05 wt% of GQD was the optimal concentration in terms of gas selectivity. The Pebax/GQD (0.05 wt%) membrane revealed a 155% increase of the CO₂

permeability and a 130% improvement of the CO₂/N₂ selectivity as compared to the pristine Pebax[®] membrane. The higher GQD concentration provoked agglomeration and selectivity performance decreased.

Rajabi *et al* [141] fabricated poly(vinyl chloride)(PVC)-based composite membranes containing raw and functionalized carbon nanotubes (MWCNTs) by solution casting method. The gas permeability of PVC/MWCNTs and PVC/functionalized MWCNTs was found to be higher than that of pure PVC membrane. Also, functionalized MWCNTs had higher gas permeability and CO₂ selectivity as compared to raw MWCNTs. The CO₂ permeability of PVC/functionalized-MWCNTs (3 wt%) was 11.08 Barrer. For comparison, only 0.25 Barrer was measured for pure PVC. In addition, the CO₂/CH₄ and CO₂/N₂ selectivity was 52.76 and 28.41 as compared to 31.25 and 12.50, respectively, for pure PVC. The vertical orientation of MWCNTs to the membrane surface facilitates the rapid diffusion of gas molecules, since MWCNTs serve as pinholes. The formation of network channels and the increase of the MWCNTs content also increase the membrane free volume. Besides, the introduction of MWCNTs into a polymer matrix leads to the formation of voids between the polymer chains and MWCNTs. These voids become more pronounced when the MWCNTs concentration increases. These spaces serve as favorable locations to gas sorption, resulting in increased permeability. Moreover, the functionalized MWCNTs are better dispersed in PVC and, therefore, such membrane has better gas permeability and selectivity.

Sainath *et al* [142] reported the influence of graphene oxide nanosheets on the performance of PSF-based hollow fiber membranes. The PSF/GO hollow fiber composite membrane with 0.2 wt% of GO sheets demonstrated exceptional performance in separating CO₂ from CH₄. The membrane displayed 36% increase in CO₂ permeance and 201% increase in CO₂/CH₄ selectivity as compared to pure PSF hollow fiber membrane. The abundance of oxygenated functional groups on GO nanosheets enables them to interact with polar gas CO₂, thereby enhancing CO₂ permeance. Conversely, the non-polar CH₄ exhibited lower permeance owing to its limited interaction with GO nanosheets.

Acrylonitrile-butadiene-styrene (ABS) including two micro-mesoporous activated carbons (AC) composite membranes were prepared and CO₂/CH₄ separation properties were investigated by Anson *et al* [143]. ABS/AC membranes exhibited a concomitant enhancement in CO₂ gas permeability (40-600%) and CO₂/CH₄ selectivity (40-100%) as compared to pure ABS due to the CO₂ adsorption

capacity of AC and interfacial contact between ABS and AC.

1.4.2.5 Ionic liquids (ILs)

ILs are a class of salts with organic cation and (in)organic anion, also known as low-temperature molten salts [144]. ILs as green solvents have been widely used over the past few decades in biological catalysis as well as in electrochemistry owing to their outstanding properties, such as negligible vapor pressure, high thermal stability, excellent gas solubility and tunable properties [119,120,145,146]. The ILs anion and cation structure determines directly their physical and chemical properties. Different cations (Figure 1-5) and anions (Figure 1-6) can be combined to create over 10⁶ different ILs, each with specific physical-chemical features [121,122]. In the field of gas separation, ILs are often used to improve the gas separation performance of polymers. The introduction of CO₂-philic groups to functionalized ILs usually improves the CO₂ absorption capacity due to the strong interactions between CO₂ and ILs. In order to improve stability and gas separation performance, the three-components composite membranes containing IL, polymer and porous fillers are considered to be promising materials for gas separation [147].

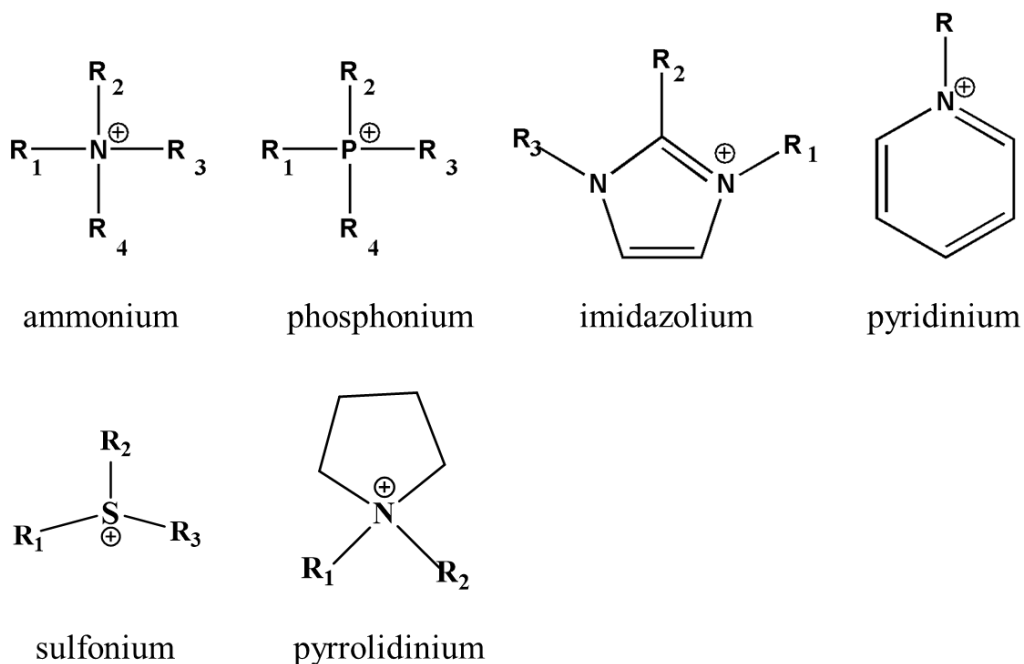


Figure 1-5 Commonly used IL cations

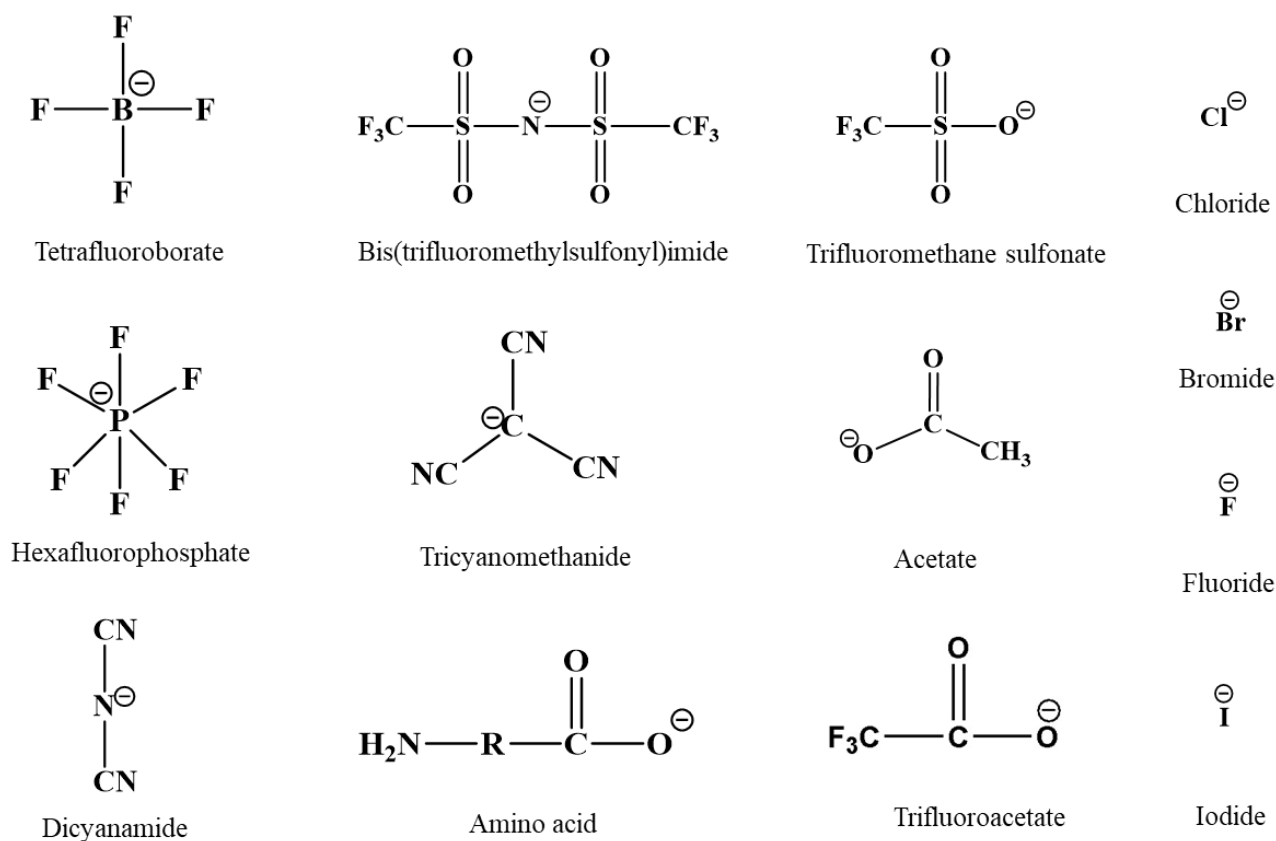


Figure 1-6 Commonly used IL anions

Rabiee *et al* studied Pebax[®]-based composite membranes for the CO₂ separation from light gases (H₂, CH₄, N₂) [148]. The separation performance and transport properties of Pebax[®]1657/1-ethyl-3-methylimidazolium tetrafluoroborate ([Emim][BF₄]) with 20, 40, 60, 80, 100 wt% loadings were measured in different conditions (operating pressure of 2-20 bar and temperature of 25-65°C). The CO₂, H₂, N₂ and CH₄ permeability of neat Pebax[®]1657 and Pebax[®]/IL increased and the selectivity of CO₂/H₂, CO₂/N₂, CO₂/CH₄ decreased with increasing temperature at 2 bars. There was a slight increase of the CO₂ permeability with increasing the operating pressure at 25°C, but the N₂, CH₄, H₂ permeability increase was less pronounced. Therefore, the CO₂/H₂, CO₂/N₂ and CO₂/CH₄ selectivity increased due to CO₂ affinity with ILs. A novel membrane based on polyimide and ILs was reported by Mittenthal *et al* [149]. Polyimide-ionene hybrids were prepared by grafting imidazolium cations to the polymer backbone. Such membranes were then soaked in 1-butyl-3-methylimidazolium bis(trifluoromethylsulfonyl)imide ([C₄mim][Tf₂N]) in order to obtain composite polyimide-ionene

hybrids/IL membranes. The gas permeability of neat ionic polyimide was rather low: for CO₂ - 0.9, H₂ - 1.6, N₂ - 0.03 and CH₄ - 0.03 Barrer. Owing to gas diffusivity increase through the membrane due to the presence of imidazolium cations of IL, CO₂, N₂ and CH₄ permeability rised by 1800-2700%. However, H₂ permeability of polyimide-ionene hybrids increased only by 200%. This can be explained by the fact that the cavities of polyimide-ionene hybrids may be sufficiently large that H₂ takes the same diffusion pathway than in case of the neat ionic polyimide. Composite membranes with the γ -alumina layer of a tubular porous asymmetric membrane filled with 1-ethyl-3-methylimidazolium tris(pentafluoroethyl)tri-fluorophosphate ([Emmim][FAP]) were studied by Althuluth *et al* [150] to purify natural gas including CO₂, CH₄, ethane C₂H₆ and propane C₃H₈. The permeability of pure gases was tested at 0.7 MPa and 40°C, and the next order was found: P_{CO₂} > P_{CH₄} > P_{C₂H₆} > P_{C₃H₈}. The permselectivity of CO₂/CH₄ (50/50%, v/v) was found to be much lower (1.15) than the ideal permselectivity (3.12) because of water negatively affecting the performance of composite membranes. The water (which is present in natural gas) could compete with CO₂ for some free volume of the composite membrane. Secondly, the possible interactions between water and IL may change the polarity, thus reducing CO₂ permeability. Therefore, this kind of composite membrane is a less promising candidate for the removal of CO₂ from natural gas. Estahbanati *et al* [151] aimed to enhance the CO₂ affinity of Pebax[®]1657 with 1-butyl-3-methylimidazolium tetrafluoroborate ([Bmim][BF₄]) ionic liquid. The gas permeability of Pebax[®]/IL membrane was tested at 2-10 bar and 35°C. Due to the affinity between [Bmim][BF₄] and CO₂, the solubility of CO₂ was found to be higher than that of CH₄ and N₂ in [Bmim][BF₄]. The CO₂ permeability of Pebax[®]/IL (50 wt%) (190 Barrer) was 1.73 times higher than pure Pebax[®] (110 Barrer) at 35°C and 10 bar. The related CO₂/CH₄ and CO₂/N₂ selectivities were increased from 20.8 to 24.4 and from 78.6 to 105.6, respectively. O'Harra *et al* [152] worked on gas separation membranes containing 6FDA-based polyimide-ionenes with ionic liquids. Composite membranes of 3 novel 6FDA-based polyimide-ionenes with imidazolium moieties and varying regiochemistry (*para*-, *meta*- and *ortho*-connectivity) and three ILs (3-ethyl-1-methyl-1H-imidazol-3-ium bis((trifluoromethyl) sulfonyl)amide [C₂mim][Tf₂N], 3-butyl-1-methyl-1H-imidazol-3-ium bis((trifluoromethyl) sulfonyl)amide [C₄mim][Tf₂N], 3-butyl-1-methyl-1H-imidazol-3-ium bis((trifluoromethyl) sulfonyl)amide [Bnmim][Tf₂N]) were prepared as gas separation membranes. All composites exhibited good compatibility and thermostability, and [6FDA I4A pXy][Tf₂N]

ionene/[C₄mim][Tf₂N] and [6FDA I4A pXy][Tf₂N] ionene (*para*-connectivity)/[Bnmim][Tf₂N] membranes presented a good affinity for CO₂ due to enhanced physical adsorption between ILs and CO₂. The CO₂ permeability of hybrid membranes was increased by more than two times (P([6FDA I4A pXy][Tf₂N] ionene): 2.15, P([6FDA I4A pXy][Tf₂N] ionene/[C₄mim][Tf₂N]): 4.57, P([6FDA I4A pXy][Tf₂N] ionene/[C₄mim][Tf₂N]/[Bnmim][Tf₂N]): 6.32 Barrer). Compared to the pure membrane, the permselectivities α of the composite membranes with [C₄mim][Tf₂N] and [Bmim][Tf₂N] were also remarkably increased ([6FDA I4A pXy][Tf₂N]: $\alpha_{\text{CO}_2/\text{N}_2}$ =20.9, $\alpha_{\text{CO}_2/\text{CH}_4}$ =13.4; [6FDA I4A pXy][Tf₂N]/[C₄mim][Tf₂N]: $\alpha_{\text{CO}_2/\text{N}_2}$ =19.1, $\alpha_{\text{CO}_2/\text{CH}_4}$ =24.8; [6FDA I4A pXy][Tf₂N]/[Bnmim][Tf₂N]: $\alpha_{\text{CO}_2/\text{N}_2}$ =22.4, $\alpha_{\text{CO}_2/\text{CH}_4}$ =21.5).

It is known that ionic liquids containing CO₂-affinity groups, such as amino and ether groups, can improve the membrane CO₂ permeability, thus further improving the CO₂ selectivity. In the case of amino groups, owing to the interaction of -NH₂ with CO₂ (equations 1-3 and 1-4), the membrane affinity with CO₂ can be enhanced. Poly(ethylene glycol) (PEG) and poly(ethylene oxide) (PEO), which are characterized by a high CO₂ solubility owing to the interactions of ether groups with CO₂, are widely used for gas separation.

Kasahara *et al* [153] studied the influence of the amino-group density of functionalized ionic liquids on the facilitated transport properties in case of CO₂ separation. Tetrabutylammonium glycinate ([N₄₄₄₄][Gly]), tetramethylammonium glycinate ([N₁₁₁₁][Gly]) and 1,1,1-trimethylhydrazinium glycinate ([aN₁₁₁][Gly]) were used to prepare a facilitated transport membrane (FTM). The results show that higher relative humidity and higher IL amino group density facilitate the CO₂ transport through FTM as a [aN₁₁₁][Gly]-CO₂ complex can be formed *via* a reaction of the second amino group at higher RHs. [aN₁₁₁][Gly]-based FTM showed higher CO₂ permeability (at 50% RH: [aN₁₁₁][Gly] ~ 200 000, [N₄₄₄₄][Gly] ~ 100 000, [N₁₁₁₁][Gly] ~ 160 000 Barrer) and higher CO₂ selectivity (at 50% RH: [aN₁₁₁][Gly] ~ 5900, [N₄₄₄₄][Gly] ~ 200, [N₁₁₁₁][Gly] ~ 5000) against N₂ than [N₄₄₄₄][Gly] and [N₁₁₁₁][Gly] over a wide RH range at 100°C. PEG-based epoxy-amine networks for CO₂ separation membranes (crosslinked PEG diglycidyl ether (PEGDE) with a diamine (2,2'-(ethylenedioxy)bis(ethylamine)) and a polyamine-based ionic liquid (triethylenetetramine trifluoroacetate ([Teta][TfA])) were reported by Dai *et al* [154]. Owing to the amine-based crosslinking agents and PEG ether groups, the membrane CO₂ affinity was enhanced. PEGDE with an average

molecular weight of 250 g/mol was also added as a plasticizer to improve mechanical compatibility and gas transport properties of the resulting network. The result showed that the PEG crosslinked with [Teta][TfA] and 80% of free PEGDE had high CO₂ permeability (117.2 Barrer) and CO₂/N₂ and CO₂/CH₄ selectivities (131.1 and 70.3, respectively). Deng *et al* [155] developed a series of composite membranes based on ether-functionalized pyridinium-based ionic liquids ([EnPy][Tf₂N], n = 1, 2) and CA polymer matrix to improve the CO₂ separation performance. Ether-functionalized pyridinium-based ILs (CA/[EnPy][Tf₂N]) and non-functionalized analogous ILs (CA/[CnPy][Tf₂N]) composite membranes were prepared and studied. The CO₂/N₂ and CO₂/CH₄ permselectivities were affected by plasticizing effect and the affinity of ILs to gases. The plasticizing effect was dominant and permselectivities dropped when the IL amount in membranes was lower than 20 wt%. When the IL concentration grew, the permselectivity of CO₂/N₂ was improved and the permselectivity of CO₂/CH₄ decreased due to the CO₂ affinity between ether groups of [E₁Py][Tf₂N] and CA. The results showed that the CA/[E₁Py][Tf₂N] (40 wt%) composite membrane exhibited approximately a seven-fold increase of the CO₂ permeability as compared with the permeability of pure CA membrane with CO₂/N₂ and CO₂/CH₄ ideal selectivities of 32 and 24, respectively. In addition, the more ether groups were present, the higher the compatibility between [E₁Py][Tf₂N] and CA was, and the less was the CO₂ permeability increase. However, [E₁Py][Tf₂N] can improve the ideal selectivity of CO₂/N₂ and CO₂/CH₄ showing the higher CO₂ permeability increase in comparison with N₂ and CH₄.

Recently, a new approach, the combination of ionic liquids with other fillers, was adopted to enhance the membrane gas permeability and selectivity. SAPO zeolites were modified by an imidazolium-based ionic liquid ([Emim][Tf₂N]) in case of polysulfone asymmetric membranes for CO₂ gas separation by Ahmad *et al* [156]. It was found that the dispersion of modified SAPO-34 particles was better than that of pure SAPO-34 particles in terms of CO₂ selectivity, and the CO₂/CH₄ and CO₂/N₂ selectivities were enhanced to 20.35 (PSF ~ 3.24) and 18.82 (PSF ~ 6.15), respectively. The high specific surface area and porosity of zeolite made it selective for gas adsorption. The IL modification did not affect the crystal structure of SAPO-34 zeolite, but slightly reduced both surface area and pore volume of zeolite. Graphene oxide modified by ionic liquid (1-(3-aminopropyl)-3-methylimidazolium bromide) was also introduced into Pebax[®] to enhance the CO₂ capture [157]. Compared with the pristine membranes, 0.05 wt% of GO can improve the composite membrane CO₂

permeability by 23%, CO₂/N₂ selectivity by 71%, and CO₂/H₂ selectivity by 31%. However, when the added amount was 0.5 wt%, the performance of each gas decreased due to the GO agglomeration. When modified with IL-NH₂, the interlayer space between the GO-IL sheets increased (for GO: interlayer space was ca. 0.79 nm, and for IL-NH₂ GO it was 0.88 nm). This result is important when higher GO content should be used. The presence of IL-NH₂ on the surface of the GO sheets also improved the CO₂ transport due to the reaction of -NH₂ with CO₂. It was found that Pebax[®]/GO-IL (0.2 wt%) had the highest CO₂ permeability (118.6 Barrer), and CO₂/N₂ (71) and CO₂/H₂ (9.5) selectivities. The mixed matrix membranes formed by zeolite particles (SAPO-34 nanocrystalline, ca. 300 nm; SSZ-13 nanoparticles, ca. 500 nm), crosslinked poly(ionic liquids) (poly([Smim][Tf₂N]), poly([Vmim][Tf₂N]), poly([Vhim][Tf₂N])), and RTILs ([Emim][Tf₂N], [Smim][Tf₂N], [Vmim][Tf₂N], [Vhim][Tf₂N]) were studied by Singh *et al* [158] for CO₂/CH₄ separation. In order to solve the problem of defects at the interface and the easy hardening of the interface between zeolite and poly(ionic liquid), RTILs was introduced. It was found that the CO₂/CH₄ separation order was: poly([Smim][Tf₂N]) ≥ poly([Vmim][Tf₂N]) > poly([Vhim][Tf₂N]), and while the majority of CO₂ was rapidly permeated, both zeolite and poly(ionic liquid) with smaller fractional free volume (FFV) had a slower CH₄ permeation. The sample with 50 wt% of poly([Smim][Tf₂N]/[Emim][Tf₂N] (20 wt%)/SAPO-34 (30 wt%) displayed exceptional performance of CO₂/CH₄ selectivity of 90 and CO₂ permeability of 260 Barrer. Yao *et al* [123] focused on ionic liquids modified MOF-polymer membranes prepared with imidazolium-based ionic liquid-decorated UiO-66 type nanoparticles and an isocyanate-terminated polyurethane oligomer. UiO-66/IL-PF₆, UiO-66/IL-SO₃CF₃ and UiO-66/IL-ClO₄ were synthesized and used to prepare membranes for CO₂ separation. UiO-66/IL-ClO₄ polyurethane showed that the covalent bonding had a positive influence on enhancing the interfacial interaction between MOF and polymer, improving the MOF dispersion within the polymer. The best selectivity of composite films was noted when [ClO₄]⁻ was used as anion, the ideal CO₂/N₂ and CO₂/CH₄ selectivities of the sample with 50 wt% UiO-66-ClO₄ were 39.1 and 25.1, respectively, at 25°C and 10 bar.

1.4.3 Gas properties

The transport of permeants inside a polymer matrix is influenced by their inherent characteristics. The properties of CO₂, N₂ and O₂ molecules are gathered in Table 1-5. The gases diffusion within a polymer is usually correlated with the gas's molecular kinetic diameter. Typically, the gas diffusivity decreases as the gas molecular size increases [159,160]. The gas permeation *via* a composite membrane includes the diffusion of gas molecules across the membrane. This diffusion process is impacted by the relative size and shape of gas molecules in relation to the dimension of the free volume present within the membrane. Furthermore, the impact of gas molecule size and shape on molecular permeability is more pronounced in glassy polymers as compared to rubbery polymers (Table 1-8) [161]. The solubility of gases or vapors is significantly influenced by their condensability and molecular interactions, which are directly related to their critical temperature and Lennard-Jones force constant, respectively. Generally, polymers have higher solubility in the case of gases or vapors with higher condensability and strong intermolecular interactions. The solubilities of N₂, CO₂, CH₄, C₂H₆, C₃H₈, and C₃F₈ were determined in Hyflon[®] AD 80 at 35°C [162]. The results showed the solubilities of these gases increase in the next order: N₂ < CH₄ < CO₂ ≈ C₂H₆ < C₃F₈ < C₃H₈ (pressure < 5 atm). This is also the order of gas critical temperature used. At high pressure (pressure > 5 atm), interactions with the polymer have a more pronounced effect on solubility as penetrant molecules are sorb preferentially into more densified polymer regions. Because of its chemical similarity with the polymer, C₃F₈ has more favorable interactions with this fluoropolymer. When the pressure > 5 atm, C₃F₈ solubility (2.6 cm³(STP)/(cm³atm)) exceeds that of C₃H₈ (2.4 cm³(STP)/(cm³atm)).

Table 1-8 Diffusion and solubility coefficients of PE and PLA [163]

Polymer	State at experiment temperature	Diffusion (10 ⁻⁹ cm ² /s)			Solubility (cm ³ (STP)/(cm ³ ·atm))		
		CO ₂	N ₂	O ₂	CO ₂	N ₂	O ₂
PE	Rubbery	676	505	1800	0.550	0.100	0.150
PLA	Glassy	5.22	13.7	47.2	2.31	0.036	0.0070

1.4.4 Operation parameters

1.4.4.1 Temperature

The gas permeability properties of composite membranes can be significantly affected by temperature. In general, it can be observed that an increase of temperature leads to an increase of the gas permeability through the membrane. Gas molecules exhibit increased kinetic energy as temperature rises, resulting in increased frequency of interactions with the membrane and thus, enhanced permeation. Simultaneously, with the temperature increase, intensification of polymer chains movement can take place, resulting in an increased availability of free volume inside membranes for gas molecules to permeate. As reported by Wang *et al* [164], the Tröger-base polymer (TB) was synthesized and used to fabricate mixed matrix membranes with ZIF-8 modified by polydopamine (PDA). TB/ZIF-8@PDA (30 wt%) was tested for CO₂ and CH₄ transport at different temperatures (35, 45, 55°C) under 4 bar. The results showed that CO₂ and CH₄ permeabilities increased with permeation temperature (CO₂: 196.8 Barrer (35°C), 240 Barrer (55°C); CH₄: 11.3 Barrer (35°C), 18.5 Barrer (55°C)). Polymer chain flexibility and mobility are improved at higher temperature, thus increasing the gas permeability due to improved diffusion. The smaller kinetic diameter of CO₂ molecule (3.30 Å) was less sensitive to temperature changes than CH₄ (3.82 Å). As a result, CO₂/CH₄ selectivity decreased from 18.1 to 12.8 with temperature increasing.

1.4.4.2 Pressure

Pressure can also influence the gas permeation properties of composite membranes. The permeation rate is directly correlated with the pressure difference (ΔR) across the membrane, and the pressure gradient increase across a composite membrane often results in increasing the gas permeation rate. The correlation between pressure and permeability is commonly described by Darcy's law (Equation 1-5) [165], which postulates that the flow rate Q is directly proportional to the pressure difference ΔR and the membrane permeability P .

$$P \propto Q = -k_1 A \frac{\Delta R}{L} \quad (\text{Equation 1-5})$$

where A is the membrane area to the direction of flow, L is the thickness of membrane and k_1 is a constant.

As the pressure increases, the gas molecules enter in more frequent collisions with the membrane, provoking higher permeability. Also, in case of composite membranes with components that possess adsorptive characteristics (such as zeolites or activated carbon), gas adsorption can be influenced by pressure, thus impacting gas permeation. Elevated pressure can enhance the gas adsorption onto adsorptive materials, hence modifying the composite membrane gas transport characteristics. Yousef *et al* [166] studied CO₂, CH₄, N₂ and H₂ permeability performance of polyethersulfone membranes under different pressures (1-6 bar). The result showed that the permeability of CO₂, CH₄, N₂ and H₂ under 6 bar was increased by 13.2%, 4.6%, 15.1% and 11%, respectively, as compared to the results obtained at 1 bar at the same temperature (20°C). A high pressure can increase the void volume in the membrane and kinetic energy of molecular motions, so that gases can be easily transported through the polymer membrane.

1.4.4.3 Humidity

The effect of humidity on the gas permeability of composite membranes is critical, especially for gases sensitive to RH [167]. The water solubility can influence the permeability of specific gases. When exposed to humidity, gases (such as CO₂ and NH₃) can exhibit enhanced solubility, leading to an increase in their permeability across the membrane. On the other hand, it should be noted that some gases (such as O₂ and N₂) demonstrate lower solubility in water and may have diminished permeability when exposed to humid environment. In some cases, moisture can potentially compete with the target gases for available adsorption sites, thereby decreasing gas permeability. Deng *et al* [168] reported CO₂/N₂ separation through Pebax[®]/zeolitic imidazolate framework cuboid (ZIF-C) mixed matrix membranes under different humidity conditions (0~100%). Pebax[®]/ZIF-C (10 wt%) showed CO₂ and N₂ permeability decreased when RH was lower than 70% (CO₂: 141.7 Barrer at 0 RH%; 108.6 Barrer at 70 RH%. N₂: 3.5 Barrer at 0 RH%; 2.5 Barrer at 70 RH%). This fact results from the competition between gas and water molecules for free volume. Also, the impact of water molecules on the permeability is greater than the impact of increased CO₂ solubility. On the contrary, when RH was

100%, CO₂ and N₂ permeability increased to 259.2 and 4.5 Barrer, respectively. This can be explained by the greater effect of gas solubility at this RH value. In addition, more free volume is formed in swollen Pebax[®] chains.

In addition, the composite membrane components exhibit a reversible interaction with gas, and the introduction of water enhances the reaction kinetics and facilitates gas penetration through the composite membrane. Barooah *et al* [169] investigated the CO₂ separation performance of PVA/PEG/amine-functionalized silica filler mixed matrix membranes under sweep water flow (0.0–0.075 mL/min). The PVA (38 wt%)/PEG (9 wt%)/PEI (25 wt%)/triethylenetetramine (15 wt%)/KOH (10 wt%)/3-aminopropyltrimethoxysilane (APTMS) functionalized silica nanoparticle loading (AFSNP) (3 wt%) membrane labelled as AFSNP-03, revealed CO₂ permeance and CO₂/N₂ selectivity of 10 GPU and 76, respectively, at a sweep water flow rate of 0.01 mL/min and temperature of 100°C. However, at a sweep water flow rate of 0.04 mL/min and temperature of 100°C this membrane showed CO₂ permeance of 36 GPU and CO₂/N₂ selectivity of 325. The presence of water increased the CO₂-amine reversible reaction mechanism as shown in Equations 1-3, 1-4 and 1-6.



1.5 Summary and outlook

It is an urgent need to develop an energy-efficient technology to separate CO₂ from other gases to reduce the greenhouse effect and face energy gas challenges. Among the different separation methods proposed (absorption, adsorption, cryogenic distillation, hydrate and membrane technology), due to its advantages (such as ease of operation, small footprint and low maintenance) membrane technology has emerged as the most promising for CO₂ separation.

In fact, polymer membranes, inorganic membranes and mixed matrix membranes have been studied for CO₂ separation. As compared to inorganic and mixed matrix membranes, polymer membranes have significant benefits (such as low fabrication cost and gas separation performance), which are essential for industrial applications. When selecting a polymer matrix, glassy polymers are

a favorable choice due to their high gas selectivity as compared to the selectivity of rubbery polymer. However, the gas permeation of polymer membranes is limited by Robeson's upper bound.

Although ILs are ecotoxic, they are being investigated as potential CO₂ absorbents since they present favorable properties for CO₂ capture, like high uptake capacity, negligible vapor pressure, wide liquid temperature range and tunable solvent capacity. Therefore, ILs are considered as the most suitable choice for enhancing the gas separation performance of polymer membranes by overcoming Robeson's upper bound.

In the last years, numerous studies have been reported on the IL use in CO₂ separation composite membranes, indicating that research in this area is growing rapidly. Despite significant progress, there are still some challenges for ILs-based CO₂ separation composite membranes, namely:

1. improving their stability,
2. recovery-based reuse,
3. to balance between CO₂ permeability and selectivity,
4. reducing the cost of membrane separation technology.

The present PhD research aims to obtain high CO₂ permeability and selectivity polymer-based membranes, that is why PSF and PES (both glassy polymers) were chosen.

PSF (Figure 1-7) stands out as a suitable polymer for membrane production thanks to its exceptional physicochemical properties, including notable thermal stability (weight loss starts at about 400°C) [170], robust chemical resistance to various substances (bases, acids, and chlorine) [171], excellent mechanical strength (tensile stress around 55 MPa) [172], and efficient processability [173]. Therefore, PSF-based membranes are applied in a wide range of fields, including water and wastewater treatment [174], membrane distillation [175], pollutant removal [176], gas separation [177], as separators for lithium-ion battery [178], and supports of composite membranes [179].

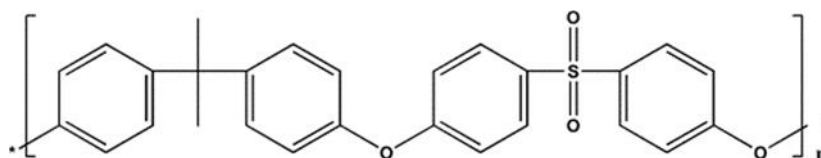


Figure 1-7 Chemical structure of PSF

PES (Figure 1-8) exhibits excellent characteristics, such as thermal stability and transparency

[180]. Additionally, PES demonstrates exceptional mechanical strength, resistance to hydrolysis, thermal stability, chemical durability, remarkable antioxidant properties, and ability to form films [181–183]. Therefore, PES is highly suitable for the fabrication of membranes with diverse surface properties and pore dimensions, with applications in many fields, such as water/oil separation [184,185] and blood purification [186]. Thus, PES has shown great potential in the manufacture of gas separation membranes [187], and has been proven to be effective in N₂ generation, H₂ recovery, and CO₂ capture [187,188]. PES, as a glassy polymer, presents high gas selectivity and low gas permeation - at 5 bars ~ 2.86 Barrer and at 25 bars ~ 2.42 Barrer for CO₂ permeation [189].

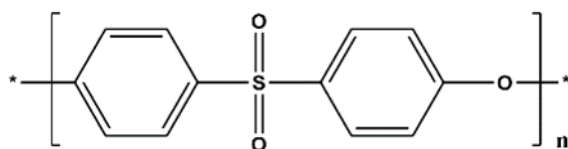


Figure 1-8 Chemical structure of PES

To overcome the tradeoff between permeability and selectivity, limited by Robeson's upper bound (Figure 1-2), of polymer materials, ILs will be introduced into PSF and PES to fabricate dense composite membranes with high CO₂ permeability and selectivity.

References

- [1] F. Chien, K.Y. Chau, M. Sadiq, G.L. Diep, T.K. Tran, T.H.A. Pham, What role renewable energy consumption, renewable electricity, energy use and import play in environmental quality, *Energy Reports* 10 (2023) 3826–3834.
- [2] A. Akaev, O. Davydova, Climate and Energy: Energy Transition Scenarios and Global Temperature Changes Based on Current Technologies and Trends, in: V. Sadovnichy, A. Akaev, I. Ilyin, S. Malkov, L. Grinin, A. Korotayev (Eds.), *Reconsidering the Limits to Growth: A Report to the Russian Association of the Club of Rome*, Springer International Publishing, Cham, 2023: pp. 53–70.
- [3] L. Chandra Voumik, M. Ridwan, Md. Hasanur Rahman, A. Raihan, An investigation into the primary causes of carbon dioxide releases in Kenya: Does renewable energy matter to reduce carbon emission, *Renewable Energy Focus* 47 (2023) 100491.
- [4] L.R. López, P. Dessì, A. Cabrera-Codony, L. Rocha-Melogno, B. Kraakman, V. Naddeo, M.D. Balaguer, S. Puig, CO₂ in indoor environments: From environmental and health risk to potential renewable carbon source, *Science of The Total Environment* 856 (2023) 159088.
- [5] A. Richard, et al. Climate change 2007: The physical science basis. Contribution of Working Group I to the Fourth Assessment Report of the Intergovernmental Panel on Climate Change. Summary for Policymakers. IPCC Secretariat, Geneva, Switzerland. 21p, 2007, 980.
- [6] M.K. Mondal, H.K. Balsora, P. Varshney, Progress and trends in CO₂ capture/separation technologies: A review, *Energy* 46 (2012) 431–441.
- [7] M.R. Atelge, H. Senol, M. Djaafri, T.A. Hansu, D. Krisa, A. Atabani, C. Eskicioglu, H. Muratçobanoğlu, S. Unalan, S. Kalloum, N. Azbar, H.D. Kıvrak, A Critical Overview of the State-of-the-Art Methods for Biogas Purification and Utilization Processes, *Sustainability* 13 (2021) 11515.
- [8] S. Lu, L. Zhang, Corrosion in CO₂ Capture and Transportation, in: L. Zhang (Ed.), *Corrosion in CO₂ Capture, Transportation, Geological Utilization and Storage: Causes and Mitigation Strategies*, Springer Nature, Singapore, 2023: pp. 31–46.
- [9] M. Shen, L. Tong, S. Yin, C. Liu, L. Wang, W. Feng, Y. Ding, Cryogenic technology progress for CO₂ capture under carbon neutrality goals: A review, *Separation and Purification Technology* 299 (2022) 121734.
- [10] C. Song, Q. Liu, N. Ji, S. Deng, J. Zhao, Y. Li, Y. Song, H. Li, Alternative pathways for efficient CO₂ capture by hybrid processes—A review, *Renewable and Sustainable Energy Reviews* 82 (2018) 215–231.
- [11] S.C. Tiwari, A. Bhardwaj, K.D.P. Nigam, K.K. Pant, S. Upadhyayula, A strategy of development and selection of absorbent for efficient CO₂ capture: An overview of properties and performance, *Process Safety and Environmental Protection* 163 (2022) 244–273.
- [12] B. Aghel, S. Janati, S. Wongwises, M.S. Shadloo, Review on CO₂ capture by blended amine

- solutions, *International Journal of Greenhouse Gas Control* 119 (2022) 103715.
- [13] P. Zang, J. Tang, X. Zhang, L. Cui, J. Chen, P. Zhao, Y. Dong, Strategies to improve CaO absorption cycle stability and progress of catalysts in Ca-based DFMs for integrated CO₂ capture-conversion: A critical review, *Journal of Environmental Chemical Engineering* 11 (2023) 111047.
- [14] S. Lian, C. Song, Q. Liu, E. Duan, H. Ren, Y. Kitamura, Recent advances in ionic liquids-based hybrid processes for CO₂ capture and utilization, *Journal of Environmental Sciences* 99 (2021) 281–295.
- [15] W. Faisal Elmobarak, F. Almomani, M. Tawalbeh, A. Al-Othman, R. Martis, K. Rasool, Current status of CO₂ capture with ionic liquids: Development and progress, *Fuel* 344 (2023) 128102.
- [16] V.M. Shama, A.R. Swami, R. Aniruddha, I. Sreedhar, B.M. Reddy, Process and engineering aspects of carbon capture by ionic liquids, *Journal of CO₂ Utilization* 48 (2021) 101507.
- [17] X. Zhu, Z. Chen, H. Ai, Amine-functionalized ionic liquids for CO₂ capture, *J Mol Model* 26 (2020) 345.
- [18] O. Akeeb, L. Wang, W. Xie, R. Davis, M. Alkasrawi, S. Toan, Post-combustion CO₂ capture via a variety of temperature ranges and material adsorption process: A review, *Journal of Environmental Management* 313 (2022) 115026.
- [19] A.G. Olabi, K. Obaideen, K. Elsaid, T. Wilberforce, E.T. Sayed, H.M. Maghrabie, M.A. Abdelkareem, Assessment of the pre-combustion carbon capture contribution into sustainable development goals SDGs using novel indicators, *Renewable and Sustainable Energy Reviews* 153 (2022) 111710.
- [20] D. Liu, B. Li, J. Wu, Y. Liu, Sorbents for hydrogen sulfide capture from biogas at low temperature: a review, *Environ Chem Lett* 18 (2020) 113–128.
- [21] R. Bai, X. Song, W. Yan, J. Yu, Low-energy adsorptive separation by zeolites, *National Science Review* 9 (2022) 064.
- [22] R.-B. Lin, Z. Zhang, B. Chen, Achieving High Performance Metal–Organic Framework Materials through Pore Engineering, *Acc. Chem. Res.* 54 (2021) 3362–3376.
- [23] H. Duo, X. Lu, S. Wang, X. Liang, Y. Guo, Preparation and applications of metal-organic framework derived porous carbons as novel adsorbents in sample preparation, *TrAC Trends in Analytical Chemistry* 133 (2020) 116093.
- [24] H. Zhang, X. Hu, T. Li, Y. Zhang, H. Xu, Y. Sun, X. Gu, C. Gu, J. Luo, B. Gao, MIL series of metal organic frameworks (MOFs) as novel adsorbents for heavy metals in water: A review, *Journal of Hazardous Materials* 429 (2022) 128271.
- [25] M.A. Qyyum, J. Haider, K. Qadeer, V. Valentina, A. Khan, M. Yasin, M. Aslam, G. De Guido, L.A. Pellegrini, M. Lee, Biogas to liquefied biomethane: Assessment of 3P’s–Production, processing, and prospects, *Renewable and Sustainable Energy Reviews* 119 (2020) 109561.
- [26] S.U. Nandanwar, D.R. Corbin, M.B. Shiflett, A Review of Porous Adsorbents for the

- Separation of Nitrogen from Natural Gas, *Ind. Eng. Chem. Res.* 59 (2020) 13355–13369.
- [27] Z. Cheng, S. Li, Y. Liu, Y. Zhang, Z. Ling, M. Yang, L. Jiang, Y. Song, Post-combustion CO₂ capture and separation in flue gas based on hydrate technology: A review, *Renewable and Sustainable Energy Reviews* 154 (2022) 111806.
- [28] G. Pandey, T. Poothia, A. Kumar, Hydrate based carbon capture and sequestration (HBCCS): An innovative approach towards decarbonization, *Applied Energy* 326 (2022) 119900.
- [29] G. Chen, G. Liu, Y. Pan, G. Liu, X. Gu, W. Jin, N. Xu, Zeolites and metal–organic frameworks for gas separation: the possibility of translating adsorbents into membranes, *Chem. Soc. Rev.* 52 (2023) 4586–4602.
- [30] D. Shi, X. Yu, W. Fan, V. Wee, D. Zhao, Polycrystalline zeolite and metal-organic framework membranes for molecular separations, *Coordination Chemistry Reviews* 437 (2021) 213794.
- [31] S.S. Hosseini, M. Azadi Tabar, I.F.J. Vankelecom, J.F.M. Denayer, Progress in high performance membrane materials and processes for biogas production, upgrading and conversion, *Separation and Purification Technology* 310 (2023) 123139.
- [32] V.R. Moreira, J.V. Raad, J.X. Lazarini, L.V.S. Santos, M.C.S. Amaral, Recent progress in membrane distillation configurations powered by renewable energy sources and waste heat, *Journal of Water Process Engineering* 53 (2023) 103816.
- [33] P. Gkotsis, E. Peleka, A. Zouboulis, Membrane-Based Technologies for Post-Combustion CO₂ Capture from Flue Gases: Recent Progress in Commonly Employed Membrane Materials, *Membranes* 13 (2023) 898.
- [34] T. Chen, X. Wei, Z. Chen, D. Morin, S.V. Alvarez, Y. Yoon, Y. Huang, Designing energy-efficient separation membranes: Knowledge from nature for a sustainable future, *Advanced Membranes* 2 (2022) 100031.
- [35] M. Khodakarami, H. Zeng, Chapter 16 - Membranes based on biodegradable polymer nanocomposite for gas separation applications, in: K. Deshmukh, M. Pandey (Eds.), *Biodegradable and Biocompatible Polymer Nanocomposites*, Elsevier, 2023: pp. 555–598.
- [36] N.H. Solangi, A. Anjum, F.A. Tanjung, S.A. Mazari, N.M. Mubarak, A review of recent trends and emerging perspectives of ionic liquid membranes for CO₂ separation, *Journal of Environmental Chemical Engineering* 9 (2021) 105860.
- [37] C. Algieri, E. Drioli, Zeolite membranes: Synthesis and applications, *Separation and Purification Technology* 278 (2021) 119295.
- [38] L. Lei, L. Bai, A. Lindbråthen, F. Pan, X. Zhang, X. He, Carbon membranes for CO₂ removal: Status and perspectives from materials to processes, *Chemical Engineering Journal* 401 (2020) 126084.
- [39] N. Sazali, A comprehensive review of carbon molecular sieve membranes for hydrogen production and purification, *Int J Adv Manuf Technol* 107 (2020) 2465–2483.

- [40] H. Xia, H. Jin, Y. Zhang, H. Song, J. Hu, Y. Huang, Y. Li, A long-lasting TIF-4 MOF glass membrane for selective CO₂ separation, *Journal of Membrane Science* 655 (2022) 120611.
- [41] A.R. Kamble, C.M. Patel, Z.V.P. Murthy, A review on the recent advances in mixed matrix membranes for gas separation processes, *Renewable and Sustainable Energy Reviews* 145 (2021) 111062.
- [42] Y. Han, Y. Yang, W.S.W. Ho, Recent progress in the engineering of polymeric membranes for CO₂ capture from flue gas, *Membranes* 10 (2020) 365.
- [43] R. Sidhikku Kandath Valappil, N. Ghasem, M. Al-Marzouqi, Current and future trends in polymer membrane-based gas separation technology: A comprehensive review, *Journal of Industrial and Engineering Chemistry* 98 (2021) 103–129.
- [44] L.M. Robeson, Correlation of separation factor versus permeability for polymeric membranes, *Journal of Membrane Science* 62 (1991) 165–185.
- [45] L.M. Robeson, The upper bound revisited, *Journal of Membrane Science* 320 (2008) 390–400.
- [46] L.M. Robeson, B.D. Freeman, D.R. Paul, B.W. Rowe, An empirical correlation of gas permeability and permselectivity in polymers and its theoretical basis, *Journal of Membrane Science* 341 (2009) 178–185.
- [47] T.-S. Chung, L.Y. Jiang, Y. Li, S. Kulprathipanja, Mixed matrix membranes (MMMs) comprising organic polymers with dispersed inorganic fillers for gas separation, *Progress in Polymer Science* 32 (2007) 483–507.
- [48] X. Yan, S. Anguille, M. Bendahan, P. Moulin, Ionic liquids combined with membrane separation processes: A review, *Separation and Purification Technology* 222 (2019) 230–253.
- [49] I.K. Swati, Q. Sohaib, S. Cao, M. Younas, D. Liu, J. Gui, M. Rezakazemi, Protic/aprotic ionic liquids for effective CO₂ separation using supported ionic liquid membrane, *Chemosphere* 267 (2021) 128894.
- [50] X. Li, S. Ding, J. Zhang, Z. Wei, Optimizing microstructure of polymer composite membranes by tailoring different ionic liquids to accelerate CO₂ transport, *International Journal of Greenhouse Gas Control* 101 (2020) 103136.
- [51] E. Ghasemi Estahbanati, M. Omidkhah, A. Ebadi Amooghin, Interfacial design of ternary mixed matrix membranes containing Pebax 1657/Silver-nanopowder/[BMIM][BF₄] for improved CO₂ separation performance, *ACS Appl. Mater. Interfaces* 9 (2017) 10094–10105.
- [52] J. Yin, C. Zhang, Y. Yu, T. Hao, H. Wang, X. Ding, J. Meng, Tuning the microstructure of crosslinked poly(ionic liquid) membranes and gels via a multicomponent reaction for improved CO₂ capture performance, *Journal of Membrane Science* 593 (2020) 117405.
- [53] F. Moghadam, E. Kamio, H. Matsuyama, High CO₂ separation performance of amino acid ionic liquid-based double network ion gel membranes in low CO₂ concentration gas mixtures under humid conditions, *Journal of Membrane Science* 525 (2017) 290–297.
- [54] C.F. Martins, L.A. Neves, R. Chagas, L.M. Ferreira, I.M. Coelho, J.G. Crespo, Removing

- CO₂ from Xenon anaesthesia circuits using an amino-acid ionic liquid solution in a membrane contactor, *Separation and Purification Technology* 275 (2021) 119190.
- [55] J.G. Wijmans, R.W. Baker, The solution-diffusion model: a review, *Journal of Membrane Science* 107 (1995) 1–21.
- [56] S. Janakiram, J.L. Martín Espejo, X. Yu, L. Ansaloni, L. Deng, Facilitated transport membranes containing graphene oxide-based nanoplatelets for CO₂ separation: Effect of 2D filler properties, *Journal of Membrane Science* 616 (2020) 118626.
- [57] T. Araújo, G. Bernardo, A. Mendes, Cellulose-based carbon molecular sieve membranes for gas separation: a review, *Molecules* 25 (2020) 3532.
- [58] Y. Yuan, Z. Qiao, J. Xu, J. Wang, S. Zhao, X. Cao, Z. Wang, M.D. Guiver, Mixed matrix membranes for CO₂ separations by incorporating microporous polymer framework fillers with amine-rich nanochannels, *Journal of Membrane Science* 620 (2021) 118923.
- [59] C. Ma, M. Wang, Z. Wang, M. Gao, J. Wang, Recent progress on thin film composite membranes for CO₂ separation, *Journal of CO₂ Utilization* 42 (2020) 101296.
- [60] E.V. Perez, C. Karunaweera, I.H. Musselman, K.J. Balkus, J.P. Ferraris, Origins and evolution of inorganic-based and MOF-based mixed-matrix membranes for gas separations, *Processes* 4 (2016) 32.
- [61] M. Liu, A. Seeger, R. Guo, Cross-linked polymer membranes for energy-efficient gas separation: innovations and perspectives, *Macromolecules* 56 (2023) 7230–7246.
- [62] Z. Chen, M. Sarakha, J. Christmann, Consequences of sequential photooxidation of polycarbonate: Relating microscopic modifications to the change of oxygen permeability, *Journal of Applied Polymer Science* 140 (2023) 54397.
- [63] S. Rafiq, L. Deng, M.-B. Hägg, Role of facilitated transport membranes and composite membranes for efficient CO₂ capture – a review, *ChemBioEng Reviews* 3 (2016) 68–85.
- [64] S. Nithin Mithra, S.S. Ahankari, Nanocellulose-based membranes for CO₂ separation from biogas through the facilitated transport mechanism: a review, *Materials Today Sustainability* 19 (2022) 100191.
- [65] H. Ohno, K. Fukumoto, Amino acid ionic liquids, *Acc. Chem. Res.* 40 (2007) 1122–1129.
- [66] A.R. Shaikh, M. Ashraf, T. AlMayef, M. Chawla, A. Poater, L. Cavallo, Amino acid ionic liquids as potential candidates for CO₂ capture: Combined density functional theory and molecular dynamics simulations, *Chemical Physics Letters* 745 (2020) 137239.
- [67] J. Guzmán, C. Ortega-Guevara, R.G. de León, R. Martínez-Palou, Absorption of CO₂ with amino acid-based ionic liquids and corresponding amino acid precursors, *Chemical Engineering & Technology* 40 (2017) 2339–2345.
- [68] Z. Chen, P. Zhang, H. Wu, S. Sun, X. You, B. Yuan, J. Hou, C. Duan, Z. Jiang, Incorporating amino acids functionalized graphene oxide nanosheets into Pebax membranes for CO₂ separation, *Separation and Purification Technology* 288 (2022) 120682.

- [69] M. Mubashir, L.F. Dumée, Y.Y. Fong, N. Jusoh, J. Lukose, W.S. Chai, P.L. Show, Cellulose acetate-based membranes by interfacial engineering and integration of ZIF-62 glass nanoparticles for CO₂ separation, *Journal of Hazardous Materials* 415 (2021) 125639.
- [70] X. Wang, C. Chi, K. Zhang, Y. Qian, K.M. Gupta, Z. Kang, J. Jiang, D. Zhao, Reversed thermo-switchable molecular sieving membranes composed of two-dimensional metal-organic nanosheets for gas separation, *Nat Commun* 8 (2017) 14460.
- [71] M. Hou, L. Li, Z. He, R. Xu, Y. Lu, J. Zhang, Z. Pan, C. Song, T. Wang, High-performance carbon molecular sieving membrane derived from a novel hydroxyl-containing polyetherimide precursor for CO₂ separations, *Journal of Membrane Science* 656 (2022) 120639.
- [72] X. Cao, Z. Wang, Z. Qiao, S. Zhao, J. Wang, Penetrated COF channels: amino environment and suitable size for CO₂ preferential adsorption and transport in mixed matrix membranes, *ACS Appl. Mater. Interfaces* 11 (2019) 5306–5315.
- [73] Z. Qiao, M. Sheng, J. Wang, S. Zhao, Z. Wang, Metal-induced polymer framework membrane with high performance for CO₂ separation, *AIChE Journal* 65 (2019) 239–249.
- [74] Y. Yuan, Z. Qiao, J. Xu, J. Wang, S. Zhao, X. Cao, Z. Wang, M.D. Guiver, Mixed matrix membranes for CO₂ separations by incorporating microporous polymer framework fillers with amine-rich nanochannels, *Journal of Membrane Science* 620 (2021) 118923.
- [75] T. Corrado, R. Guo, Macromolecular design strategies toward tailoring free volume in glassy polymers for high performance gas separation membranes, *Molecular Systems Design & Engineering* 5 (2020) 22–48.
- [76] Y. Yampolskii, Polymeric Gas Separation Membranes, *Macromolecules* 45 (2012) 3298–3311.
- [77] M. Yoshino, K. Ito, H. Kita, K.-I. Okamoto, Effects of hard-segment polymers on CO₂/N₂ gas-separation properties of poly(ethylene oxide)-segmented copolymers, *Journal of Polymer Science Part B: Polymer Physics* 38 (2000) 1707–1715.
- [78] H. Riasat Harami, A. Dashti, P. Ghahramani Pirsalami, S.K. Bhatia, A.F. Ismail, P.S. Goh, Molecular simulation and computational modeling of gas separation through polycarbonate/p-nitroaniline/zeolite 4A mixed matrix membranes, *Ind. Eng. Chem. Res.* 59 (2020) 16772–16785.
- [79] Y.-C. Huang, L.-F. Chen, Y.-H. Huang, C.-C. Hu, C.-H. Wu, R.-J. Jeng, Recyclable nanocomposites for carbon dioxide fixation and membrane separation using waste polycarbonate, *Chemical Engineering Journal* 452 (2023) 139262.
- [80] R. Kumar, Kamakshi, M. Kumar, K. Awasthi, UV-irradiation assisted functionalization and binding of Pd nanoparticles in polycarbonate membranes for hydrogen separation, *Environ Sci Pollut Res* 28 (2021) 46404–46413.
- [81] V. Vatanpour, M.E. Pasaoglu, H. Barzegar, O.O. Teber, R. Kaya, M. Bastug, A. Khataee, I. Koyuncu, Cellulose acetate in fabrication of polymeric membranes: A review, *Chemosphere* 295 (2022) 133914.

- [82] M. Mubashir, L.F. Dumée, Y.Y. Fong, N. Jusoh, J. Lukose, W.S. Chai, P.L. Show, Cellulose acetate-based membranes by interfacial engineering and integration of ZIF-62 glass nanoparticles for CO₂ separation, *Journal of Hazardous Materials* 415 (2021) 125639.
- [83] M. Mubashir, Y.F. Yeong, K.K. Lau, T.L. Chew, Effect of spinning conditions on the fabrication of cellulose acetate hollow fiber membrane for CO₂ separation from N₂ and CH₄, *Polymer Testing* 73 (2019) 1–11.
- [84] M. Mubashir, Y. Yin fong, C.T. Leng, L.K. Keong, N. Jusoh, Study on the effect of process parameters on CO₂/CH₄ binary gas separation performance over NH₂-MIL-53(Al)/cellulose acetate hollow fiber mixed matrix membrane, *Polymer Testing* 81 (2020) 106223.
- [85] Q. Wang, F. Huang, C.J. Cornelius, Y. Fan, Carbon molecular sieve membranes derived from crosslinkable polyimides for CO₂/CH₄ and C₂H₄/C₂H₆ separations, *Journal of Membrane Science* 621 (2021) 118785.
- [86] M.Z. Ahmad, P. Izak, V. Fila, CO₂ separation of fluorinated 6FDA-based polyimides, performance-improved ZIF-incorporated mixed matrix membranes and gas permeability model evaluations, *Journal of Environmental Chemical Engineering* 10 (2022) 108611.
- [87] T. Wang, L. Jiang, Y. Zhang, L. Wu, H. Chen, C. Li, Fabrication of polyimide mixed matrix membranes with asymmetric confined mass transfer channels for improved CO₂ separation, *Journal of Membrane Science* 637 (2021) 119653.
- [88] H.A. Mannan, D.F. Mohshim, H. Mukhtar, T. Murugesan, Z. Man, M.A. Bustam, Synthesis, characterization, and CO₂ separation performance of polyether sulfone/[EMIM][Tf₂N] ionic liquid-polymeric membranes (ILPMs), *Journal of Industrial and Engineering Chemistry* 54 (2017) 98–106.
- [89] B. Tüzün-Antepli, L. Yılmaz, H. Kalıpçılar, Investigating the state of skin layer of asymmetric polyethersulfone (PES) - zeolitic imidazole framework-8 (ZIF-8) mixed matrix gas separation membranes and its effect on gas separation performance, *ChemistrySelect* 7 (2022) e202200014.
- [90] A. Mohamed, S. Yousef, A. Tonkonogovas, V. Makarevicius, A. Stankevičius, High performance of PES-GNs MMMs for gas separation and selectivity, *Arabian Journal of Chemistry* 15 (2022) 103565.
- [91] K. Asif, S.S.M. Lock, S.A.A. Taqvi, N. Jusoh, C.L. Yiin, B.L.F. Chin, A molecular simulation study on amine-functionalized silica/polysulfone mixed matrix membrane for mixed gas separation, *Chemosphere* 311 (2023) 136936.
- [92] B. Sasikumar, G. Arthanareeswaran, Concurrent enhancement of CO₂-philic pathway and interfacial compatibilization in ZIF-67 based polysulfone membranes through [Bmim][Tf₂N] for CO₂ separation, *Applied Surface Science* 606 (2022) 154900.
- [93] M. Farrokhara, F. Dorosti, New high permeable polysulfone/ionic liquid membrane for gas separation, *Chinese Journal of Chemical Engineering* 28 (2020) 2301–2311.
- [94] A. Pulyalina, V. Rostovtseva, G. Polotskaya, L. Vinogradova, Z. Zoolshoev, M. Simonova, A.

- Hairullin, A. Toikka, Z. Pientka, Hybrid macromolecular stars incorporated poly(phenylene oxide) membranes: Organization, physical, and gas separation properties, *Polymer* 172 (2019) 355–364.
- [95] P.R. Sruthi, S. Anas, An overview of synthetic modification of nitrile group in polymers and applications, *Journal of Polymer Science* 58 (2020) 1039–1061.
- [96] M. Hussain, A. König, Mixed-matrix membrane for gas separation: polydimethylsiloxane filled with zeolite, *Chemical Engineering & Technology* 35 (2012) 561–569.
- [97] M. Nour, K. Berean, M.J. Griffin, G.I. Matthews, M. Bhaskaran, S. Sriram, K. Kalantar-zadeh, Nanocomposite carbon-PDMS membranes for gas separation, *Sensors and Actuators B: Chemical* 161 (2012) 982–988.
- [98] G. Defontaine, A. Barichard, S. Letaief, C. Feng, T. Matsuura, C. Detellier, Nanoporous polymer–Clay hybrid membranes for gas separation, *Journal of Colloid and Interface Science* 343 (2010) 622–627.
- [99] S. Bandehali, A. Moghadassi, F. Parvizian, S.M. Hosseini, T. Matsuura, E. Joudaki, Advances in high carbon dioxide separation performance of poly (ethylene oxide)-based membranes, *Journal of Energy Chemistry* 46 (2020) 30–52.
- [100] D.J. Harrigan, J.A. Lawrence, H.W. Reid, J.B. Rivers, J.T. O’Brien, S.A. Sharber, B.J. Sundell, Tunable sour gas separations: Simultaneous H₂S and CO₂ removal from natural gas via crosslinked telechelic poly(ethylene glycol) membranes, *Journal of Membrane Science* 602 (2020) 117947.
- [101] T. Hong, Y. Li, S. Wang, Y. Li, X. Jing, Polyurethane-based gas separation membranes: a review and perspectives, *Separation and Purification Technology* 301 (2022) 122067.
- [102] M.S.A. Wahab, A.R. Sunarti, Development of PEBAX based membrane for gas separation: a review, *International Journal of Membrane Science and Technology* 2 (2015) 78–84.
- [103] M. Farnam, H. bin Mukhtar, A. bin Mohd Shariff, A review on glassy and rubbery polymeric membranes for natural gas purification, *ChemBioEng Reviews* 8 (2021) 90–109.
- [104] S. Kim, T.W. Pechar, E. Marand, Poly(imide siloxane) and carbon nanotube mixed matrix membranes for gas separation, *Desalination* 192 (2006) 330–339.
- [105] M. Sadeghi, M.A. Semsarzadeh, H. Moadel, Enhancement of the gas separation properties of polybenzimidazole (PBI) membrane by incorporation of silica nano particles, *Journal of Membrane Science* 331 (2009) 21–30.
- [106] Y. Hirayama, Y. Kase, N. Tanihara, Y. Sumiyama, Y. Kusuki, K. Haraya, Permeation properties to CO₂ and N₂ of poly(ethylene oxide)-containing and crosslinked polymer films, *Journal of Membrane Science* 160 (1999) 87–99.
- [107] G.-L. Zhuang, H.-H. Tseng, M.-Y. Wey, Preparation of PPO-silica mixed matrix membranes by in-situ sol–gel method for H₂/CO₂ separation, *International Journal of Hydrogen Energy* 39 (2014) 17178–17190.

- [108] B. Molki, W.M. Aframehr, R. Bagheri, J. Salimi, Mixed matrix membranes of polyurethane with nickel oxide nanoparticles for CO₂ gas separation, *Journal of Membrane Science* 549 (2018) 588–601.
- [109] M. Klepić, K. Setničková, M. Lanč, M. Žák, P. Izák, M. Dendisová, A. Fuoco, J.C. Jansen, K. Friess, Permeation and sorption properties of CO₂-selective blend membranes based on polyvinyl alcohol (PVA) and 1-ethyl-3-methylimidazolium dicyanamide ([EMIM][DCA]) ionic liquid for effective CO₂/H₂ separation, *Journal of Membrane Science* 597 (2020) 117623.
- [110] J. Li, S. Wang, K. Nagai, T. Nakagawa, A.W.-H. Mau, Effect of polyethyleneglycol (PEG) on gas permeabilities and permselectivities in its cellulose acetate (CA) blend membranes, *Journal of Membrane Science* 138 (1998) 143–152.
- [111] T.-H. Bae, J.S. Lee, W. Qiu, W.J. Koros, C.W. Jones, S. Nair, A high-performance gas-separation membrane containing sub micrometer-sized metal–organic framework crystals, *Angewandte Chemie* 122 (2010) 10059–10062.
- [112] E.G. Estahbanati, M. Omidkhah, A.E. Amooghin, Interfacial design of ternary mixed matrix membranes containing Pebax 1657/silver-nanopowder/[BMIM][BF₄] for improved CO₂ separation performance, *ACS Appl. Mater. Interfaces* 9 (2017) 10094–10105.
- [113] S. Kim, Y.M. Lee, High performance polymer membranes for CO₂ separation, *Current Opinion in Chemical Engineering* 2 (2013) 238–244.
- [114] M. Zabihzadeh Khajavi, A. Ebrahimi, M. Yousefi, S. Ahmadi, M. Farhoodi, A. Mirza Alizadeh, M. Taslikh, Strategies for producing improved oxygen barrier materials appropriate for the food packaging sector, *Food Eng Rev* 12 (2020) 346–363.
- [115] A. Guinault, C. Sollogoub, S. Domenek, A. Grandmontagne, V. Ducruet, Influence of crystallinity on gas barrier and mechanical properties of pla food packaging films, *Int J Mater Form* 3 (2010) 603–606.
- [116] M.M. Zagho, M.K. Hassan, M. Khraisheh, M.A.A. Al-Maadeed, S. Nazarenko, A review on recent advances in CO₂ separation using zeolite and zeolite-like materials as adsorbents and fillers in mixed matrix membranes (MMMs), *Chemical Engineering Journal Advances* 6 (2021) 100091.
- [117] X. Tan, S. Robijns, R. Thür, Q. Ke, N. De Witte, A. Lamaire, Y. Li, I. Aslam, D. Van Havere, T. Donckels, T. Van Assche, V. Van Speybroeck, M. Dusselier, I. Vankelecom, Truly combining the advantages of polymeric and zeolite membranes for gas separations, *Science* 378 (2022) 1189–1194.
- [118] L.D. Anbealagan, T.Y.S. Ng, T.L. Chew, Y.F. Yeong, S.C. Low, Y.T. Ong, C.-D. Ho, Z.A. Jawad, Modified Zeolite/Polysulfone mixed matrix membrane for enhanced CO₂/CH₄ separation, *membranes* 11 (2021) 630.
- [119] R. Lin, L. Ge, H. Diao, V. Rudolph, Z. Zhu, Ionic Liquids as the MOFs/polymer interfacial binder for efficient membrane separation, *ACS Appl. Mater. Interfaces* 8 (2016) 32041–32049.
- [120] Q. Luo, B. An, M. Ji, J. Zhang, Hybridization of metal–organic frameworks and task-specific

- ionic liquids: fundamentals and challenges, *Materials Chemistry Frontiers* 2 (2018) 219–234.
- [121] J. Ma, Y. Ying, X. Guo, H. Huang, D. Liu, C. Zhong, Fabrication of mixed-matrix membrane containing metal–organic framework composite with task-specific ionic liquid for efficient CO₂ separation, *J. Mater. Chem. A* 4 (2016) 7281–7288.
- [122] M. Zeeshan, V. Nozari, M.B. Yagci, T. Isik, U. Unal, V. Ortalan, S. Keskin, A. Uzun, Core–Shell Type Ionic Liquid/Metal Organic Framework Composite: An Exceptionally High CO₂/CH₄ Selectivity, *J. Am. Chem. Soc.* 140 (2018) 10113–10116.
- [123] B.-J. Yao, L.-G. Ding, F. Li, J.-T. Li, Q.-J. Fu, Y. Ban, A. Guo, Y.-B. Dong, Chemically cross-linked MOF membrane generated from imidazolium-based ionic liquid-decorated UiO-66 type NMOF and its application toward CO₂ separation and conversion, *ACS Appl. Mater. Interfaces* 9 (2017) 38919–38930.
- [124] P. Moradihamedani, N.A. Ibrahim, D. Ramimoghadam, W.M.Z.W. Yunus, N.A. Yusof, Polysulfone/zinc oxide nanoparticle mixed matrix membranes for CO₂/CH₄ separation, *Journal of Applied Polymer Science* 16 (2014) 131t.
- [125] B. Molki, W.M. Aframehr, R. Bagheri, J. Salimi, Mixed matrix membranes of polyurethane with nickel oxide nanoparticles for CO₂ gas separation, *Journal of Membrane Science* 549 (2018) 588–601.
- [126] A.A. Abd, S.Z. Naji, A.S. Hashim, M.R. Othman, Carbon dioxide removal through physical adsorption using carbonaceous and non-carbonaceous adsorbents: a review, *Journal of Environmental Chemical Engineering* 8 (2020) 104142.
- [127] K. Friess, M. Lanč, K. Pilnáček, V. Fíla, O. Vopička, Z. Sedláková, M.G. Cowan, W.M. McDanel, R.D. Noble, D.L. Gin, P. Izak, CO₂/CH₄ separation performance of ionic-liquid-based epoxy-amine ion gel membranes under mixed feed conditions relevant to biogas processing, *Journal of Membrane Science* 528 (2017) 64–71.
- [128] W.M. McDanel, M.G. Cowan, N.O. Chisholm, D.L. Gin, R.D. Noble, Fixed-site-carrier facilitated transport of carbon dioxide through ionic-liquid-based epoxy-amine ion gel membranes, *Journal of Membrane Science* 492 (2015) 303–311.
- [129] H. Rabiee, A. Ghadimi, T. Mohammadi, Gas transport properties of reverse-selective poly(ether-b-amide6)/[Emim][BF₄] gel membranes for CO₂/light gases separation, *Journal of Membrane Science* 476 (2015) 286–302.
- [130] H. Wang, M. Wang, X. Liang, J. Yuan, H. Yang, S. Wang, Y. Ren, H. Wu, F. Pan, Z. Jiang, Organic molecular sieve membranes for chemical separations, *Chem. Soc. Rev.* 50 (2021) 5468–5516.
- [131] R. Wijiyanti, I.S. Caralin, A.R. Widyanto, T. Gunawan, Z.A. Karim, A.F. Ismail, M. Nomura, N. Widiastuti, Evaluation of different carbon-modified zeolite derivatives preparation methods as a filler in mixed matrix membrane on their gas separation performance, *Microporous and Mesoporous Materials* 359 (2023) 112650.
- [132] R. Ebadi, H. Maghsoudi, A.A. Babaluo, Fabrication and characterization of Pebax-1657 mixed

matrix membrane loaded with Si-CHA zeolite for CO₂ separation from CH₄, *Journal of Natural Gas Science and Engineering* 90 (2021) 103947.

- [133] K. Zarshenas, A. Raisi, A. Aroujalian, Mixed matrix membrane of nano-zeolite NaX/poly(ether-block-amide) for gas separation applications, *Journal of Membrane Science* 510 (2016) 270–283.
- [134] Y. He, Z. Wang, H. Wang, Z. Wang, G. Zeng, P. Xu, D. Huang, M. Chen, B. Song, H. Qin, Y. Zhao, Metal-organic framework-derived nanomaterials in environment related fields: Fundamentals, properties and applications, *Coordination Chemistry Reviews* 429 (2021) 213618.
- [135] S. Ahmadipouya, F. Ahmadijokani, H. Molavi, M. Rezakazemi, M. Arjmand, CO₂/CH₄ separation by mixed-matrix membranes holding functionalized NH₂-MIL-101(Al) nanoparticles: Effect of amino-silane functionalization, *Chemical Engineering Research and Design* 176 (2021) 49–59.
- [136] J. Gao, H. Mao, H. Jin, C. Chen, A. Feldhoff, Y. Li, Functionalized ZIF-7/Pebax[®] 2533 mixed matrix membranes for CO₂/N₂ separation, *Microporous and Mesoporous Materials* 297 (2020) 110030.
- [137] J. Ahmad, M.B. Hågg, Polyvinyl acetate/titanium dioxide nanocomposite membranes for gas separation, *Journal of Membrane Science* 445 (2013) 200–210.
- [138] M. Ariazadeh, Z. Farashi, N. Azizi, M. Khajouei, Influence of functionalized SiO₂ nanoparticles on the morphology and CO₂/CH₄ separation efficiency of Pebax-based mixed-matrix membranes, *Korean J. Chem. Eng.* 37 (2020) 295–306.
- [139] G. Maduraiveeran, W. Jin, Carbon nanomaterials: Synthesis, properties and applications in electrochemical sensors and energy conversion systems, *Materials Science and Engineering: B* 272 (2021) 115341.
- [140] F. Shi, Q. Tian, J. Wang, Q. Wang, F. Shi, Y. Li, S.P. Nunes, Carbon quantum dot-enabled tuning of the microphase structures of poly(ether-b-amide) membrane for CO₂ separation, *Ind. Eng. Chem. Res.* 59 (2020) 14960–14969.
- [141] Z. Rajabi, A.R. Moghadassi, S.M. Hosseini, M. Mohammadi, Preparation and characterization of polyvinylchloride based mixed matrix membrane filled with multi walled carbon nano tubes for carbon dioxide separation, *Journal of Industrial and Engineering Chemistry* 19 (2013) 347–352.
- [142] K. Sainath, A. Modi, J. Bellare, CO₂/CH₄ mixed gas separation using graphene oxide nanosheets embedded hollow fiber membranes: Evaluating effect of filler concentration on performance, *Chemical Engineering Journal Advances* 5 (2021) 100074.
- [143] M. Anson, J. Marchese, E. Garis, N. Ochoa, C. Pagliero, ABS copolymer-activated carbon mixed matrix membranes for CO₂/CH₄ separation, *Journal of Membrane Science* 243 (2004) 19–28.
- [144] J. Salgado, J.J. Parajó, M. Villanueva, J.R. Rodríguez, O. Cabeza, L.M. Varela, Liquid range

- of ionic liquid – metal salt mixtures for electrochemical applications, *The Journal of Chemical Thermodynamics* 134 (2019) 164–174.
- [145] W. Fam, J. Mansouri, H. Li, J. Hou, V. Chen, Gelled graphene oxide–ionic liquid composite membranes with enriched ionic liquid surfaces for improved CO₂ separation, *ACS Appl. Mater. Interfaces* 10 (2018) 7389–7400.
- [146] H.T.V. Nguyen, T.H.A. Ngo, K.D. Do, M.N. Nguyen, N.T.T. Dang, T.T.H. Nguyen, V. Vien, T.A. Vu, Preparation and characterization of a hydrophilic polysulfone membrane using graphene oxide, *Journal of Chemistry* 2019 (2019) 3164373.
- [147] A.R. Nabais, L.A. Neves, L.C. Tomé, Mixed-Matrix Ion Gel Membranes for Gas Separation, *ACS Appl. Polym. Mater.* 4 (2022) 3098–3119.
- [148] Gas transport properties of reverse-selective poly(ether-b-amide6)/[Emim][BF₄] gel membranes for CO₂/light gases separation, *Journal of Membrane Science* 476 (2015) 286–302.
- [149] M.S. Mittenenthal, B.S. Flowers, J.E. Bara, J.W. Whitley, S.K. Spear, J.D. Roveda, D.A. Wallace, M.S. Shannon, R. Holler, R. Martens, D.T. Daly, Ionic Polyimides: Hybrid polymer architectures and composites with ionic liquids for advanced gas separation membranes, *Ind. Eng. Chem. Res.* 56 (2017) 5055–5069.
- [150] M. Althuluth, J.P. Overbeek, H.J. van Wees, L.F. Zubeir, W.G. Haije, A. Berrouk, C.J. Peters, M.C. Kroon, Natural gas purification using supported ionic liquid membrane, *Journal of Membrane Science* 484 (2015) 80–86.
- [151] E. Ghasemi Estahbanati, M. Omidkhan, A. Ebadi Amooghin, Preparation and characterization of novel ionic liquid/Pebax membranes for efficient CO₂/light gases separation, *Journal of Industrial and Engineering Chemistry* 51 (2017) 77–89.
- [152] K.E. O’Harra, I. Kammakam, E.M. Devriese, D.M. Noll, J.E. Bara, E.M. Jackson, Synthesis and performance of 6FDA-based polyimide-ionenes and composites with ionic liquids as gas separation membranes, *Membranes* 9 (2019) 79.
- [153] S. Kasahara, E. Kamio, A.R. Shaikh, T. Matsuki, H. Matsuyama, Effect of the amino-group densities of functionalized ionic liquids on the facilitated transport properties for CO₂ separation, *Journal of Membrane Science* 503 (2016) 148–157.
- [154] Z. Dai, R.D. Noble, D.L. Gin, X. Zhang, L. Deng, Combination of ionic liquids with membrane technology: A new approach for CO₂ separation, *Journal of Membrane Science* 497 (2016) 1–20.
- [155] J. Deng, L. Bai, S. Zeng, X. Zhang, Y. Nie, L. Deng, S. Zhang, Ether-functionalized ionic liquid based composite membranes for carbon dioxide separation, *RSC Adv.* 6 (2016) 45184–45192.
- [156] N.N.R. Ahmad, C.P. Leo, A.W. Mohammad, A.L. Ahmad, Modification of gas selective SAPO zeolites using imidazolium ionic liquid to develop polysulfone mixed matrix membrane for CO₂ gas separation, *Microporous and Mesoporous Materials* 244 (2017) 21–30.
- [157] G. Huang, A.P. Isfahani, A. Muchtar, K. Sakurai, B.B. Shrestha, D. Qin, D. Yamaguchi, E.

- Sivaniah, B. Ghalei, Pebax/ionic liquid modified graphene oxide mixed matrix membranes for enhanced CO₂ capture, *Journal of Membrane Science* 565 (2018) 370–379.
- [158] Z.V. Singh, M.G. Cowan, W.M. McDanel, Y. Luo, R. Zhou, D.L. Gin, R.D. Noble, Determination and optimization of factors affecting CO₂/CH₄ separation performance in poly(ionic liquid)-ionic liquid-zeolite mixed-matrix membranes, *Journal of Membrane Science* 509 (2016) 149–155.
- [159] S.G. Charati, S.A. Stern, Diffusion of gases in silicone polymers: molecular dynamics simulations, *Macromolecules* 31 (1998) 5529–5535.
- [160] T.C. Merkel, V.I. Bondar, K. Nagai, B.D. Freeman, I. Pinnau, Gas sorption, diffusion, and permeation in poly(dimethylsiloxane), *Journal of Polymer Science Part B: Polymer Physics* 38 (2000) 415–434.
- [161] S.C. George, S. Thomas, Transport phenomena through polymeric systems, *Progress in Polymer Science* 26 (2001) 985–1017.
- [162] R.S. Prabhakar, B.D. Freeman, I. Roman, Gas and vapor sorption and permeation in poly(2,2,4-trifluoro-5-trifluoromethoxy-1,3-dioxole-co-tetrafluoroethylene), *Macromolecules* 37 (2004) 7688–7697.
- [163] S. Kanehashi, A. Kusakabe, S. Sato, K. Nagai, Analysis of permeability; solubility and diffusivity of carbon dioxide; oxygen; and nitrogen in crystalline and liquid crystalline polymers, *Journal of Membrane Science* 365 (2010) 40–51.
- [164] X. Wang, L. Wu, N. Li, Y. Fan, Sealing Tröger base/ZIF-8 mixed matrix membranes defects for improved gas separation performance, *Journal of Membrane Science* 636 (2021) 119582.
- [165] J. Hart, M.J. Battrum, W.J. Thomas, Axial pressure gradients during the pressurization and depressurization steps of a PSA gas separation cycle, *Gas Separation & Purification* 4 (1990) 97–102.
- [166] S. Yousef, J. Šereika, A. Tonkonogovas, T. Hashem, A. Mohamed, CO₂/CH₄, CO₂/N₂ and CO₂/H₂ selectivity performance of PES membranes under high pressure and temperature for biogas upgrading systems, *Environmental Technology & Innovation* 21 (2021) 101339.
- [167] Z. Qin, X. Feng, D. Yin, B. Xin, Z. Jin, Y. Deng, L. Yang, L. Yao, W. Jiang, C. Liu, Z. Dai, Impact of humidity on the CO₂/N₂ separation performance of Pebax-MOF mixed matrix membranes, *Ind. Eng. Chem. Res.* 62 (2023) 14034–14046.
- [168] J. Deng, Z. Dai, J. Hou, L. Deng, Morphologically Tunable MOF Nanosheets in Mixed Matrix Membranes for CO₂ Separation, *Chem. Mater.* 32 (2020) 4174–4184.
- [169] M. Barooah, B. Mandal, B. Su, Enhanced CO₂ separation performance of mixed matrix membrane by incorporating amine-functionalized silica filler, *Journal of Applied Polymer Science* 138 (2021) 51438.
- [170] S.-C. Lu, A.L. Khan, I.F.J. Vankelecom, Polysulfone-ionic liquid based membranes for CO₂/N₂ separation with tunable porous surface features, *Journal of Membrane Science* 518 (2016) 10–

20.

- [171] S. Kheirieh, M. Asghari, M. Afsari, Application and modification of polysulfone membranes, *Reviews in Chemical Engineering* 34 (2018) 657–693.
- [172] M. Farrokhara, F. Dorosti, New high permeable polysulfone/ionic liquid membrane for gas separation, *Chinese Journal of Chemical Engineering* 28 (2020) 2301–2311.
- [173] O.S. Serbanescu, S.I. Voicu, V.K. Thakur, Polysulfone functionalized membranes: Properties and challenges, *Materials Today Chemistry* 17 (2020) 100302.
- [174] S.C. Mamah, P.S. Goh, A.F. Ismail, N.D. Suzaimi, L.T. Yogarathinam, Y.O. Raji, T.H. El-badawy, Recent development in modification of polysulfone membrane for water treatment application, *Journal of Water Process Engineering* 40 (2021) 101835.
- [175] H. Fan, A. Gao, G. Zhang, S. Zhao, J. Cui, Y. Yan, A facile strategy towards developing amphiphobic polysulfone membrane with double re-entrant structure for membrane distillation, *Journal of Membrane Science* 602 (2020) 117933.
- [176] T.D. Kusworo, N. Ariyanti, D.P. Utomo, Effect of nano-TiO₂ loading in polysulfone membranes on the removal of pollutant following natural-rubber wastewater treatment, *Journal of Water Process Engineering* 35 (2020) 101190.
- [177] K. Asif, S.S.M. Lock, S.A.A. Taqvi, N. Jusoh, C.L. Yiin, B.L.F. Chin, A.C.M. Loy, A molecular simulation study of silica/polysulfone mixed matrix membrane for mixed gas separation, *polymers* 13 (2021) 2199.
- [178] B. Yu, Y. Fan, S. Mateti, D. Kim, C. Zhao, S. Lu, X. Liu, Q. Rong, T. Tao, K.K. Tanwar, X. Tan, S.C. Smith, Y.I. Chen, An ultra-long-life flexible lithium–sulfur battery with lithium cloth anode and polysulfone-functionalized separator, *ACS Nano* 15 (2021) 1358–1369.
- [179] S. Benkhaya, H. Lgaz, S. Chraibi, A.A. Alrashdi, M. Rafik, H.-S. Lee, A. El Harfi, Polysulfone/Polyetherimide Ultrafiltration composite membranes constructed on a three-component Nylon-fiberglass-Nylon support for azo dyes removal: Experimental and molecular dynamics simulations, *Colloids and Surfaces A: Physicochemical and Engineering Aspects* 625 (2021) 126941.
- [180] A. Korycki, C. Garnier, A. Abadie, V. Nassiet, C.T. Sultan, F. Chabert, Poly(etheretherketone)/Poly(ethersulfone) Blends with Phenolphthalein: Miscibility, Thermomechanical Properties, Crystallization and Morphology, *Polymers* 13 (2021) 1466.
- [181] A. Heidari, E. Abdollahi, T. Mohammadi, A.A. Asadi, Improving permeability, hydrophilicity and antifouling characteristic of PES hollow fiber UF membrane using carboxylic PES: A promising substrate to fabricate NF layer, *Separation and Purification Technology* 270 (2021) 118811.
- [182] N.A. Mohamad Nor, M.A. Mohamed, J. Jaafar, Modified sulfonated polyphenylsulfone proton exchange membrane with enhanced fuel cell performance: a review, *Journal of Industrial and Engineering Chemistry* 116 (2022) 32–59.

- [183] M.T. Tsehaye, S. Velizarov, B. Van der Bruggen, Stability of polyethersulfone membranes to oxidative agents: A review, *Polymer Degradation and Stability* 157 (2018) 15–33.
- [184] R. Wang, X. Zhao, Y. Lan, L. Liu, C. Gao, In situ metal-polyphenol interfacial assembly tailored superwetting PES/SPES/MPN membranes for oil-in-water emulsion separation, *Journal of Membrane Science* 615 (2020) 118566.
- [185] A.A.R. Abdel-Aty, Y.S.A. Aziz, R.M.G. Ahmed, I.M.A. ElSherbiny, S. Panglisch, M. Ulbricht, A.S.G. Khalil, High performance isotropic polyethersulfone membranes for heavy oil-in-water emulsion separation, *Separation and Purification Technology* 253 (2020) 117467.
- [186] X. Song, H. Ji, W. Zhao, S. Sun, C. Zhao, Hemocompatibility enhancement of polyethersulfone membranes: Strategies and challenges, *Advanced Membranes* 1 (2021) 100013.
- [187] T.H. Novita, W.W. Lestari, J.H. Pratama, T. Gunawan, N. Widiastuti, D.S. Handayani, Novel mixed matrix membranes (MMMs) based on metal–organic framework (MOF) [Mg₃(BTC)₂]/poly-ether sulfone (PES): preparation and application for CO₂ gas separation, *J Polym Res* 28 (2021) 434.
- [188] S. Yousef, S. Tuckute, A. Tonkonogovas, A. Stankevičius, A. Mohamed, Ultra-permeable CNTs/PES membranes with a very low CNTs content and high H₂/N₂ and CH₄/N₂ selectivity for clean energy extraction applications, *Journal of Materials Research and Technology* 15 (2021) 5114–5127.
- [189] S. Yousef, J. Šereika, A. Tonkonogovas, T. Hashem, A. Mohamed, CO₂/CH₄, CO₂/N₂ and CO₂/H₂ selectivity performance of PES membranes under high pressure and temperature for biogas upgrading systems, *Environmental Technology & Innovation* 21 (2021) 101339.

Chapter 2
**Synthesis and characterization of ionic
liquids**

Prior research has demonstrated that the CO₂ absorption capacity of ILs is influenced by both anion and cation nature, with anions exerting a more significant impact [1–3]. Furthermore, it has been reported that imidazolium-based and alkanolamine-based ILs exhibit excellent thermal stability and CO₂ absorption capacity [4–6]. To obtain imidazolium-based ILs with superior thermal stability and to study the impact of imidazolium-based ILs featuring different cations on the gas permeation of composite membranes, [Meim]⁺ and [Vim]⁺ cations were chosen. [TFSO₃]⁻ and [Tf₂N]⁻ as anions were adopted due to the strong affinity of CO₂ with fluorine atom. Concerning alkanolamine-based ILs ligands, the strategic choice was made to exploit the reaction involving the amino groups of 2,2'-(ethylenedioxy)bis(ethylamine) (DOBA) and 2-hydroxyethylenediamine (HDA) with CO₂.

In this Chapter, the synthesis of six ILs is described:

- vinyl imidazolium trifluoromethane sulfonate [Vim][TFSO₃] (Figure 2-1),
- methyl imidazolium trifluoromethane sulfonate [Meim][TFSO₃] (Figure 2-1),
- vinyl imidazolium bis(trifluoromethylsulfonyl)imide ([Vim][Tf₂N]) (Figure 2-2),
- methyl imidazolium bis(trifluoromethylsulfonyl)imide ([Meim][Tf₂N]) (Figure 2-2),
- lithium bis(trifluoromethylsulfonyl)imide salt-2,2'-(ethylenedioxy)bis(ethylamine) (Li(DOBA)[Tf₂N]) (Figure 2-3),
- and lithium bis(trifluoromethylsulfonyl)imide salt-2-hydroxyethylenediamine (Li(HDA)[Tf₂N]) (Figure 2-3).

Their chemical structure was analyzed by ¹H NMR and FT-IR analysis, while their thermal properties were characterized by DSC and TGA.

2.1 Synthesis of ionic liquids

2.1.1 [Meim][TFSO₃] and [Vim][TFSO₃]

[Meim][TFSO₃] and [Vim][TFSO₃] (Figure 2-1) were synthesized according to the literature [7]. 150 mmol of 1-methylimidazole (Meim) (12.32 g) or *N*-vinylimidazole (Vim) (14.12 g) were dissolved in dry diethylether (200 mL) at 0°C under an argon atmosphere. Then, 150 mmol of trifluoromethanesulfonic acid (32.72 g) were dropwise added to the solution under stirring and maintained around 5°C. White crystals of ionic liquid began to precipitate after 15-20 min. The reaction mixture was stirred for 2 h at 10°C and additional 2 h at 25°C. Then, the obtained white crystals were filtrated off and washed 5 times with 250 mL of chloroform. The obtained salt was vacuum dried at

150 mbar and 120°C for 48 h.

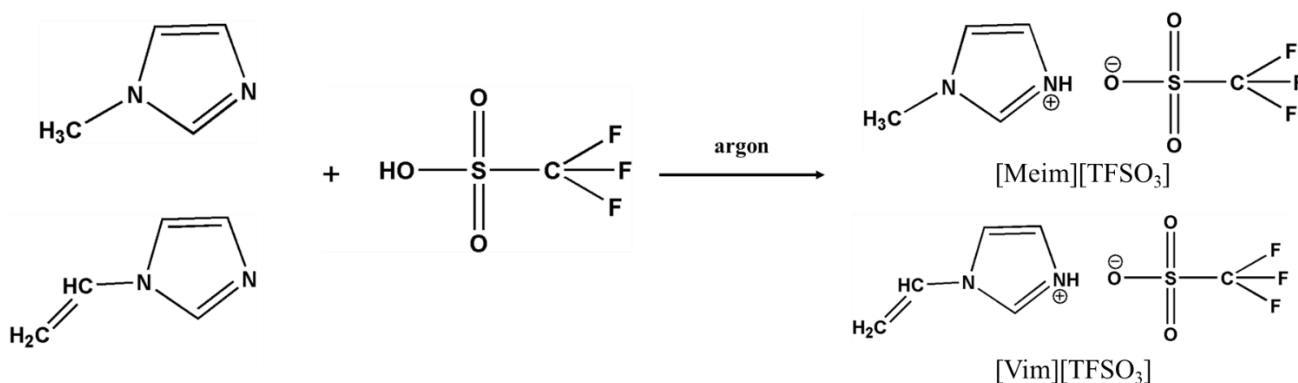


Figure 2-1 Synthetic route of [Meim][TfSO₃] and [Vim][TfSO₃] preparation

2.1.2 [Meim][Tf₂N] and [Vim][Tf₂N]

[Meim][Tf₂N] and [Vim][Tf₂N] (Figure 2-2) were synthesized according to the literature [8]. Dry ethanol (30 mL) was added to a two-necked round-bottom flask equipped with a magnetic stirrer, a thermometer and a drip funnel under an argon atmosphere. Then, 150 mmol of bis(trifluoromethanesulfonyl)imide (Tf₂N) (42.17 g) were slowly added, the solution was cooled down to 0°C, and 150 mmol of 1-methylimidazole (12.32 g) or N-vinylimidazole (14.12 g) were added dropwise. The temperature was increased to 22°C and the mixture was stirred overnight. IL was dried under vacuum at 150 mbar and 100°C for 48 h.

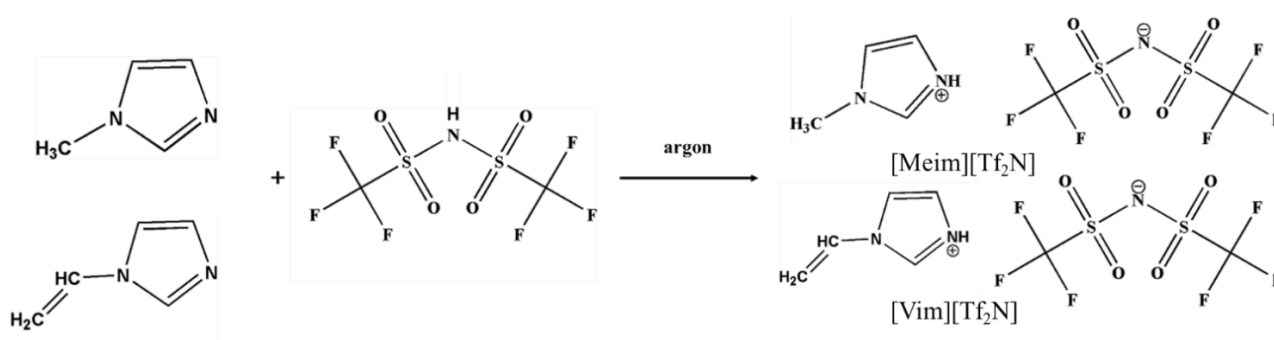


Figure 2-2 Synthetic route of [Vim][Tf₂N] and [Meim][Tf₂N] preparation

2.1.3 Li(DOBA)[Tf₂N] and Li(HDA)[Tf₂N]

Li(DOBA)[Tf₂N] and Li(HDA)[Tf₂N] (Figure 2-3) were prepared according to the literature [6]

by equimolar mixing of lithium bis(trifluoromethylsulfonyl)imide salt (LiTf_2N) (43.06 g) and 2,2'-(ethylenedioxy)bis(ethylamine) (DOBA) (22.23 g) or 2-hydroxyethylenediamine (HDA) (15.62 g). The mixture was stirred 24 h at 50°C . The obtained IL was dried under vacuum (150 mbar) for 24 h at 80°C .

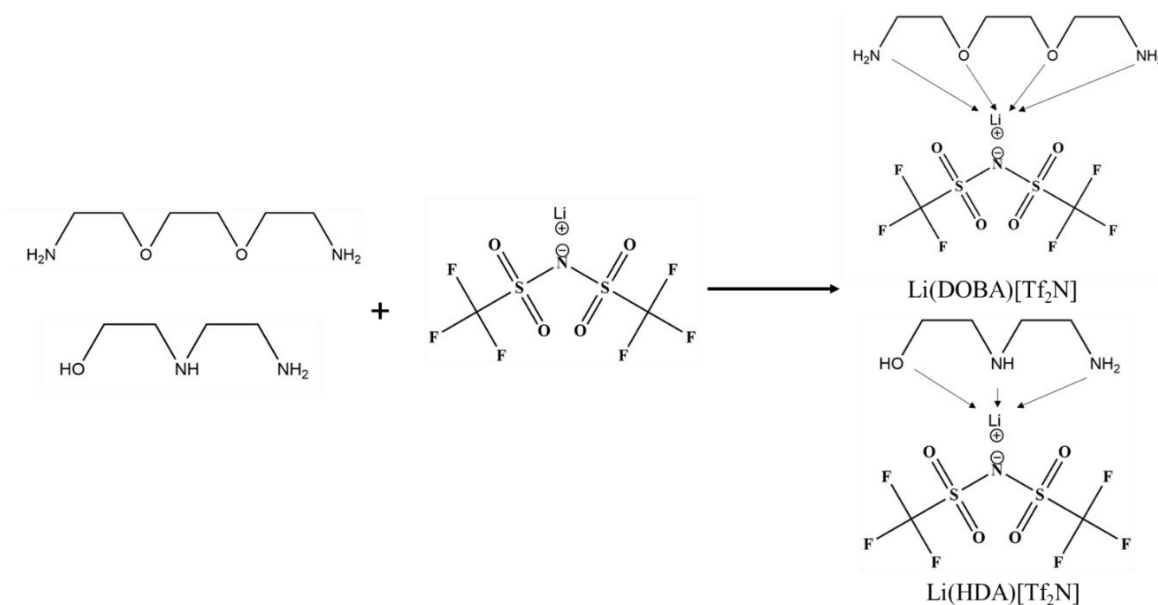


Figure 2-3 Synthetic route of $\text{Li}(\text{DOBA})[\text{Tf}_2\text{N}]$ and $\text{Li}(\text{HDA})[\text{Tf}_2\text{N}]$ preparation

2.2 Characterization of ILs

2.2.1 Structural characterization

2.2.1.1 FT-IR analysis

FT-IR spectroscopy was used to analyze the vibrations of the characteristic bonds of the ILs functional groups (Figure 2-4).

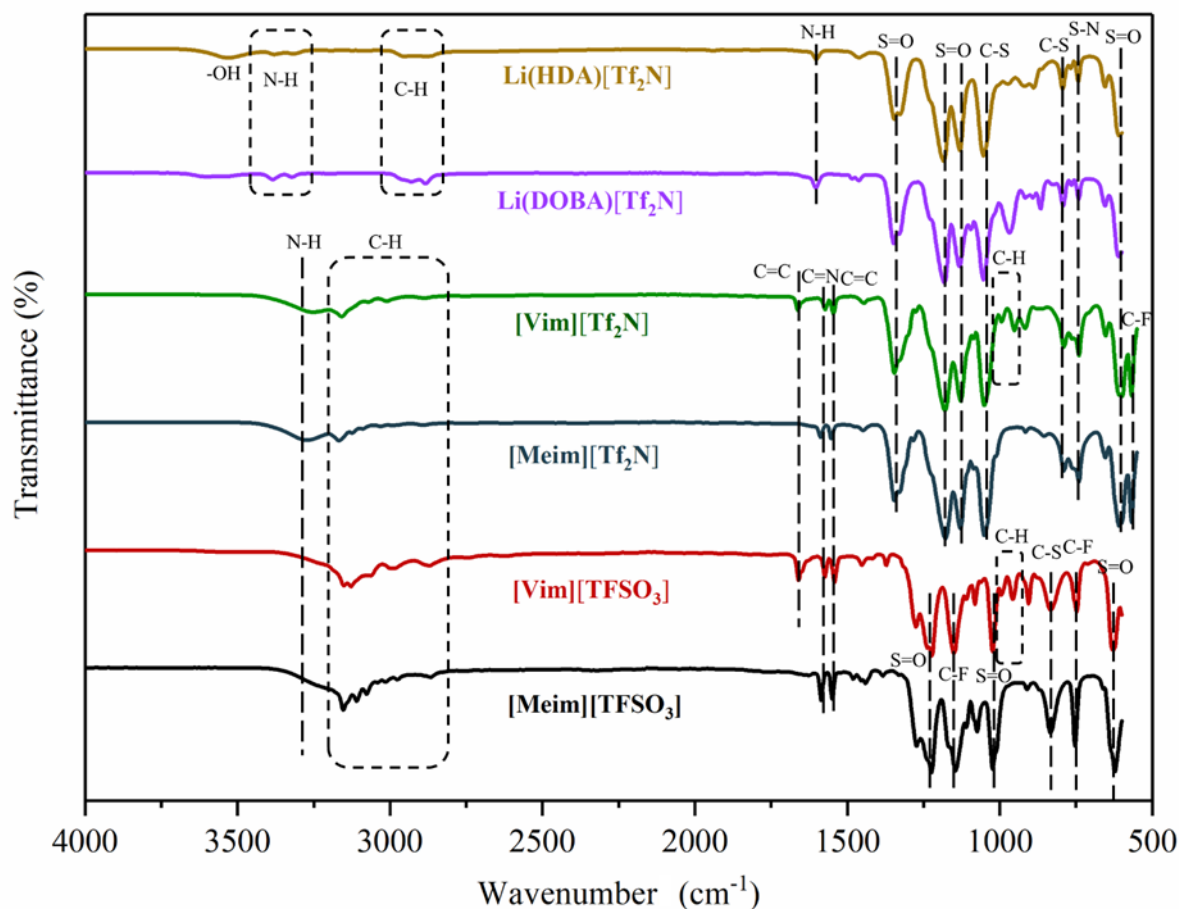


Figure 2-4 FT-IR spectra of synthesized ILs

For easier comparison, the signals of the same cations and anions were analyzed together.

For [Vim][TfSO₃], [Meim][TfSO₃], [Meim][Tf₂N] and [Vim][Tf₂N], all the characteristic vibrations of the cationic imidazole ring (N-H, C-H, C=N and C=C stretch at 3268, 2800-3200, 1576 and 1542 cm⁻¹) can be observed and are consistent with the literature [9]. The signals at 1660 cm⁻¹ and 950-1000 cm⁻¹, corresponding to the C=C substituent characteristic peak and C-H bending of vinyl imidazolium, revealed the difference between [Vim]⁺ and [Meim]⁺ as already observed [10]. For anions, the characteristic peaks were more pronounced and intense. The S=O bending of [TfSO₃]⁻ appeared at 632, 1020 and 1226 cm⁻¹, while the -SO₂ groups of [Tf₂N]⁻ were observed at 614, 1128, 1186 and 1346 cm⁻¹. The characteristic strong bands of C-F were observed at 752 and 1146 cm⁻¹ for [TfSO₃]⁻ and 572 cm⁻¹ for [Tf₂N]⁻. Also, the C-S bending of [TfSO₃]⁻ at 834 cm⁻¹ and [Tf₂N]⁻ at 794 and 1056 cm⁻¹ were observed. Finally, the S-N bending of [Tf₂N]⁻ appeared at 742 cm⁻¹. All these results are consistent with the literature [8,11].

The characteristic peaks of alkanolamine-based ILs were also analyzed. The C-H and N-H signals

of DOBA and HDA appeared at 2800-3000 and 3200-3420 cm^{-1} , respectively [6]. The broad peak at 3420-3680 cm^{-1} was assigned to the -OH groups of HDA [12]. The N-H bending of DOBA and HDA was observed around 1600 cm^{-1} [13].

To sum up, the peaks of all ILs are consistent with the targeted structures and with the literature.

2.2.1.2 ^1H NMR spectroscopy

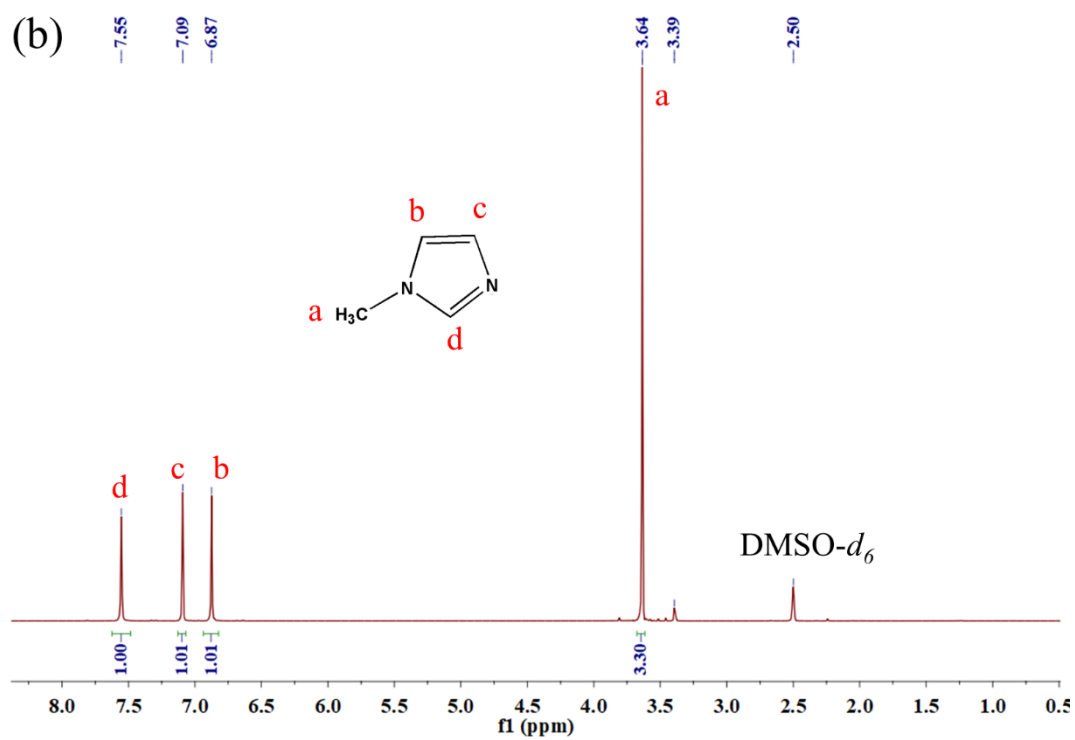
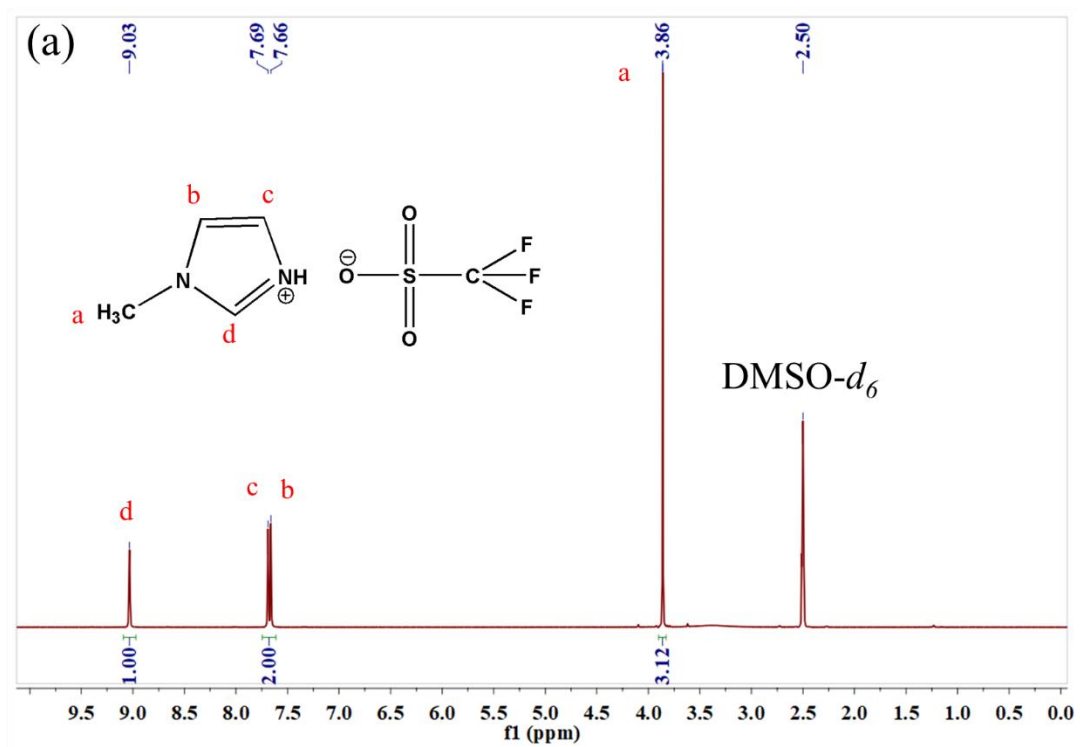
In order to validate FT-IR results, ^1H NMR analysis was carried out to confirm the ILs structures. The corresponding chemical shifts were gathered in Table 2-1 and are consistent with the literature [6,8].

For a clearer presentation, [Meim][TFSO₃] and Li(DOBA)[Tf₂N] were taken as typical examples of imidazolium-based and alkanolamine-based ILs, respectively, and the results are detailed thereafter.

The ^1H NMR spectrum of [Meim][TFSO₃] (Figure 2-5 (a)) exhibited the signals of the imidazolium ring *b*, *c*, *d* at 7.66 (1H), 7.69 (1H) and 9.03 (1H) ppm, and the proton *a* of the side methyl chain at 3.86 (3H) ppm, fully concordant with the expected structure. The obtained signals are quite different from the spectrum of Meim (Figure 2-5 (b)), for which the signals *a*, *b*, *c*, *d* at 3.64 (3H), 6.87 (1H), 7.09 (1H) and 7.55 (1H) ppm can be seen. Such difference is due to the different intramolecular interactions brought by the anion [14]. The signal of trifluoromethanesulfonic acid (Figure 2-5 (c)) at 13.65 ppm could not be detected on the spectrum of IL, indicating that no initial reagent remained. Therefore, the results of ^1H NMR analysis confirm the successful synthesis of [Meim][TFSO₃].

Table 2-1 ^1H NMR chemical shifts of synthesized ILs

ILs (solvent)	^1H NMR shifts (ppm)
[Meim][TFSO ₃] (<i>d</i> ₆ -DMSO)	9.03 (s, 1H), 7.69 (t, 1H), 7.66 (t, 1H), 3.86 (s, 3H)
[Vim][TFSO ₃] (<i>d</i> ₆ -DMSO)	9.32 (t, 1H), 8.17 (t, 1H), 7.79 (t, 1H), 7.29 (m, 1H), 5.99 (dd, 1H), 5.42 (dd, 1H)
[Meim][Tf ₂ N] (<i>d</i> ₆ -DMSO)	9.03 (s, 1H), 7.69 (t, 1H), 7.66 (t, 1H), 3.86 (s, 3H)
[Vim][Tf ₂ N] (<i>d</i> ₆ -DMSO)	9.33 (t, 1H), 8.17 (t, 1H), 7.80 (t, 1H), 7.29 (m, 1H), 5.99 (dd, 1H), 5.42 (dd, 1H)
Li(DOBA)[Tf ₂ N] (D ₂ O)	3.67 (s, 2H), 3.56 (t, 2H), 2.78 (t, 2H)
Li(HDA)[Tf ₂ N] (D ₂ O)	3.66 (t, 2H), 2.70 (m, 6H)



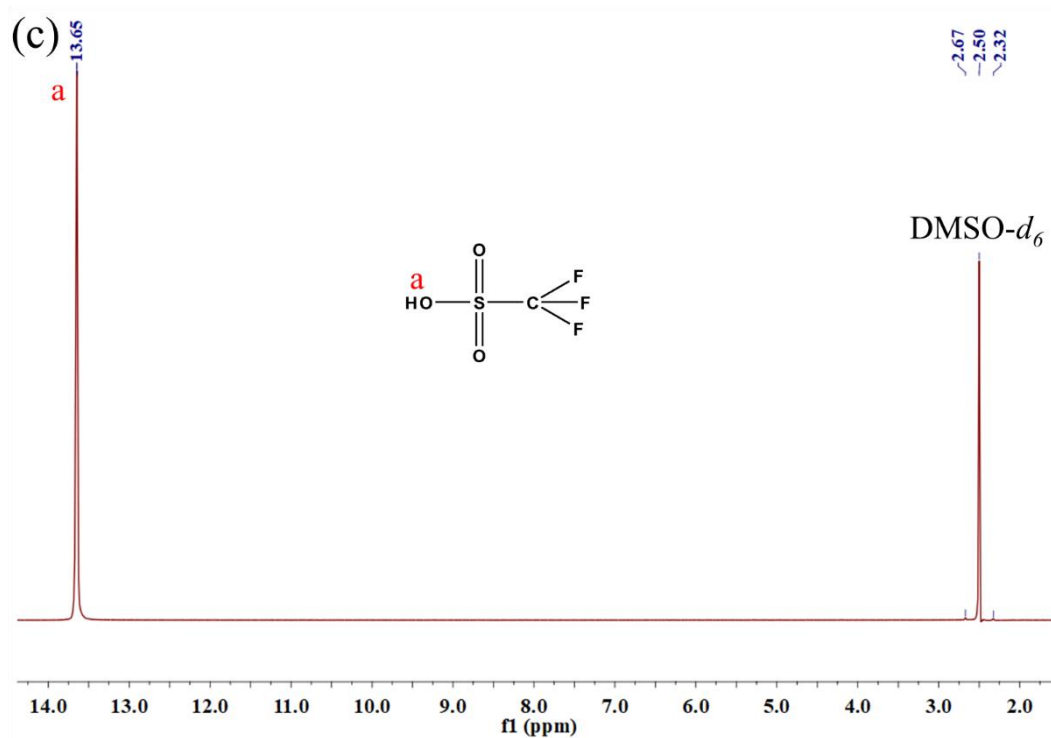
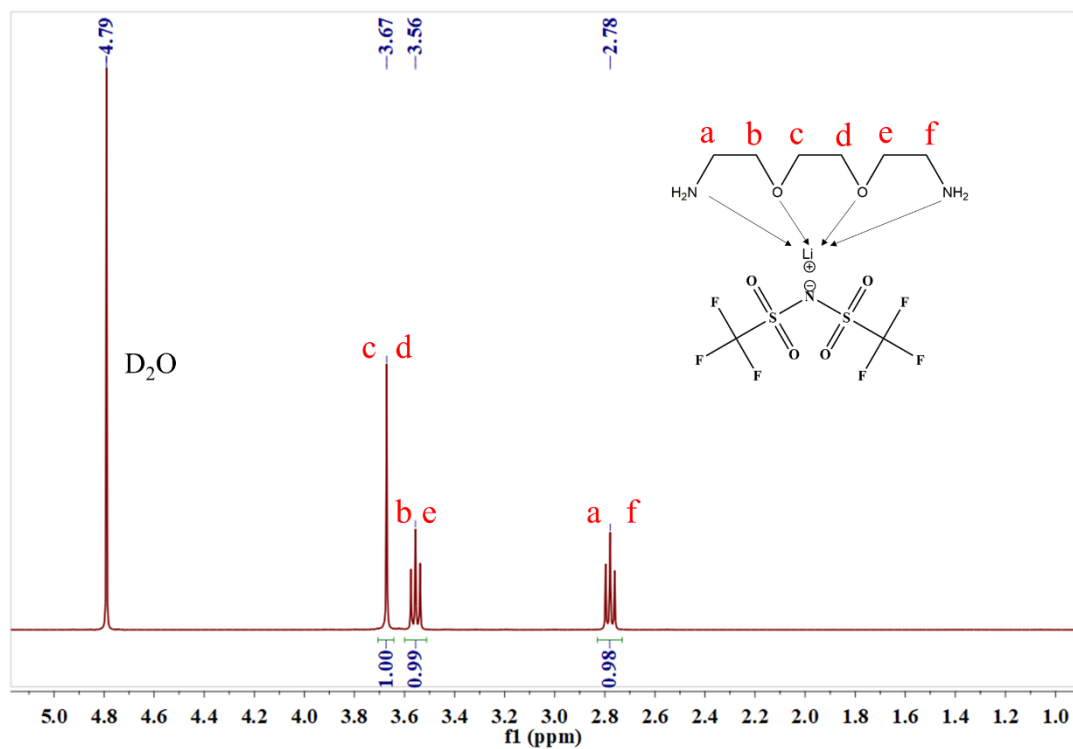


Figure 2-5 ^1H NMR spectra of [Meim][TfSO₃] (a), 1-methylimidazole (b), and trifluoromethanesulfonic acid (c)

The ^1H NMR spectrum of Li(DOBA)[Tf₂N] is presented in Figure 2-6. The protons at 3.67 (2H), 3.56 (2H) and 2.78 (2H) ppm were found, very close to the literature values (3.66 (2H), 3.53 (2H) and 2.88 (2H)) [6]. To conclude, the ^1H NMR analysis confirms the successful synthesis of Li(DOBA)[Tf₂N].

Figure 2-6 ^1H NMR spectra of $\text{Li}(\text{DOBA})[\text{Tf}_2\text{N}]$

The ^1H NMR spectra of $[\text{Vim}][\text{TFSO}_3]$, $[\text{Meim}][\text{Tf}_2\text{N}]$, $[\text{Vim}][\text{Tf}_2\text{N}]$, and $\text{Li}(\text{HDA})[\text{Tf}_2\text{N}]$ are presented in Figure 2-7, Figure 2-8, Figure 2-9 and Figure 2-10, respectively. The ^1H NMR spectra of other raw chemicals (Vim and Tf_2N) are presented in Annex 3.

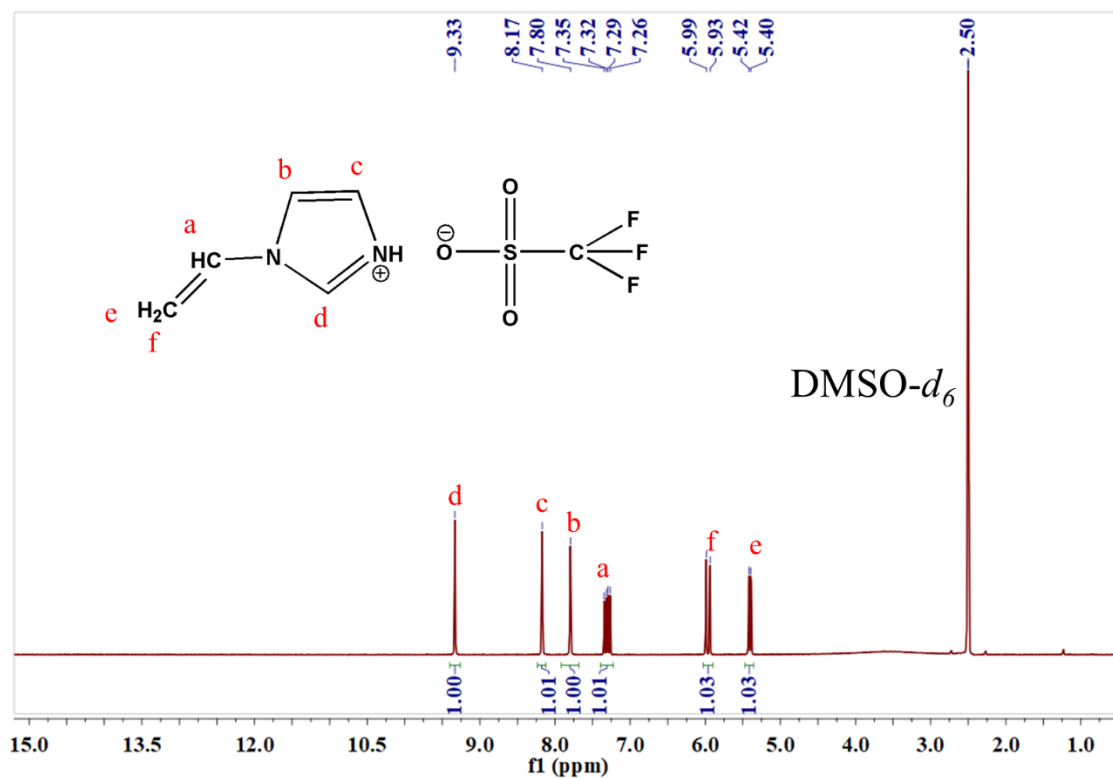


Figure 2-7 ¹H NMR spectra of [Vim][TFSO₃]

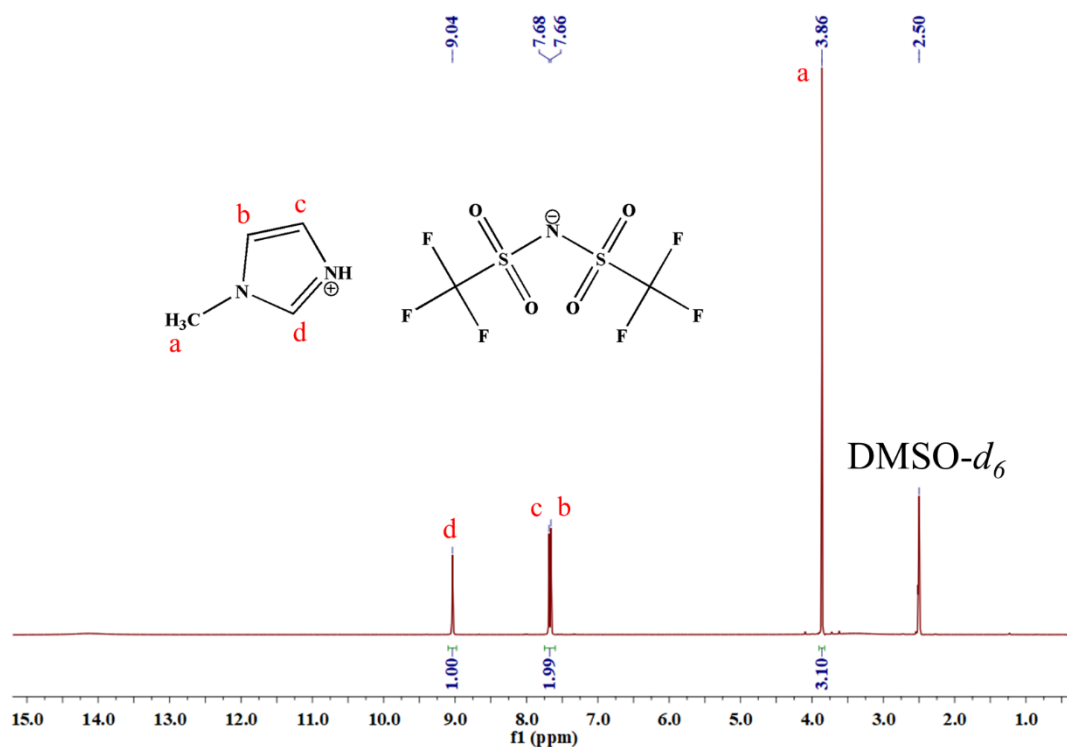


Figure 2-8 ¹H NMR spectra of [Meim][Tf₂N]

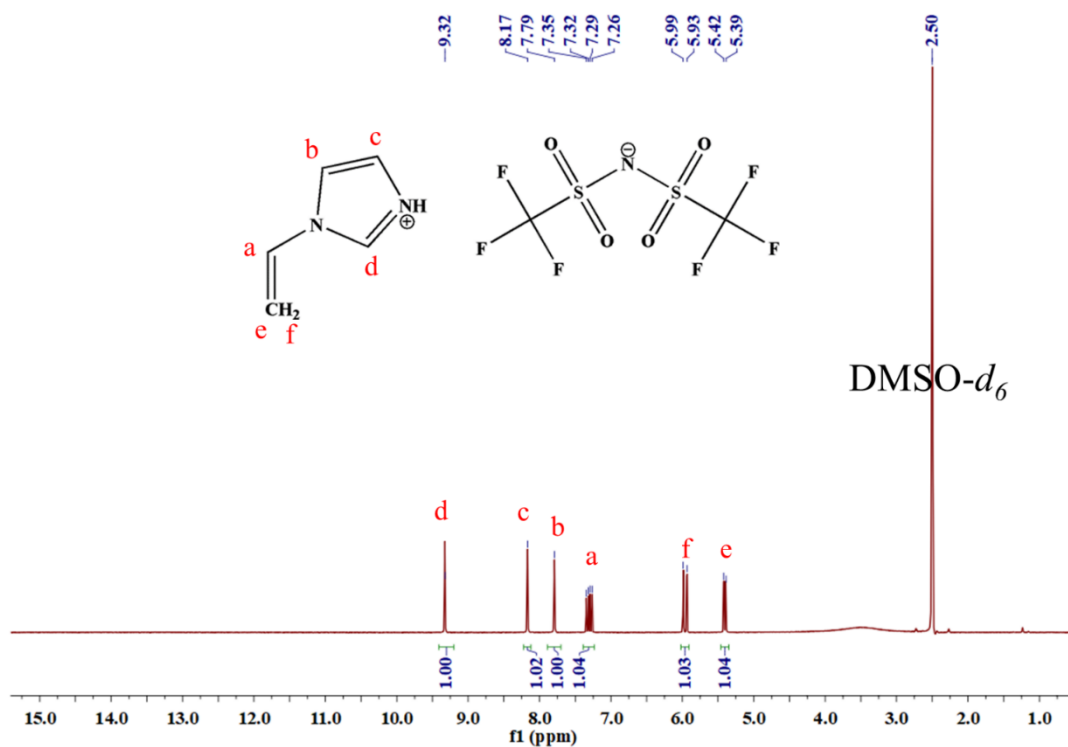


Figure 2-9 ^1H NMR spectra of $[\text{Vim}][\text{Tf}_2\text{N}]$

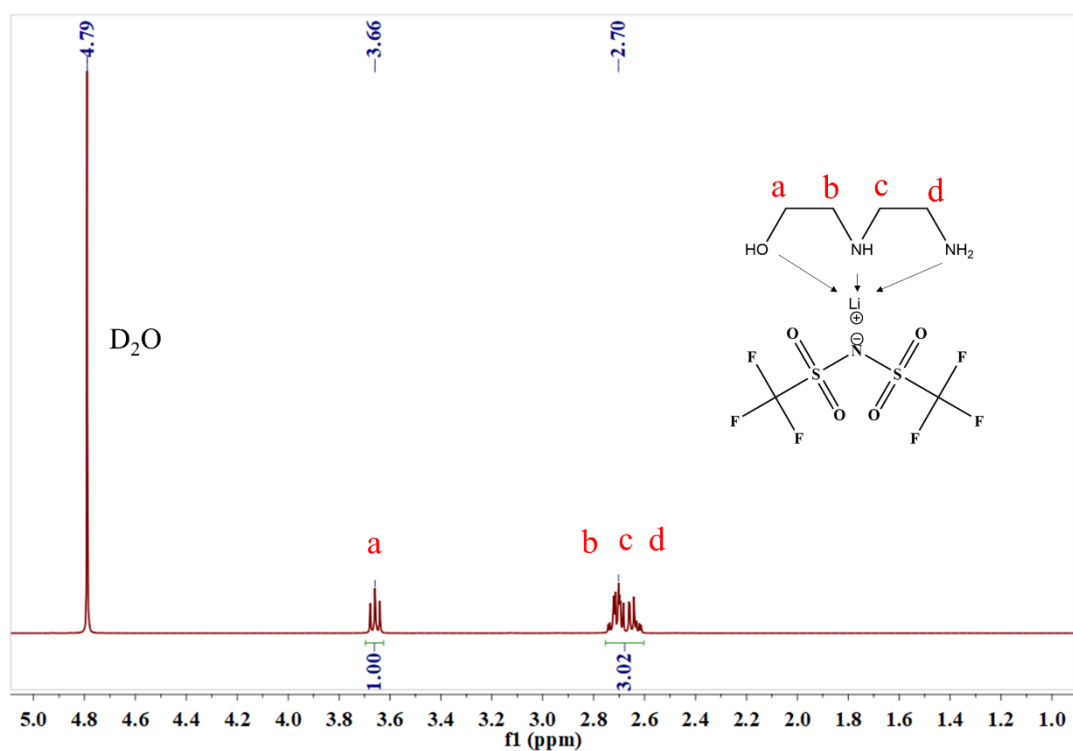


Figure 2-10 ^1H NMR spectra of $\text{Li}(\text{HDA})[\text{Tf}_2\text{N}]$

2.2.2 Thermal characterization

2.2.2.1 Thermal stability

The thermal stability of ILs, which is a crucial parameter both during production and membrane use [15], was studied from 30 to 800°C by thermal gravimetric analysis (Figure 2-11 and Table 2-2).

One can see that the 5% weight loss temperature ($T_{5\%}$) of imidazolium-based ILs is 314, 289, 323 and 287°C for [Meim][TFSO₃], [Vim][TFSO₃], [Meim][Tf₂N] and [Vim][Tf₂N], respectively. The $T_{5\%}$ value of Meim and Vim is 56 and 42°C, respectively, indicating that the thermal stability of [Meim]⁺ and [Vim]⁺ is higher than that of Meim and Vim due to the ionic bonding. Furthermore, [Meim][TFSO₃] and [Meim][Tf₂N] exhibit higher degradation temperatures, with a one-step degradation, than that of [Vim][TFSO₃] and [Vim][Tf₂N], with a two-step degradation. This result can be explained by the higher thermal stability of the methyl groups as compared to the stability of vinyl ones, while [TFSO₃]⁻ and [Tf₂N]⁻ anions have minimal impact on the $T_{5\%}$ value of ILs.

It can be seen that $T_{5\%}$ of alkanolamine-based ILs are 241°C for Li(DOBA)[Tf₂N] and 238°C for Li(HDA)[Tf₂N], which is much higher than the temperature of DOBA (81°C) and HDA (93°C) (Table 2-2). Such improvement of the thermal stability is due to the coordination between Li⁺ and nitrogen and oxygen atoms [6,16]. Also, the coordination atoms and coordination number affect the thermal stability of alkanolamine-based ILs, therefore Li(DOBA)[Tf₂N] is slightly more stable than Li(HDA)[Tf₂N].

The thermal stability of imidazolium-based ILs is superior to the stability of alkanolamine-based ILs, with a degradation starting around 290 and 240°C, respectively. Besides [Meim]-based ILs are the most stable, with no observed degradation below 314°C.

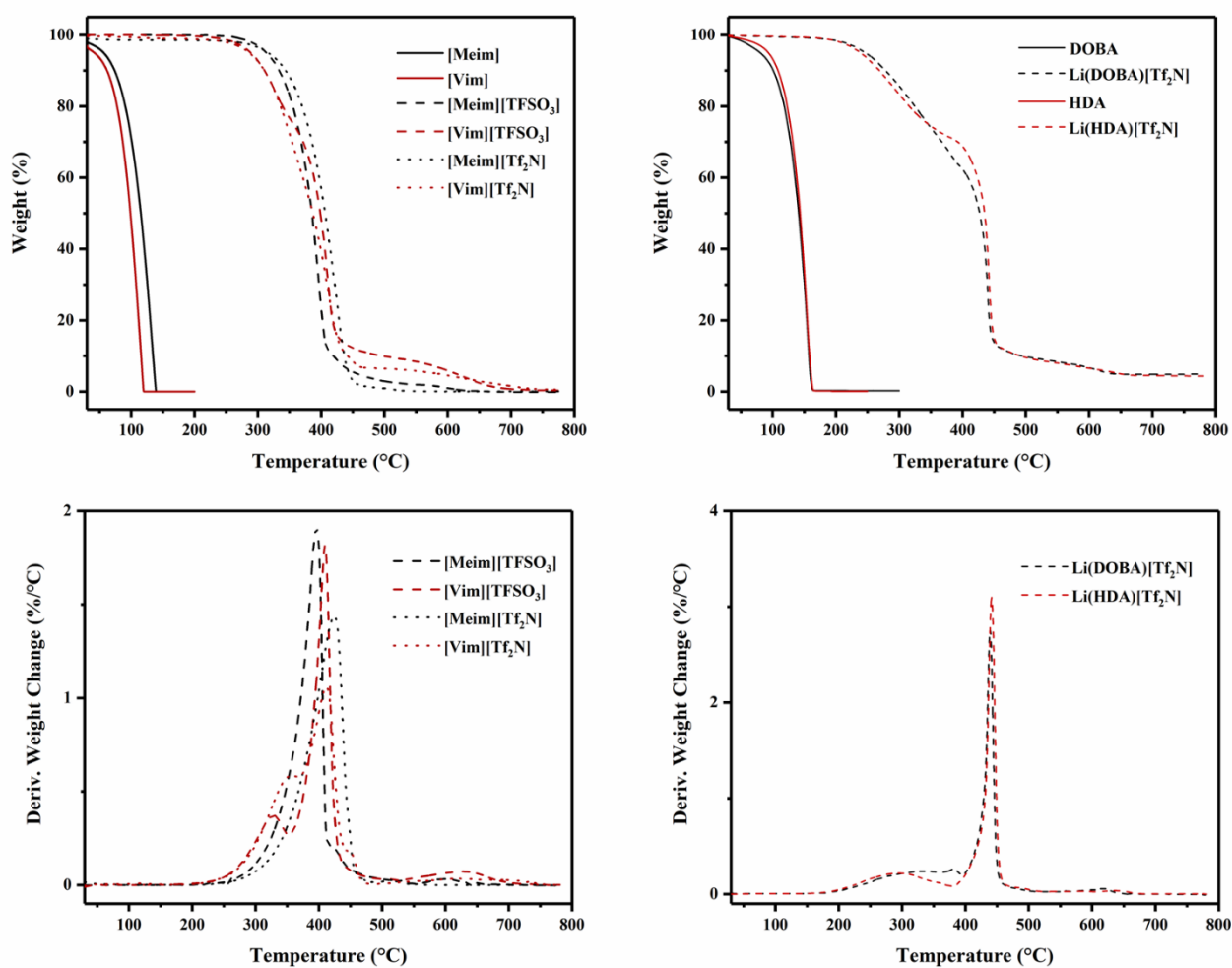


Figure 2-11 TGA and DTG curves of ILs

Table 2-2 TGA data ($T_{5\%}$, T_{\max} and isothermal weight loss at 150°C) of ILs

IL	$T_{5\%}$ ($^{\circ}\text{C}$)	T_{\max} ($^{\circ}\text{C}$)	Weight loss (150°C , 800 min) (%)
[Meim][TFSO ₃]	314	396	0.8
[Vim][TFSO ₃]	289	409	1.3
[Meim][Tf ₂ N]	323	423	1.2
[Vim][Tf ₂ N]	287	412	3.5
Li(DOBA)[Tf ₂ N]	241	440	5.8
Li(HDA)[Tf ₂ N]	238	441	6.7

$T_{5\%}$ - 5% weight loss temperature; T_{\max} - temperature at maximum degradation rate

One of the possible ways to prepare composite membranes is the solvent evaporation method. The final step consists in a complete drying of the obtained membrane, since residual solvent can plasticize the polymer matrix and change its overall properties. The solvents generally used for PSF and PES membranes, dimethylformamide (boiling temperature 153°C) and *N*-methyl-2-pyrrolidone (boiling temperature 202°C) [17], must be eliminated in a 15 mbar vacuum oven at a temperature of 150°C during 10 h. In order to confirm that these drying conditions are compatible with the thermal stability of ILs, TGA was carried out at 150°C for 800 min (Figure 2-12 and Table 2-2). All ILs are rather stable at 150°C for 800 min, showing limited weight loss-around 1-7%. These results indicate that both imidazolium-based and alkanolamine-based ILs have good thermal stability and could be used for the preparation of PSF-based and PES-based membranes.

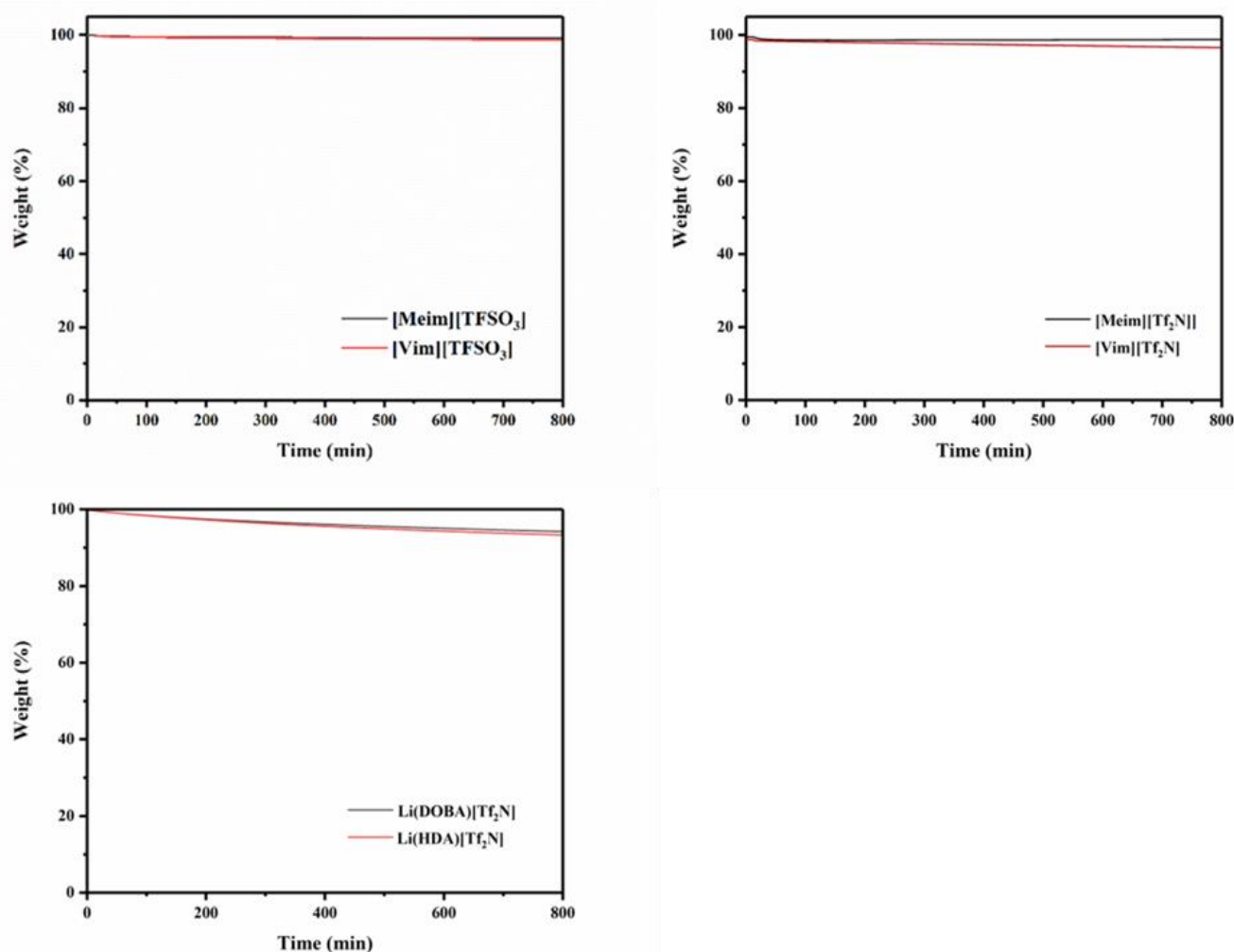


Figure 2-12 TGA isothermal curves of ILs at 150°C

2.2.2.2 Differential scanning calorimetry (DSC)

DSC measurements were carried out to determine the melting (T_m), crystallization (T_c) and glass transition (T_g) temperatures of ILs (Table 2-3). Apart from the first heating used to erase the thermal history (which turned out to be identical to the second one), the first cooling and second heating curves are presented in Figure 2-13. Despite quenching attempts, the T_g of imidazolium-based ILs could not be measured, so the literature data were used for some values.

Table 2-3 DSC data of ILs

IL	T_g (°C)	T_m (°C)	T_c (°C)	ΔH_m (J/g)
[Meim][TFSO ₃]	-61 [197]	61/85/110	61/81/93	70.2
[Vim][TFSO ₃]	nd	71	41	62.3
[Meim][Tf ₂ N]	-59 [197]	17/49	-43	75.6
[Vim][Tf ₂ N]	-75 [197]	31	-16	53.2
Li(DOBA)[Tf ₂ N]	-57	41	-1 ^{cc}	52.7
Li(HDA)[Tf ₂ N]	-47	nd	nd	nd

nd - no data available; cc - cold crystallization during heating

It is clear that both cation and anion structures affect the thermal behavior of ILs.

The T_g of all imidazolium-based ILs is below -50°C (-61°C for [Meim][TFSO₃], -59°C for [Meim][Tf₂N] and -75°C for [Vim][Tf₂N]). [Meim][TFSO₃] exhibits three T_m at 61°C , 85°C , and 110°C , and [Meim][Tf₂N] displays two T_m at 17°C and 49°C . In contrast, both [Vim][TFSO₃] and [Vim][Tf₂N] have a single T_m at 71°C and 31°C , respectively. This suggests that [Meim]⁺ is more prone to form polymorphism than [Vim]⁺. The T_m values reported in the literature for [Vim][TFSO₃] (77°C), [Meim][Tf₂N] (57°C) and [Vim][Tf₂N] (39°C) were quite different from the values found in this work, maybe due to the different drying condition used [8]. Additionally, the T_m of the four imidazolium-based ILs is above room temperature, so these ILs are crystalline solid at room temperature. Globally, for the same anion, [Meim]⁺ as compared to [Vim]⁺, brings higher T_g , T_m , T_c and ΔH_m , and for the same cation, [TFSO₃]⁻ brings higher T_m than [Tf₂N]⁻. These results may be explained by the fact that the smaller the size of both anion and cation is, the stronger the ionic bond is, leading to a higher melting point.

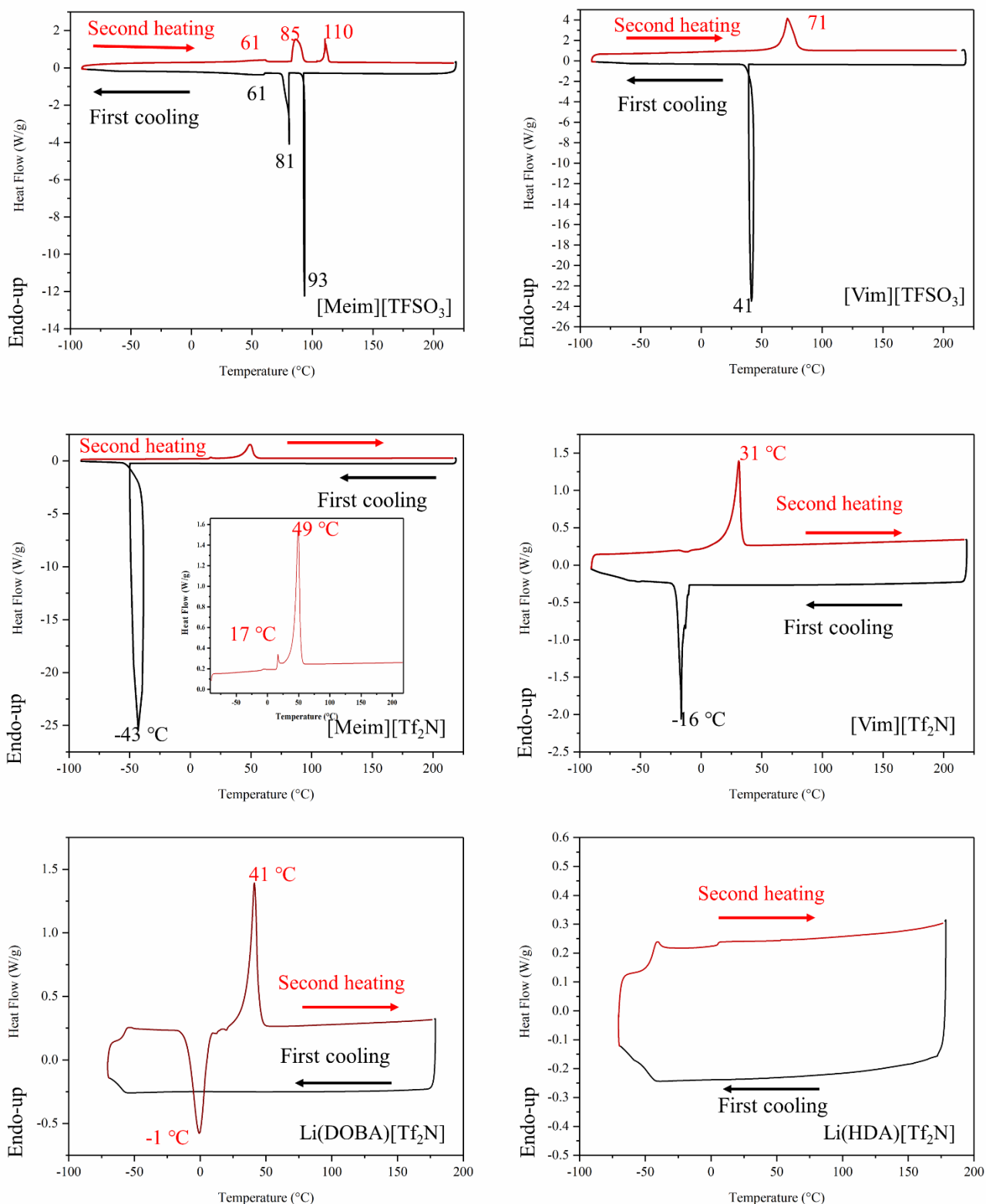


Figure 2-13 DSC curves of ILs

The T_g of Li(DOBA)[Tf₂N] (-57°C) is lower than the T_g value of Li(HDA)[Tf₂N] (-47°C) because of the ether bonds in DOBA that bring easier chain mobility than HDA. The crystallization ability of

these ILs is inferior as compared to the imidazolium-based ILs. Indeed, Li(DOBA)[Tf₂N] exhibit a cold crystallization process with no crystallization during previous cooling, with a T_m of 41°C, and Li(HDA)[Tf₂N] seems to be amorphous.

2.3 Conclusion

Four imidazolium-based ILs ([Meim][TFSO₃], [Vim][TFSO₃], [Meim][Tf₂N] and [Vim][Tf₂N]) and two alkanolamine-based ILs (Li(DOBA)[Tf₂N] and Li(HDA)[Tf₂N]) were synthesized successfully. The chemical structures were verified through rigorous analysis using ¹H NMR and FT-IR spectroscopy. The thermal stability of the ILs was examined by TGA, demonstrating stability up to 200°C and long-term stability at 150°C for 800 min, which is especially crucial for membrane preparation procedure confirming the suitability of these ILs for membrane production process. Notably, imidazolium-based ILs are more thermally stable than alkanolamine-based ILs.

Additionally, the DSC characterization emphasized the impact of both anion and cation on the IL thermal behavior, namely on T_g, T_m, T_c values and crystallization ability. For imidazolium-based ILs with the same anion, [Meim]⁺ exhibited elevated values of T_g, T_m, T_c, and ΔH_m as compared to [Vim]⁺. Similarly, when assessing the same cation, [TFSO₃]⁻ revealed a higher T_m than [Tf₂N]⁻. Meanwhile, the ILs with the [Meim]⁺ cation exhibited polymorphism. For alkanolamine-based ILs, Li(DOBA)[Tf₂N] was crystalline, whereas Li(HDA)[Tf₂N] was amorphous. The T_g of Li(DOBA)[Tf₂N] was lower than that of [Li(HDA)[Tf₂N]. Finally, the four imidazolium-based ILs showed greater crystallization ability than the alkanolamine-based ILs.

This comprehensive investigation provides valuable insight to the further utilization of these ILs in various applications, particularly in the development of advanced membranes.

References

- [1] M. Hasib-ur-Rahman, M. Sijaj, F. Larachi, Ionic liquids for CO₂ capture-Development and progress, *Chemical Engineering and Processing: Process Intensification* 49 (2010) 313–322.
- [2] J.L. Anthony, J.L. Anderson, E.J. Maginn, J.F. Brennecke, Anion Effects on Gas Solubility in Ionic Liquids, *J. Phys. Chem. B* 109 (2005) 6366–6374.
- [3] X. Zhang, X. Zhang, H. Dong, Z. Zhao, S. Zhang, Y. Huang, Carbon capture with ionic liquids: overview and progress, *Energy Environ. Sci.* 5 (2012) 6668–6681.
- [4] P. Liu, K. Cai, X. Zhang, T. Zhao, Effective absorption of SO₂ by imidazole-based protic ionic liquids with multiple active sites: Thermodynamic and mechanical studies, *AIChE Journal* 68 (2022) e17596.
- [5] M. Wang, L. Zhang, H. Liu, J. Zhang, C. Zheng, Studies on CO₂ absorption performance by imidazole-based ionic liquid mixtures, *Journal of Fuel Chemistry and Technology* 40 (2012) 1264–1268.
- [6] C. Wang, Y. Guo, X. Zhu, G. Cui, H. Li, S. Dai, Highly efficient CO₂ capture by tunable alkanolamine-based ionic liquids with multidentate cation coordination, *Chem. Commun.* 48 (2012) 6526–6528.
- [7] Ya. Kobzar, K. Fatyeyeva, Ye. Lobko, Yu. Yakovlev, T. Hrbek, S. Marais, New ionic liquid-based polyoxadiazole electrolytes for hydrogen middle- and high-temperature fuel cells, *Journal of Membrane Science* 640 (2021) 119774.
- [8] Y. Prykhodko, A. Martin, H. Oulyadi, Ya.L. Kobzar, S. Marais, K. Fatyeyeva, Imidazolium-based protic ionic liquids with perfluorinated anions: Influence of chemical structure on thermal properties, *Journal of Molecular Liquids* 345 (2022) 117782.
- [9] S. Abdollahi, H.R. Mortaheb, A. Ghadimi, M. Esmaeili, Improvement in separation performance of Matrimid®5218 with encapsulated [Emim][Tf₂N] in a heterogeneous structure: CO₂/CH₄ separation, *Journal of Membrane Science* 557 (2018) 38–48.
- [10] A.G. Kuba, Y.Y. Smolin, M. Soroush, K.K.S. Lau, Synthesis and integration of poly(1-vinylimidazole) polymer electrolyte in dye sensitized solar cells by initiated chemical vapor deposition, *Chemical Engineering Science* 154 (2016) 136–142.
- [11] V.H. Paschoal, L.F.O. Faria, M.C.C. Ribeiro, Vibrational Spectroscopy of Ionic Liquids, *Chem. Rev.* 117 (2017) 7053–7112.
- [12] D. Si, K. Chen, J. Yao, H. Li, Structures and Electronic Properties of Lithium Chelate-Based Ionic Liquids, *J. Phys. Chem. B* 120 (2016) 3904–3913.
- [13] S. Magalhães, B.J. Goodfellow, A. Nunes, FTIR spectroscopy in biomedical research: how to get the most out of its potential, *Applied Spectroscopy Reviews* 56 (2021) 869–907.
- [14] Synthesis, NMR, Raman, thermal and nonlinear optical properties of dicationic ionic liquids from experimental and theoretical studies, *Journal of Molecular Structure* 1220 (2020) 128713.
- [15] X. Wang, S. Wang, W. Wang, H. Li, X. Liu, X. Gu, S. Bourbigot, Z. Wang, J. Sun, S. Zhang, The flammability and mechanical properties of poly (lactic acid) composites containing Ni-MOF nanosheets with polyhydroxy groups, *Composites Part B: Engineering* 183 (2020) 107568.
- [16] G. Shi, H. Zhao, K. Chen, W. Lin, H. Li, C. Wang, Efficient capture of CO₂ from flue gas at

high temperature by tunable polyamine-based hybrid ionic liquids, *AIChE Journal* 66 (2020) e16779.

- [17] R. Gregorio, D.S. Borges, Effect of crystallization rate on the formation of the polymorphs of solution cast poly(vinylidene fluoride), *Polymer* 49 (2008) 4009–4016.

Chapter 3
Preparation and characterization of PSF-
based dense composite membranes

3.1 Introduction

Owing to the numerous advantageous characteristics of PSF detailed in Chapter 1 (section 1.5), PSF has been extensively studied as porous support layer in composite membranes for CO₂ separation. Martínez-Izquierdo *et al* [1] prepared PSF support layers by casting, followed by phase inversion. Then, the selective layer (Pebax[®] Renew[®] 30R51/ZIF-94 (15 wt%)/[Bmim][BF₄] (10 wt%)) was spin-coated onto the PSF support, and gave a CO₂ permeance increased by 65% up to 819 GPU as compared with the pristine Pebax[®]. This result was explained by the high CO₂-philicity of [Bmim][BF₄], the aldehyde group in ZIF-94, and the large specific surface area (645 cm²/g) of ZIF-94.

Also, PSF can serve as a selective dense layer in CO₂ separation composite membranes. However, PSF as a glassy polymer demonstrates high gas selectivity but it is constrained by limited gas permeability (CO₂ permeability is 4.3 Barrer and CO₂/CH₄ selectivity is 8.2) [2]. Farrokhara and Dorosti, [2] studied the effect of 1-ethyl-3-methylimidazolium tetrafluoroborate [Emim][BF₄] on CO₂/CH₄ separation performance of symmetric PSF membranes: PSF/[Emim][BF₄] (40 wt%) improved CO₂ permeation and CO₂/CH₄ selectivity by 98.3% and 172%, respectively, in comparison with pure PSF membrane. This enhancement was attributed to the high CO₂ affinity of [Emim][BF₄].

In this Chapter, the main objective is to obtain dense PSF-based composite membranes with high CO₂ permeability and selectivity. Firstly, the initial focus is optimizing the preparation process of dense composite membranes based on PSF and containing six synthesized ionic liquids: [Meim][TFSO₃], [Vim][TFSO₃], [Meim][Tf₂N], [Vim][Tf₂N], Li(DOBA)[Tf₂N] and Li(HDA)[Tf₂N]. Secondly, the impact of these ILs on the thermal properties, microstructure, surface energy, mechanical characteristics, and gas permeation (CO₂, N₂ and O₂) of the composite membranes will be studied and discussed.

3.2 Membrane preparation

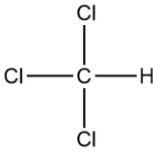
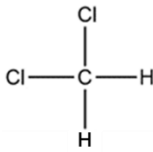

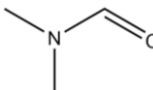
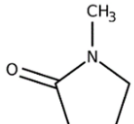
The fabrication of membranes by the casting method, especially composite membranes, is a complex process. Indeed, the membrane's quality depends on several preparation factors, including solvent selection, polymer concentration, supporting material, and solvent evaporation conditions.

3.2.1 Solvent selection

Many researchers have emphasized the critical role of casting solvents on the properties of gas separation membrane as they may change the membrane microstructure and, consequently, the gas permeability. Furthermore, the choice of a casting solvent influences the solvent removal process, contributing to the production of membranes with higher quality.

In this study, five casting solvents were tested: *N*-methyl-2-pyrrolidone (NMP) [2], dimethylformamide (DMF) [3], tetrahydrofuran (THF) [4], chloroform (CHCl₃) [5] and dichloromethane (CH₂Cl₂) [6]. Their characteristics, including boiling point, density, solubility parameter and molecular structure, are gathered in Table 3-1. It should be pointed out that the solubility parameter is rather crucial.

Table 3-1 Properties of solvents [7]

Solvent	Structure	Boiling point (°C)	Density (g/mL)	Solubility parameter (cal/cm ³)
CHCl ₃		61.2	1.498	9.3
CH ₂ Cl ₂		39.8	1.326	9.7
THF		66	0.886	9.1
DMF		153	0.944	12.1
NMP		202	1.028	11.3

Even if PSF can be successfully dissolved in CHCl₃ and CH₂Cl₂, four of the synthesized ILs ([Meim][TFSO₃], [Vim][TFSO₃], [Meim][Tf₂N], [Vim][Tf₂N]) are insoluble in these solvents. Therefore, CHCl₃ and CH₂Cl₂ cannot be used as casting solvents. Meanwhile, PSF and all ILs are soluble in THF, DMF and NMP. Therefore, these solvents were selected for dense PSF-based

membranes preparation.

3.2.2 Polymer concentration

The determination of the polymer optimal concentration is necessary to obtain a defect-free and dense CO₂ separation composite membrane. Different polymer concentrations (from 5 wt% to 25 wt%) were tested with the three selected solvents (THF, DMF and NMP). In each case, the obtained solution was casted on a glass support. Whatever the solvent used, 5 wt%, 10 wt% and 15 wt% polymer concentrations did not give solutions with sufficient viscosity to allow casting by Doctor BladeTM. In contrast, the 25 wt% polymer concentration was too high, leading to a bad quality membrane (non-smooth surface). Finally, dense pure PSF membranes with best quality were obtained with a 20 wt% polymer concentration, which was chosen for all further experiments.

3.2.3 Supporting material

The selection of the right supporting material is important to fabricate superior quality composite membranes by the casting method. Thus, different supports were considered. Among them, a PVA supporting membrane was tested and prepared by solution-casting process. 15 g of PVA were dissolved in 85 g of ultrapure water and stirred overnight at 95°C. Then, the solution was sonicated during 6 h to remove air bubbles. Finally, the solution was casted on a glass plate by Doctor BladeTM, placed in an oven at 45°C during 15 h, and dried at 85°C during 6 h.

Since the loading of ILs can change the surface energy value of the casting solution and, hence, affect the membrane formation on the support, 20 wt% PSF solutions in THF, DMF and NMP, and containing [Meim][TFSO₃] (10% w/w IL/PSF) were chosen for the tests.

The PSF/IL solutions casted on different supports (Table 3-2) successfully led to the formation of membranes only on PVA, indicating similar polarities of PVA membrane and casting solution. To conclude, PVA support was chosen for all membranes fabrication.

Table 3-2 Tested supporting materials to obtain PSF/[Meim][TFSO₃] composite membranes

Support	Surface energy (mN/m)	Solvent used		
		THF	DMF	NMP
Glass	~50	×	×	×
Glass surface grafted by imidazole	nd	×	×	×
PDMS	~20	×	×	×
Aluminum	~40	×	×	×
Steel	~45	×	×	×
PVDF	~44	×	×	×
PE	~30	×	×	×
PVA	~37	√	√	√

× - no membrane; √ - work; nd – no available data

3.2.4 Solvent evaporation conditions

The environment temperature and humidity during solvent evaporation have a strong influence on the quality and structure of membranes [8]. High humidity will promote water diffusion inside the casting solution, thus changing the membrane microstructure and creating voids. High temperature also accelerates solvent evaporation, resulting in shorter drying time but contributing to the formation of porous layers. Therefore, optimal humidity and temperature are essential for obtaining uniform and high-quality membranes.

A THF-based solution of PSF/10[Meim][TFSO₃] was casted, placed in room conditions (25°C, 40% RH) and covered by a glass dish to prevent THF from evaporating too quickly. However, the obtained composite membrane was not dense (Figure 3-1a). The DMF-based solution, casted and placed in an oven at 65°C (0% RH) also did not give a dense composite membrane (Figure 3-1b). Finally, a dense composite membrane (Figure 3-1c) was successfully prepared with NMP-based solution at 65°C and 0% RH. Therefore, NMP was chosen for PSF-based membrane preparation.

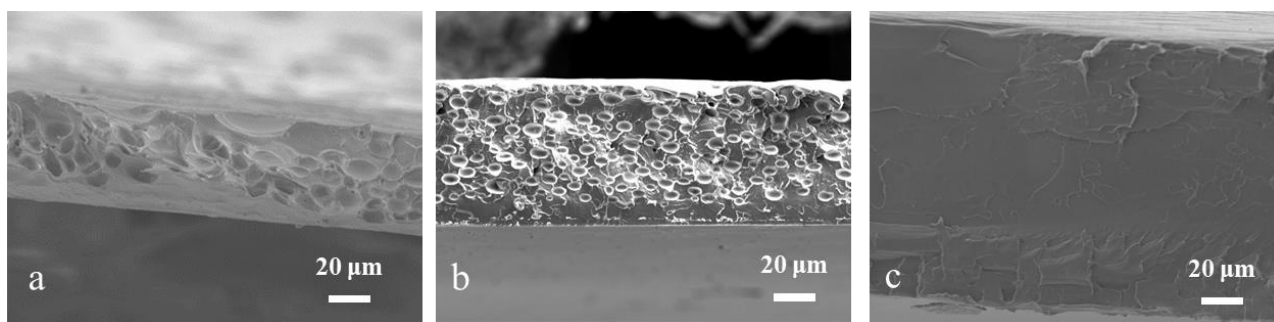


Figure 3-1 Cross-section SEM images of PSF/10[Meim][TFSO₃] membranes prepared from THF (a), DMF (b), and NMP (c) solutions

3.2.5 Optimized membrane preparation procedure

To ensure that composite membranes without defects are obtained by the solution-casting process, the polymer and ILs were placed at 100°C for 6 h to remove all moisture before use.

The preparation process of pure membranes was as follows: PSF (5 g) was dissolved in NMP (20 g) with magnetic stirring during 24 h at room temperature (25°C) to obtain a 20 wt% homogeneous solution. Then, the solution was casted on the PVA supporting membrane, placed under vacuum at 65°C, and the pressure was decreased with a rate of 5 mbar/min from atmospheric pressure down to 15 mbar. After 12 h, the obtained membrane was maintained at 85, 110 and 130°C, each time for 5 h. Finally, the membrane was dried at 150°C during 24 h (still under 15 mbar).

The composite membranes were prepared following the same procedure and a certain amount of ILs was added to the PSF solution in NMP. The upper limit for the loading capacity of imidazolium-based and alkanolamine-based ILs was 30 and 20 wt%, respectively. The names of the obtained membranes follow a common nomenclature. For example, adding 0.5 g of [Meim][TFSO₃] to the 5 g of PSF solution gave the membrane labelled PSF/10[Meim][TFSO₃], adding 1.0 g of [Meim][TFSO₃] to the 5 g of PSF solution gave the membrane labelled PSF/20[Meim][TFSO₃], and adding 1.5 g of [Meim][TFSO₃] to the 5 g of PSF solution gave the membrane labelled PSF/30[Meim][TFSO₃].

3.3 Membrane Characterization

3.3.1 Transparency of membrane

The optical images of pure PSF and PSF/IL-based composite membranes with different amounts

of ILs are showed in Figure 3-2. The pure membrane was colorless and optically transparent. As the ILs loading increased, the membranes became less transparent and turned to light yellow, especially using ILs with [Vim]⁺. The observed results may indicate an incompatibility between PSF and ILs at high IL content.

3.3.2 FT-IR spectroscopy and SEM-mapping

All membranes exhibited a characteristic peak at 1684 cm⁻¹ corresponding to a C=O stretching vibrational absorption peak (Figure 3-3). Residual solvent from casting, *N*-methyl-2-pyrrolidone, could explain this signal.

Concerning pure PSF, the peaks from 2820 cm⁻¹ to 3050 cm⁻¹ could be the aromatic and aliphatic stretching vibrations of -CH₂ group [9]. Meanwhile, the stretching vibration of the aromatic benzene rings was found from 1480 to 1590 cm⁻¹ [10]. The C-O stretching characteristic peak appeared at 1237 cm⁻¹ [11] and the S=O stretching vibration peak was found at 1149 and 1294 cm⁻¹ [12]. All these bands were observed at their distinctive places, as reported in the literature, and were observed in every composite membrane.

After incorporating different types and concentrations of ILs, the FT-IR spectra of the composite membranes changed significantly and confirmed the effective incorporation of ILs into the polymer matrix: the peak near 1024 cm⁻¹ in the composite membranes was ascribed to the S=O stretching vibrations of [TfSO₃]⁻, and the S=O absorption peak at 1182 cm⁻¹ and the C-S bonding at 1050 cm⁻¹ showed the presence of [Tf₂N]⁻. However, the bond of alkanolamine-based ILs ligand (DOBA and HDA) cannot be observed. This could be due to the overlapping of their characteristic signals with those of PSF and the inherent weakness of the N-H bond. This result confirms the effective IL incorporation inside the PSF matrix.



Figure 3-2 Optical images of PSF/ILs-based membranes

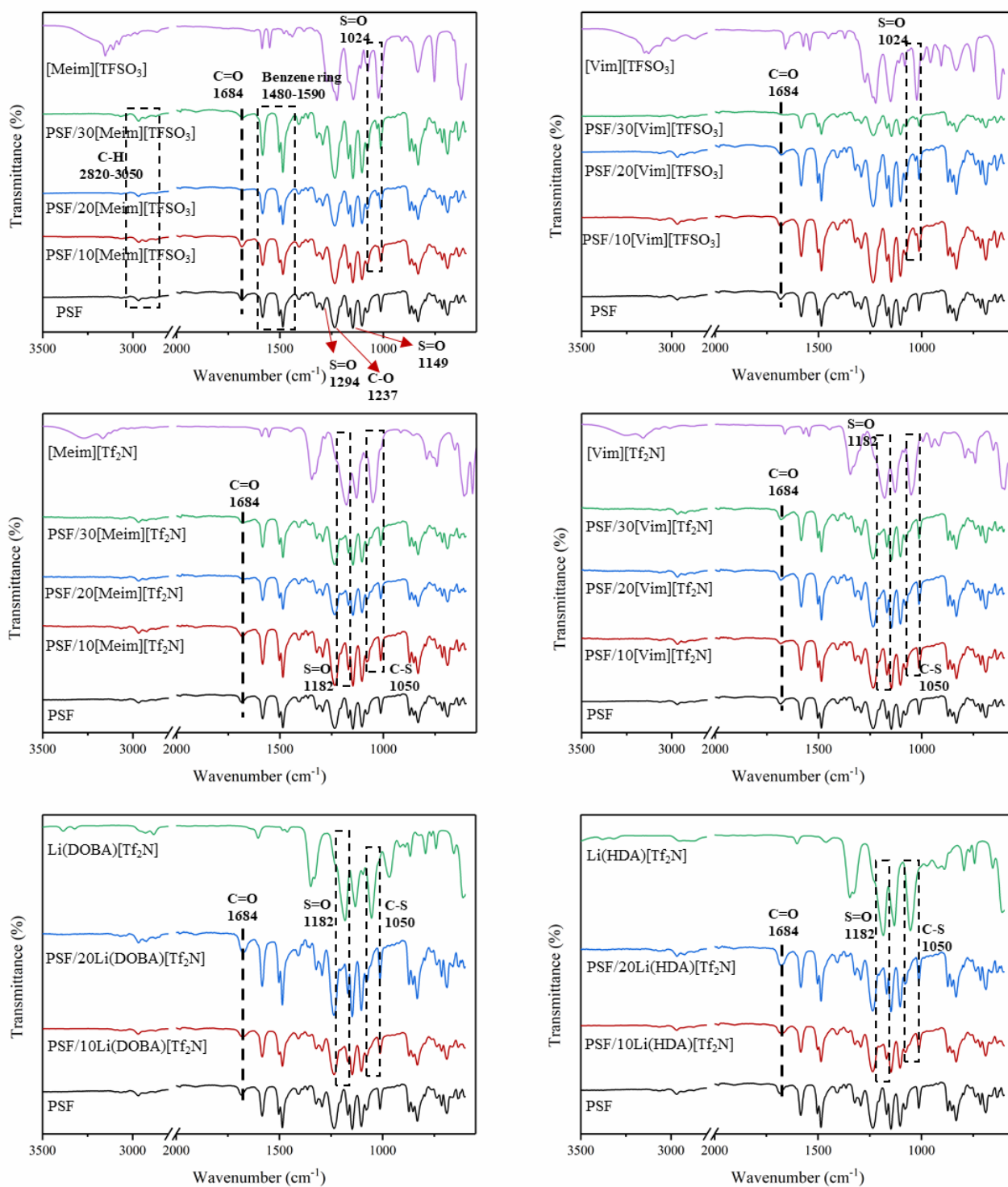


Figure 3-3 FT-IR spectra of PSF/ILs composite membranes

The microstructure of the membrane plays a decisive role in membrane permeability and mechanical properties. The pure PSF membrane has homogeneous and smooth surfaces (Figure 3-4). The SEM images of both membrane surfaces (close to air and close to PVA) containing [Meim][TfSO₃]

and [Vim][TFSO₃] are presented in Figure 3-4 and 3-5, respectively. The microscopic morphology of both sides of PSF/30[Meim][TFSO₃] exhibited a similar appearance, characterized by smooth surfaces free of observable cracks or holes. Nevertheless, the addition of [Vim][TFSO₃] to PSF resulted in a noticeable alteration in the microscopic morphology of PSF close to PVA surface: increasing the loading of [Vim][TFSO₃] made the surface rougher, so that the surface of PSF/30[Vim][TFSO₃] close to PVA exhibited numerous irregularities. A compatibility issue between PSF/[Vim][TFSO₃] and PVA could be supposed. Fluorine (F) elemental mapping of the surface, shown in Figure 3-4 and Figure 3-5, demonstrated a homogeneous distribution of ILs in PSF.

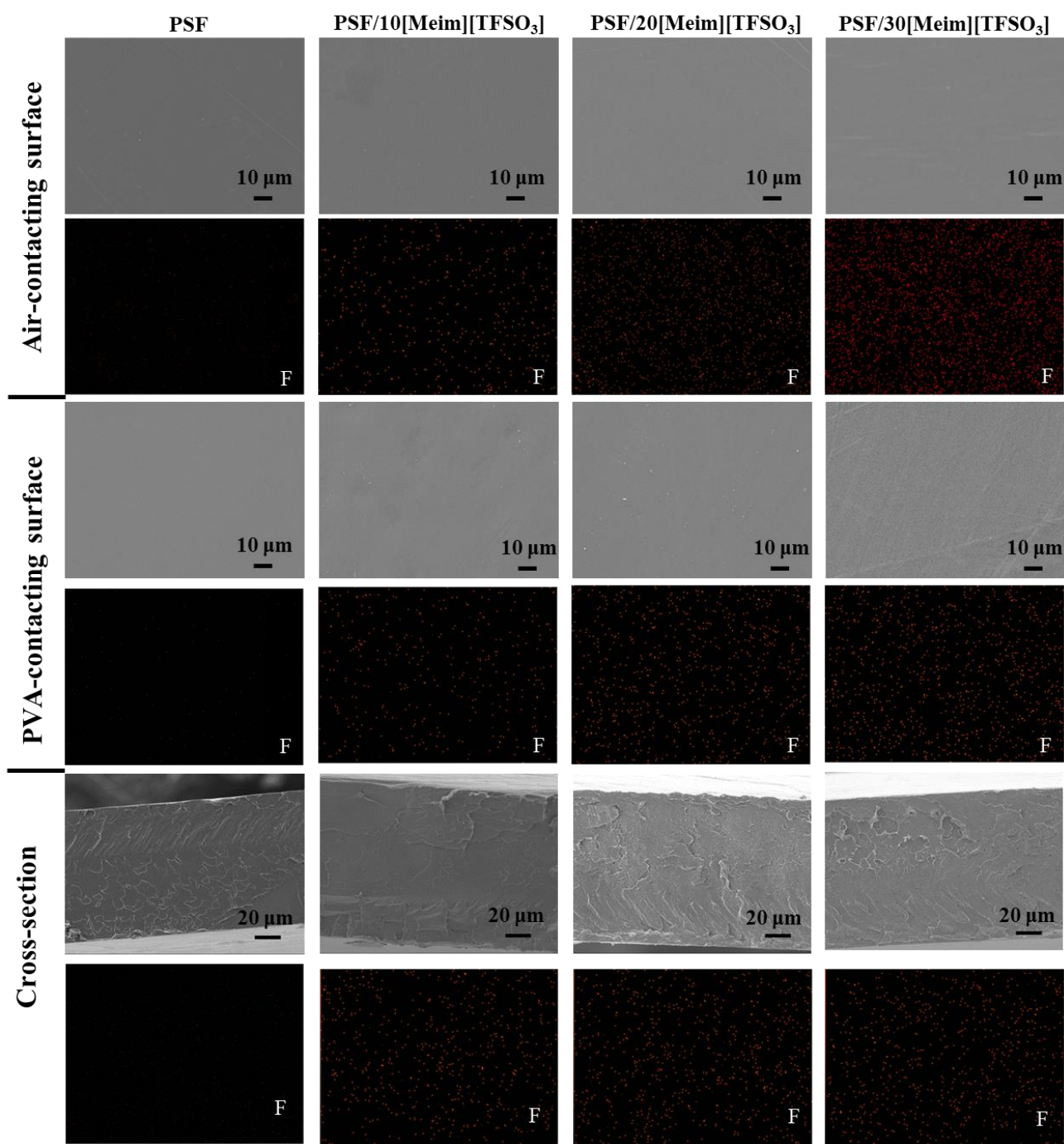
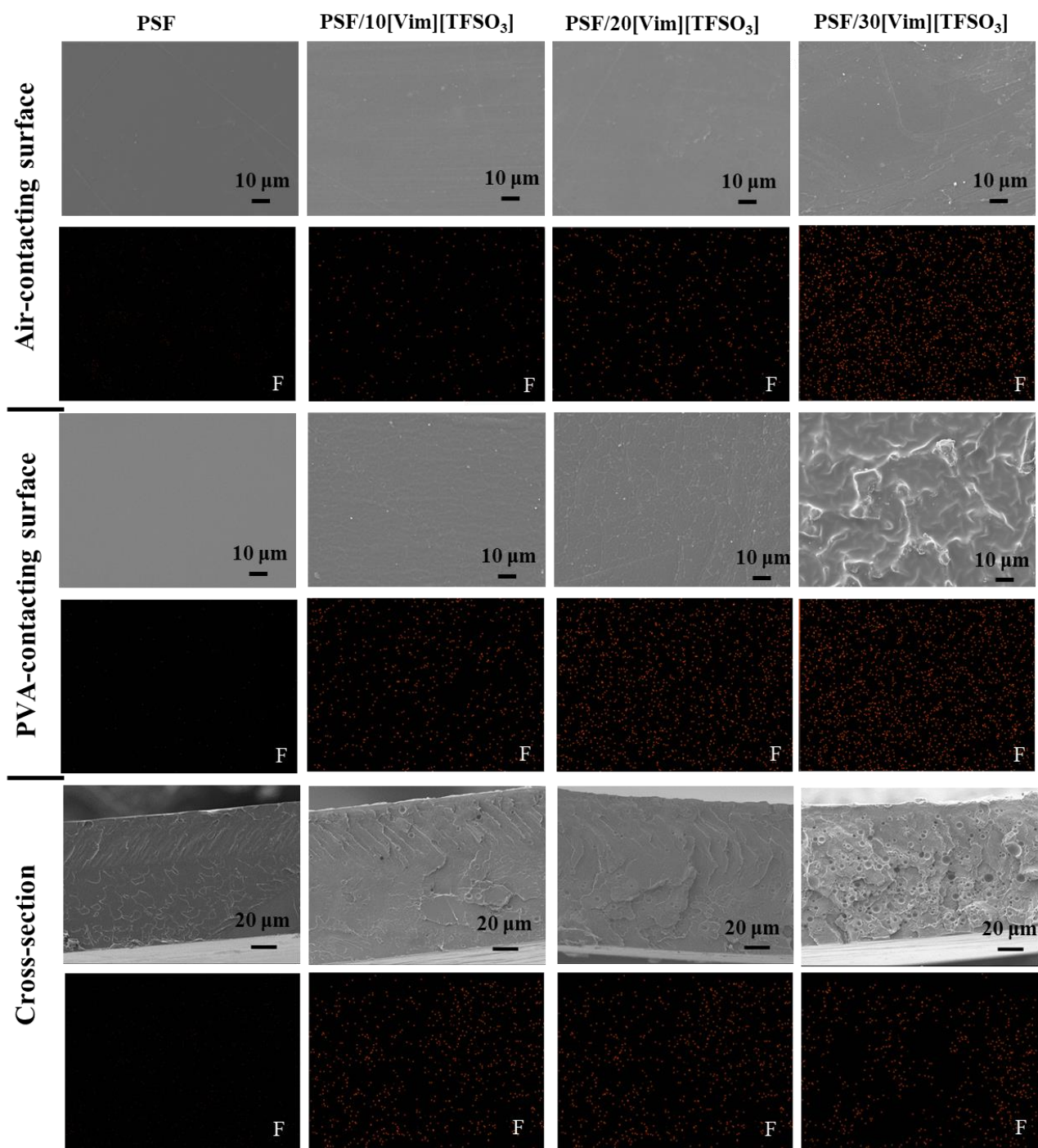


Figure 3-4 SEM images and F-mapping of PSF/[Meim][TFSO₃] membranes

Figure 3-5 SEM images and F-mapping of PSF/[Vim][TFSO₃] membranes

The SEM membrane cross-sectional images, shown in Figure 3-4 and Figure 3-5, indicated that the thickness of PSF/[Meim][TFSO₃] and PSF/[Vim][TFSO₃] was about 150 μm. The pure PSF membrane and PSF/10[Meim][TFSO₃] were dense, void-free and symmetric. However, many voids were observed in the cross-section of PSF/20[Meim][TFSO₃] and PSF/30[Meim][TFSO₃]. In contrast to PSF/[Meim][TFSO₃], the cross-sectional morphology of PSF/[Vim][TFSO₃] exhibited larger and

more abundant pores. As the loading of [Vim][TFSO₃] increased, the porosity of composite membranes also increased probably due to bad compatibility between PSF and [Vim][TFSO₃] at high IL loading. In addition, the F-mapping of membranes cross-sections showed that ILs were well distributed in the membrane thickness.

Concerning PSF/[Meim][Tf₂N] and PSF/[Vim][Tf₂N] membranes, SEM images and F-mapping of both surfaces were presented in Figure 3-6 and Figure 3-7, respectively. It can be seen from surface SEM images that there was no micro void on both surfaces, and the surfaces close to air were smooth. However, the ILs had an effect on the roughness of the surface close to PVA. As the amount of ILs increased, the rougher the surface became. When [Meim][Tf₂N] and [Vim][Tf₂N] loading was 30 wt%, it could be observed that the surface close to PVA displayed obvious textures - the same as for the PVA surface. The reason could be that the IL enhanced the interactions, more particularly hydrogen bonds F···HO between the composite membrane and the PVA support. Based on F-mapping images, F element was well distributed, indicating that [Meim][Tf₂N] and [Vim][Tf₂N] were not aggregated.

As to the membrane cross-section (Figure 3-6 and Figure 3-7), all membranes were dense except PSF/20[Vim][Tf₂N] and PSF/30[Vim][Tf₂N]: some micro voids, probably owing to a bad compatibility between PSF and [Vim][Tf₂N], could be noticed. The uniform distribution of F element in the cross-section views suggested that ILs were dispersed uniformly throughout the thickness.

To sum up, [Meim]⁺-based ILs seemed to be more appropriate than [Vim]⁺-based ILs in terms of compatibility with the PSF matrix.

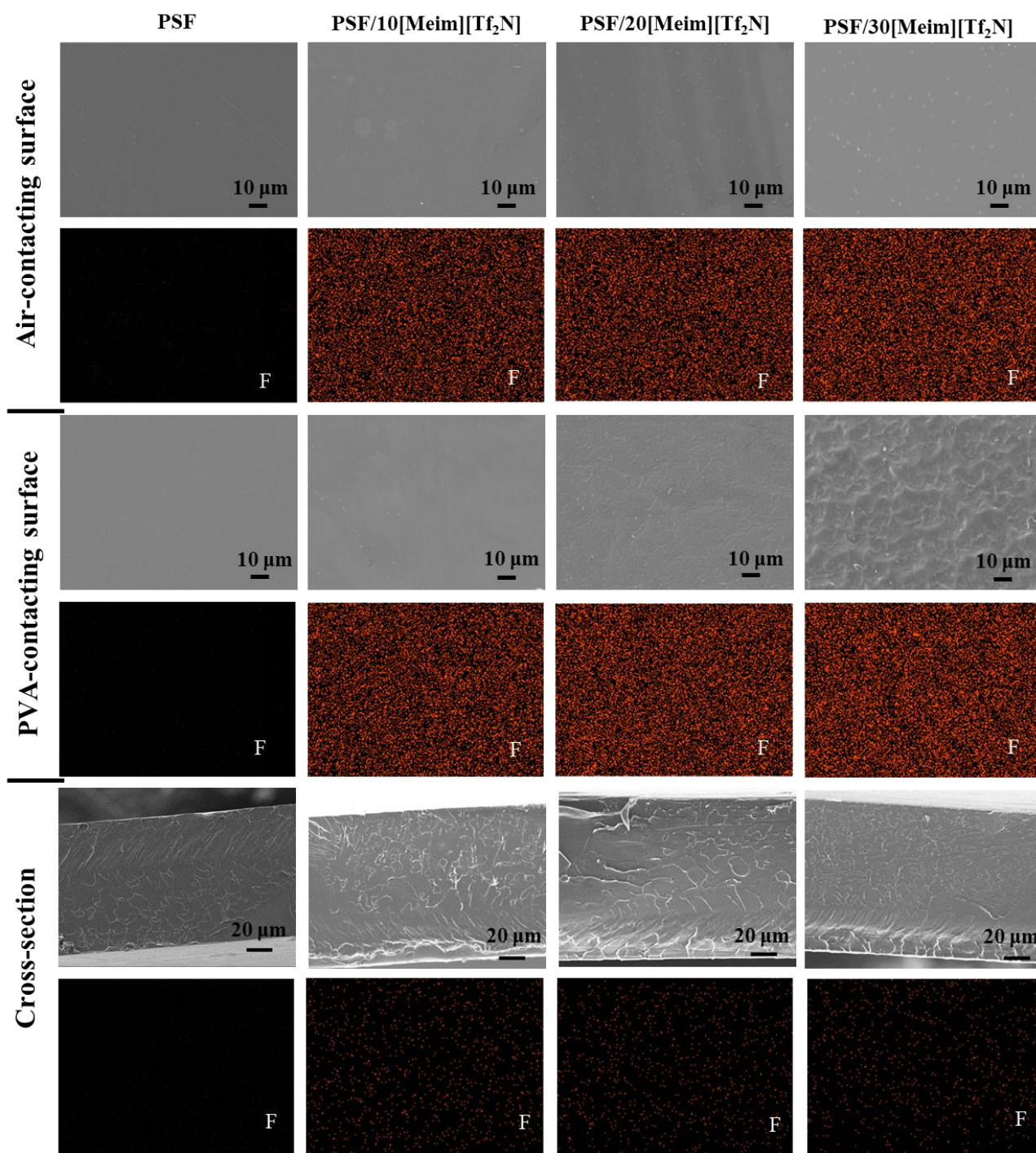
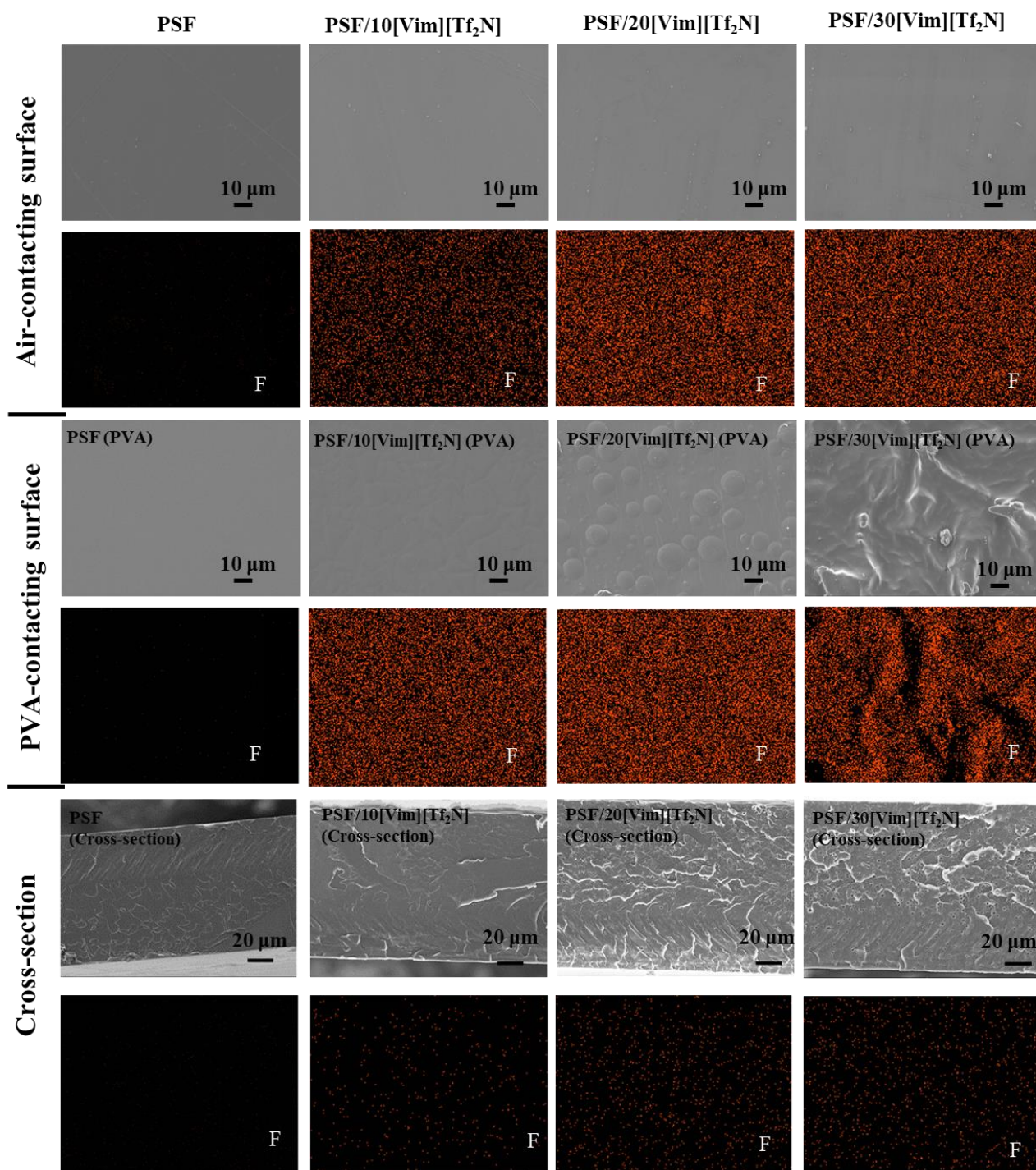


Figure 3-6 SEM images and F-mapping of PSF/[Meim][Tf₂N] membranes

Figure 3-7 SEM images and F-mapping of PSF/[Vim][Tf₂N] membranes

Concerning Li(DOBA)[Tf₂N] and Li(HDA)[Tf₂N], the SEM images and F-mapping of the surfaces (Figure 3-8) revealed the homogenous IL dispersion whatever the loading, as no agglomeration was observed. The surfaces close to air were smooth and non-porous as compared to the non-porous and non-smooth surfaces close to PVA.

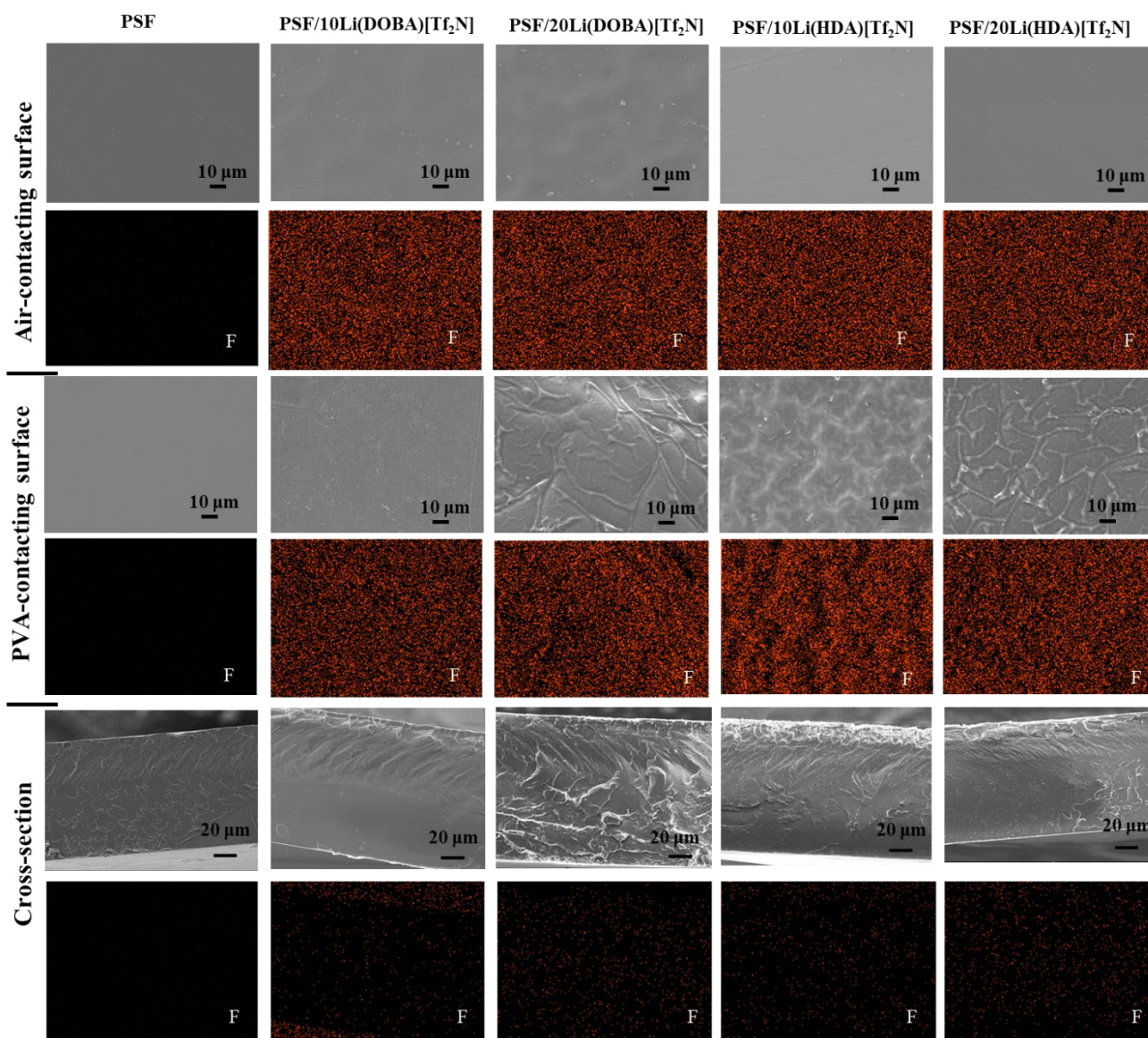


Figure 3-8 SEM images and F-mapping of PSF/Li(DOBA) [Tf₂N] and PSF/Li(HDA) [Tf₂N] membranes

The cross-section images and F-mapping (Figure 3-8) revealed that all composite membranes were dense, with a well-distributed F element in the thickness, indicating a good compatibility between PSF and Li(DOBA) [Tf₂N] or Li(HDA) [Tf₂N].

3.3.3 Thermal characterization

3.3.3.1 Thermal degradation

TGA was carried out to study the thermal stability of the composite membranes (Figure 3-9). All

membranes had a weight loss of about 6% from 175°C to 200°C, which corresponded to residual solvent, *N*-methyl-2-pyrrolidone, as previously observed in FT-IR.

Different behaviors were obtained for PSF/imidazolium-based ILs (two-step degradation) and PSF/alkanolamine-based ILs (one-step degradation) composite membranes.

For PSF/imidazolium-based ILs composite membranes, the curves of PSF/30[Meim][TFSO₃] (Figure 3-9a) and PSF/30[Vim][TFSO₃] (Figure 3-9b) were taken as example. Excluding the weight loss due to NMP, the 5 % weight loss temperature ($T_{5\%}$) of PSF membrane was 502°C, and the $T_{5\%}$ of [Meim][TFSO₃] and [Vim][TFSO₃] were 314°C and 289°C, respectively (Table 2-2). The composite membranes showed a $T_{5\%}$ of 408°C and 394°C for PSF/30[Meim][TFSO₃] and PSF/30[Vim][TFSO₃], respectively. The first stage from 394°C to 453°C, or from 380°C to 432°C, corresponded to the degradation of ILs ([Meim][TFSO₃] or [Vim][TFSO₃], respectively), with weight loss percentages corresponding to the ILs loadings (10, 20 and 30%). The ILs degradation temperature in the composite membrane was higher than the thermal degradation temperature of initial ILs, indicating that the PSF protected the ILs from degradation. The second stage of degradation corresponded to the degradation of PSF, which was lower than $T_{5\%}$ of pure PSF: the ILs catalyzed the thermal degradation of PSF.

For PSF/alkanolamine-based ILs membranes, PSF/Li(DOBA)[Tf₂N] was taken as an example (Figure 3-9e). The TGA curve of PSF/20Li(DOBA)[Tf₂N] showed a one-step degradation process with $T_{5\%} = 486^\circ\text{C}$, indicating a low decrease of the thermal stability of PSF by the IL ($T_{5\%}$ of PSF is 502°C).

In conclusion, the TGA curves demonstrated that the composite membranes exhibited sufficient thermal stability for gas separation application.

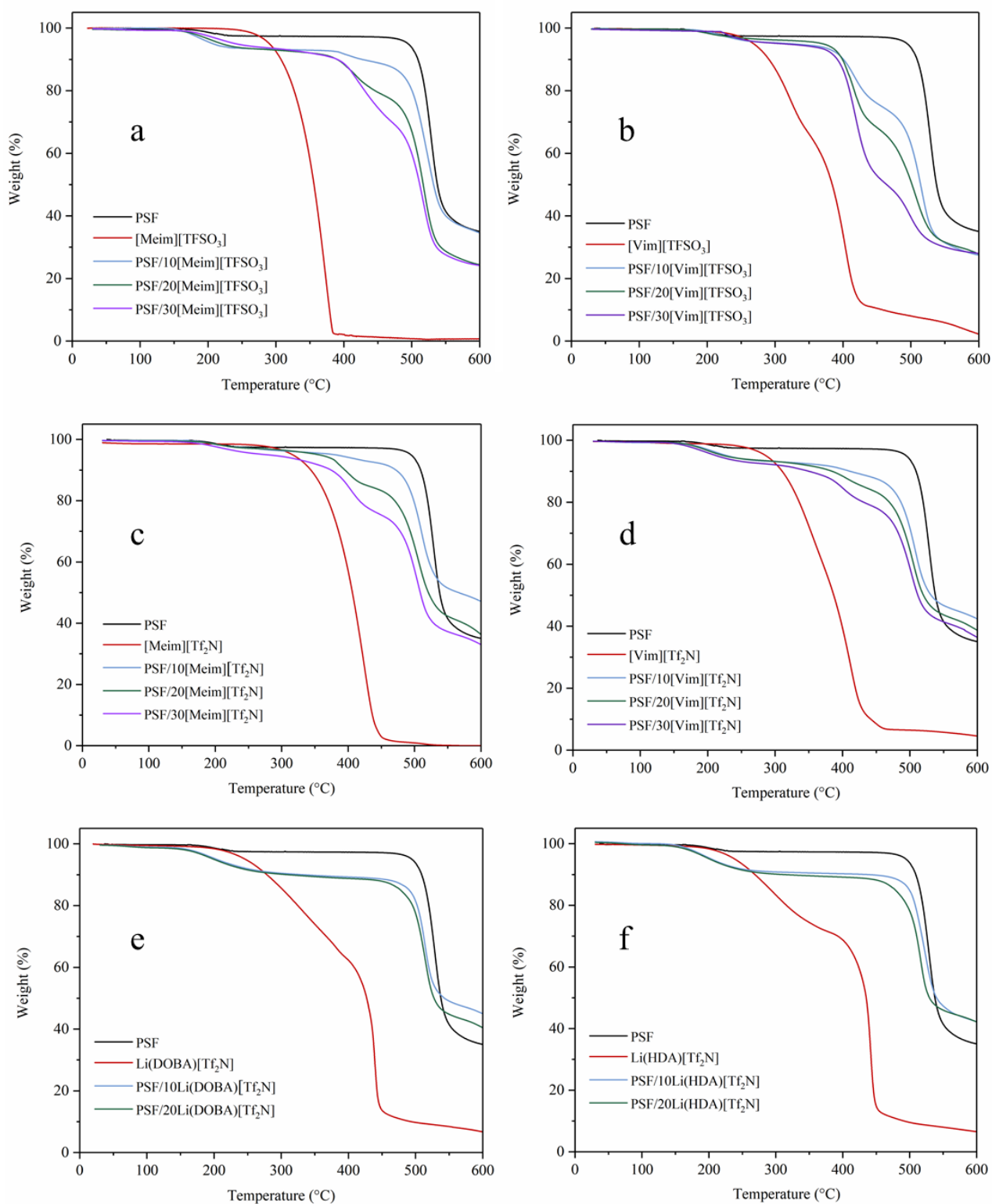


Figure 3-9 TGA curves of PSF/IL composite membranes

3.3.3.2 Differential scanning calorimetry (DSC)

The prepared composite membranes were characterized by DSC to assess the effect of ILs on their thermal properties. The obtained thermograms and the glass transition temperatures (T_g) from the second heating were shown in Annex 4 and Table 3-3. As expected, T_g of the composite membranes was lower than that of pure PSF membrane ($T_g = 180^\circ\text{C}$), with a gradual decrease by increasing the IL content. Indeed, ILs serve as plasticizer, reducing the stiffness of PSF, as already observed in the literature [13].

To estimate the glass transition temperature of homogeneous polymer blends, it is common to employ the Fox equation (Equation 3-1) [14,15] or the Gordon-Taylor equation (Equation 3-2) [16].

$$\frac{1}{T_g} = \frac{\omega_1}{T_{g1}} + \frac{\omega_2}{T_{g2}} \quad (\text{Equation 3-1})$$

$$T_g = \frac{\omega_1 \cdot T_{g1} + k \cdot \omega_2 \cdot T_{g2}}{\omega_1 + k \cdot \omega_2} \quad (\text{Equation 3-2})$$

where T_g is the glass transition temperature of the blend, ω_1 and ω_2 are the weight fractions of the two components in the blend, T_{g1} and T_{g2} are the glass transition temperatures of the individual components, and k is a constant.

Except PSF/[Vim][TFSO₃] (no T_g value obtained for this IL), all PSF-based composite membranes gave calculated T_g which are different from those obtained experimentally (Table 3-3). Therefore, Fox equation is not suited to describe PSF-based composite membranes.

If the more complete Gordon-Taylor relation is used, Equation 3-2 can be modified and linearized to give Equation 3-3, very useful to check the validity of the law and to deduce the coefficient k :

$$\frac{T_g - T_{gPSF}}{T_{gIL} - T_g} = k \frac{1 - \omega_{PSF}}{\omega_{PSF}} \quad (\text{Equation 3-3})$$

where T_g is the glass transition temperature of the composite membrane, ω_{PSF} and ω_{IL} are the weight fractions of PSF and IL in the membrane, respectively, T_{gPSF} and T_{gIL} are the glass transition temperatures of PSF and IL, respectively, and k is a constant.

Table 3-3 T_g value of PSF/IL composite membranes

Sample	T_g (°C)/Experiment	T_g (°C)/Calculated (Equation 3-1)
PSF	182	-
PSF/10[Meim][TFSO ₃]	165	139
PSF/20[Meim][TFSO ₃]	127	109
PSF/30[Meim][TFSO ₃]	114	87
PSF/10[Vim][TFSO ₃]	150	nd
PSF/20[Vim][TFSO ₃]	136	nd
PSF/30[Vim][TFSO ₃]	128	nd
PSF/10[Meim][Tf ₂ N]	152	140
PSF/20[Meim][Tf ₂ N]	131	110
PSF/30[Meim][Tf ₂ N]	101	88
PSF/10[Vim][Tf ₂ N]	144	134
PSF/20[Vim][Tf ₂ N]	106	101
PSF/30[Vim][Tf ₂ N]	99	77
PSF/10Li(DOBA)[Tf ₂ N]	148	140
PSF/20Li(DOBA)[Tf ₂ N]	90	111
PSF/10Li(HDA)[Tf ₂ N]	136	144
PSF/20Li(HDA)[Tf ₂ N]	84	116

nd – no data available

The linear fits of T_g by Gordon-Taylor equation (Figure 3-10) showed R-square values for PSF/[Meim][TFSO₃], PSF/[Meim][Tf₂N], PSF/[Vim][Tf₂N], and PSF/Li(HDA)[Tf₂N] exceeding 0.98. This revealed that these ILs were well distributed within the membrane and formed homogeneous mixtures with PSF. However, contrary to the SEM observations, Li(DOBA)[Tf₂N] seemed to be non-ideally distributed within PSF. This difference may come from the fact all membranes contained slightly different quantities of residual casting solvent (Figure 3-9), which modified differently each T_g .

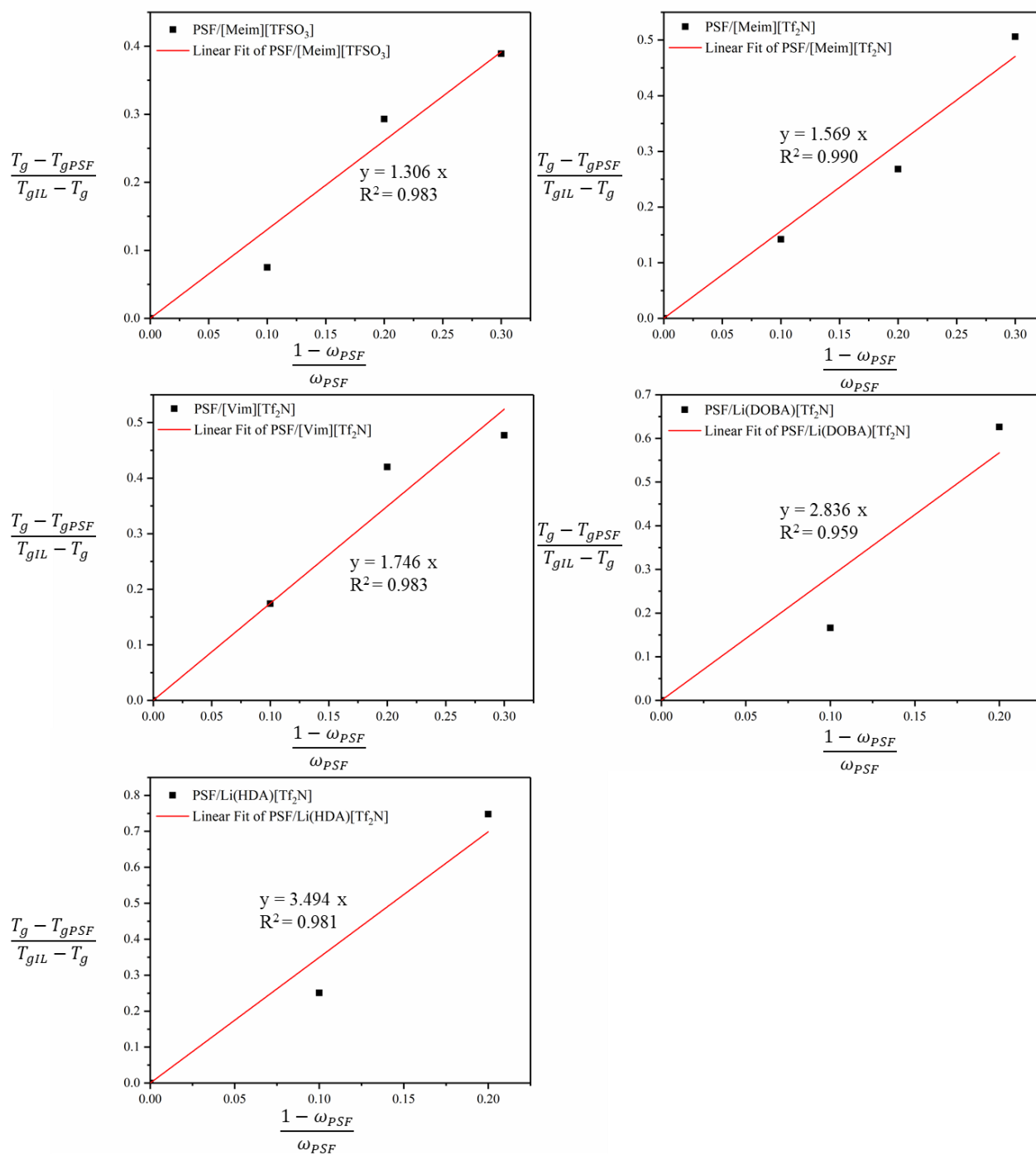


Figure 3-10 Linear fit of T_g by Gordon-Taylor equation (Equation 3-3)

3.3.4 Surface energy

The surface energy of membranes was measured by contact angle measurements in order to characterize their wettability. The contact angle values for both surfaces of PSF and PSF-based composite membranes are shown in Table 3-4 (surface close to air) and Table 3-5 (surface close to PVA). As the amount of added ILs increased, the contact angle of water and glycerol gradually decreased, and the diiodomethane contact angle gradually increased. The reason is that ILs, as hydrophilic additives containing hydrophilic groups (-NH, -NH₂ and -OH), enhanced the hydrophilicity of PSF.

The Owens - Wendt method was used to determine the surface energy (γ_s), and dispersive (γ_s^d) and polar (γ_s^p) components. The obtained results are presented in Table 3-4 and Table 3-5. As compared to pure PSF, the composite membranes had higher values of γ_s and γ_s^p due to the ILs presence. It can be seen that the difference of γ_s^p between PSF/10[Meim][TFSO₃] and PSF/10[Meim][Tf₂N] was much higher than that between PSF/10[Meim][TFSO₃] and PSF/10[Vim][TFSO₃]. The same situation was observed for all PSF/imidazolium-based IL composite membranes. Moreover, the γ_s^p value of PSF/imidazolium-based IL with [Tf₂N]⁻ was close to that of PSF/alkanolamine-based IL with [Tf₂N]⁻. Therefore, the impact of anion on the surface energy of the composite membranes is more important than that of cation due to the presence of the highly polar F element within all studied anions.

Additionally, the [Tf₂N]⁻ anion had a stronger influence on the surface energy as compared to [TFSO₃]⁻ due to a higher concentration of F elements (Figure 3-4 and Figure 3-7). Concerning imidazolium-based ILs, except the influence of anion, the cation also contains the polar component -NH, thereby exerting a pronounced impact. The inclusion of -NH₂ (DOBA), -O- (DOBA), -OH (HDA), -NH (HDA), and F ([Tf₂N]⁻) in alkanolamine-based ILs enhances the surface polarity of PSF.

Finally, one can see that the membrane surface values of γ_s^p close to air and PVA are rather similar for the same membrane, indicating that the IL distribution on both surfaces is practically the same, which is consistent with F-mapping characterization.

Table 3-4 Solvent contact angles and surface energy of PSF-based membranes (air-contacting surface)

Sample	Contact angle (°)			γ_s	γ_s^d	γ_s^p
	Water	Diiodomethane	Glycerol			
PSF	85.1 ± 0.9	21.2 ± 0.8	88.5 ± 2.0	40.7	40.0	0.7
PSF/10[Meim][TFSO ₃]	78.0 ± 1.5	23.1 ± 1.1	76.5 ± 1.6	43.6	41.3	2.3
PSF/20[Meim][TFSO ₃]	71.1 ± 1.7	25.5 ± 0.8	71.5 ± 1.1	44.9	40.2	4.6
PSF/30[Meim][TFSO ₃]	66.7 ± 1.4	31.5 ± 1.4	67.7 ± 1.0	45.2	38.2	6.9
PSF/10[Vim][TFSO ₃]	75.0 ± 1.4	23.8 ± 0.5	73.0 ± 1.4	44.6	41.3	3.2
PSF/20[Vim][TFSO ₃]	71.9 ± 1.0	35.2 ± 0.6	58.8 ± 0.9	46.3	40.5	5.8
PSF/30[Vim][TFSO ₃]	69.6 ± 1.5	40.5 ± 0.9	53.5 ± 0.7	46.6	39.0	7.6
PSF/10[Meim][Tf ₂ N]	77.9 ± 1.1	28.4 ± 0.2	80.6 ± 0.4	62.6	43.9	18.7
PSF/20[Meim][Tf ₂ N]	71.3 ± 1.0	31.5 ± 0.2	77.6 ± 0.6	63.7	43.4	20.3
PSF/30[Meim][Tf ₂ N]	65.6 ± 0.4	34.8 ± 0.3	68.3 ± 0.8	65.4	43.5	22.0
PSF/10[Vim][Tf ₂ N]	71.8 ± 0.3	32.3 ± 0.2	76.4 ± 0.3	63.7	43.5	20.3
PSF/20[Vim][Tf ₂ N]	69.2 ± 0.6	33.4 ± 0.1	72.0 ± 0.4	64.4	43.6	21.0
PSF/30[Vim][Tf ₂ N]	67.9 ± 0.6	38.1 ± 0.3	63.0 ± 0.5	65.5	43.7	21.8
PSF/10Li(DOBA)[Tf ₂ N]	70.1 ± 0.2	28.8 ± 0.2	73.7 ± 0.1	63.9	44.2	19.7
PSF/20Li(DOBA)[Tf ₂ N]	66.6 ± 1.0	36.7 ± 0.2	72.2 ± 0.3	64.8	43.1	21.8
PSF/10Li(HDA)[Tf ₂ N]	74.1 ± 0.3	26.3 ± 0.2	73.7 ± 0.2	64.1	44.5	19.6
PSF/20Li(HDA)[Tf ₂ N]	70.8 ± 1.2	31.0 ± 0.1	67.0 ± 0.1	64.8	44.2	20.6

Table 3-5 Solvent contact angles and surface energy of PSF-based membranes (PVA-contacting surface)

Sample	Contact angle (°)			γ_s	γ_s^d	γ_s^p
	Water	Diiodomethane	Glycerol			
PSF	86.6 ± 1.0	22.9 ± 0.7	88.7 ± 1.9	40.4	39.9	0.5
PSF/10[Meim][TfSO ₃]	77.9 ± 1.2	24.2 ± 0.5	77.5 ± 0.5	43.0	40.6	2.4
PSF/20[Meim][TfSO ₃]	72.0 ± 1.9	26.7 ± 0.8	73.9 ± 0.7	43.7	39.4	4.3
PSF/30[Meim][TfSO ₃]	69.9 ± 1.4	32.3 ± 1.4	70.1 ± 0.4	43.8	38.0	5.7
PSF/10[Vim][TfSO ₃]	72.9 ± 1.1	26.9 ± 0.7	76.9 ± 1.1	42.6	38.7	3.9
PSF/20[Vim][TfSO ₃]	66.8 ± 1.8	38.3 ± 1.0	65.3 ± 1.0	44.2	36.2	7.9
PSF/30[Vim][TfSO ₃]	74.5 ± 1.6	40.8 ± 0.9	74.8 ± 0.7	39.3	34.4	4.9
PSF/10[Meim][Tf ₂ N]	80.5 ± 0.4	30.4 ± 0.4	77.8 ± 0.2	62.5	44.2	18.3
PSF/20[Meim][Tf ₂ N]	77.5 ± 0.4	33.9 ± 0.3	74.7 ± 0.4	63.1	43.9	19.2
PSF/30[Meim][Tf ₂ N]	70.6 ± 0.5	37.1 ± 0.2	66.3 ± 0.6	64.9	43.8	21.1
PSF/10[Vim][Tf ₂ N]	77.3 ± 0.6	39.4 ± 0.3	77.6 ± 0.5	62.5	43.0	19.5
PSF/20[Vim][Tf ₂ N]	74.8 ± 0.8	42.9 ± 0.2	73.2 ± 0.3	63.1	42.8	20.4
PSF/30[Vim][Tf ₂ N]	72.8 ± 1.0	38.7 ± 0.1	66.2 ± 0.6	64.5	43.8	20.7
PSF/10Li(DOBA)[Tf ₂ N]	76.1 ± 0.5	45.5 ± 0.5	70.2 ± 0.2	63.1	42.8	20.4
PSF/20Li(DOBA)[Tf ₂ N]	71.3 ± 0.8	48.8 ± 0.2	66.8 ± 0.3	64.0	42.2	21.8
PSF/10Li(HDA)[Tf ₂ N]	76.8 ± 0.8	30.2 ± 0.3	70.2 ± 0.4	63.9	44.7	19.3
PSF/20Li(HDA)[Tf ₂ N]	71.5 ± 0.4	31.9 ± 0.1 ±	64.9 ± 0.2	65.2	44.5	20.6

Additionally, enhancing the surface polarity of the membrane surface tends to decrease the solubility of non-polar gases (N_2 , O_2 and CO_2). However, the gases with higher critical temperature (Table 1-5, gases critical temperature order: $CO_2 > O_2 > N_2$) are more condensable and, therefore, more soluble, this behavior being especially pronounced in membranes with high surface polarity [17]. Therefore, our membranes, with high surface polarity, are more suitable for CO_2 solubility as compared to N_2 and O_2 , which is desirable in this study.

3.3.5 Mechanical properties

In general, additives can reduce the mechanical properties of a polymer matrix because of their poor compatibility and interfacial issues [18]. The effect of ILs on the mechanical properties is shown in Table 3-6.

PSF is a brittle material with a high tensile strength (75.8 MPa), a high Young's modulus (2690 MPa) and a low strain at break (3.8%) (Table 3-6). The addition of imidazolium-based ILs decreased Young's modulus due to the plasticizing ability of ILs, thus confirming the lower glass transition temperatures measured by DSC for the composite membranes as compared with pure PSF (Table 3-3). The same trend was observed for the strain at break: it increased, and the effect was more pronounced with $[Vim]^+$ than with $[Meim]^+$, and also higher with $[TFSO_3]^-$ as compared to $[Tf_2N]^-$. The tensile strength of composite membranes decreased with higher IL concentration, certainly owing to an incompatibility between PSF and ILs that appears at high IL loading.

For PSF/alkanolamine-based ILs composite membranes, Young's modulus and tensile strength globally decreased as compared with pure PSF, while their strain at break was close to that of pure PSF (Table 3-6). Almost no difference was observed between PSF/Li(DOBA)[Tf_2N] and PSF/Li(HDA)[Tf_2N] composite membranes with the same IL loading, indicating that Li(DOBA)[Tf_2N] and Li(HDA)[Tf_2N] had the same influence on the PSF mechanical properties.

To conclude, ILs reduce the Young's modulus and the tensile strength of PSF. Additionally, the plasticizing effect of ILs on PSF has also been confirmed.

Table 3-6 Mechanical properties of PSF and PSF/ILs membranes

Sample	Young's modulus (MPa)	Tensile strength (MPa)	Strain at break (%)
PSF	2690 ± 270	75.8 ± 4.9	3.8 ± 0.3
PSF/10[Meim][TFSO ₃]	2540 ± 119	71.2 ± 6.5	9.7 ± 2.1
PSF/20[Meim][TFSO ₃]	2500 ± 160	61.3 ± 5.6	8.8 ± 2.3
PSF/30[Meim][TFSO ₃]	2240 ± 173	54.0 ± 4.1	9.1 ± 1.6
PSF/10[Vim][TFSO ₃]	2520 ± 121	60.5 ± 4.9	18.4 ± 1.3
PSF/20[Vim][TFSO ₃]	2443 ± 127	39.2 ± 5.2	15.8 ± 1.1
PSF/30[Vim][TFSO ₃]	2330 ± 169	34.0 ± 6.7	12.4 ± 0.9
PSF/10[Meim][Tf ₂ N]	2470 ± 91.8	73.7 ± 1.0	4.0 ± 0.1
PSF/20[Meim][Tf ₂ N]	2190 ± 120	60.0 ± 1.2	3.6 ± 0.3
PSF/30[Meim][Tf ₂ N]	2040 ± 130	60.5 ± 2.2	3.8 ± 0.1
PSF/10[Vim][Tf ₂ N]	2760 ± 142	70.8 ± 3.5	2.6 ± 0.2
PSF/20[Vim][Tf ₂ N]	2530 ± 123	67.2 ± 2.6	6.8 ± 0.7
PSF/30[Vim][Tf ₂ N]	2230 ± 180	46.1 ± 3.9	10.1 ± 0.4
PSF/10Li(DOBA)[Tf ₂ N]	2300 ± 144	60.2 ± 4.6	4.6 ± 0.3
PSF/20Li(DOBA)[Tf ₂ N]	2230 ± 147	57.8 ± 2.4	4.1 ± 0.2
PSF/10Li(HDA)[Tf ₂ N]	2680 ± 231	70.3 ± 2.9	3.1 ± 0.1
PSF/20Li(HDA)[Tf ₂ N]	2160 ± 170	57.7 ± 1.1	4.4 ± 0.2

3.3.6 Gas separation

Based on “time-lag method”, the pressure-time curves can be obtained. The permeability coefficient P is calculated by Equation 3-4.

$$P = \frac{L \times V_a \times T_0}{S_a \times P_1 \times P_0 \times T_m} \frac{dp_2}{dt} \quad \text{Equation (3-4)}$$

where L is the thickness of membrane, V_a is the downstream volume (256 cm³), S_a represents the

surface of membrane (11.3 cm^2), P_1 is the upstream compartment pressure (4 bars), $\frac{dp_2}{dt}$ is the slope of the P_2 -t curve, P_0 is 1 atm, T_m is the experimental (measurement) temperature (298 K). The permeation coefficient (P) unit is typically defined as Barrer and $1 \text{ Barrer} = 10^{-10} \text{ cm}^3 \text{ (STP) cm}/(\text{cm}^2 \text{ s cmHg})$.

The diffusion coefficient D is estimated from the time-lag value t_L :

$$D = \frac{L^2}{6 t_L} \quad \text{Equation (3-5)}$$

The permeability coefficient P and the ideal gas selectivity α are described in Equation 1-1 and Equation 1-2, respectively.

In general, the main factor controlling the gas sorption is the condensing capacity of the permeant gases [19]: the polymer gases solubility should follow the order: $S(\text{CO}_2) > S(\text{O}_2) > S(\text{N}_2)$. According to gases Van Der Waals volume order: $V(\text{O}_2) < V(\text{N}_2) < V(\text{CO}_2)$ [20], the gases diffusion order within a polymer should be $D(\text{O}_2) > D(\text{N}_2) > D(\text{CO}_2)$ [21]. $S(\text{CO}_2)$ is much higher than $S(\text{O}_2)$ and $S(\text{N}_2)$, therefore, the gases permeability should follow the order: $P(\text{N}_2) < P(\text{O}_2) < P(\text{CO}_2)$.

The gases (CO_2 , N_2 and O_2) permeability and selectivity coefficients are presented in Figure 3-11 and Table 3-7, respectively. The corresponding diffusion and solubility coefficients are shown in Figure 3-12 and Figure 3-13, respectively. As expected, the orders of permeability and solubility coefficients within PSF-based membranes followed the well-established order: $P(\text{N}_2) < P(\text{O}_2) < P(\text{CO}_2)$ and $S(\text{CO}_2) > S(\text{O}_2) > S(\text{N}_2)$. Meanwhile, the order of diffusion coefficient is following: $D(\text{O}_2) > D(\text{N}_2) > D(\text{CO}_2)$, except for PSF/20[Meim][TFSO₃], PSF/10Li(DOBA)[Tf₂N] and PSF/10Li(HDA)[Tf₂N]: $D(\text{N}_2) > D(\text{O}_2) > D(\text{CO}_2)$. This result can be explained by membrane morphology.

According to Equation 1-1, the gas permeability coefficient of composite membrane mainly depends on IL influence on the diffusion and solubility coefficients. The membrane solubility coefficient depends on the membrane surface polarity, free volume and IL absorption capacity. Only PSF/20[Meim][Tf₂N] membrane has higher solubility coefficient as compared to pure PSF (Figure 3-13). And this, whatever the gas is. The higher polarity and more free volume in case of composite membranes can explain this result.

One can see that the IL loading has little effect on the CO_2 diffusion coefficient (Figure 3-12) confirming no specific interactions between CO_2 and membrane components (i.e. IL and PSF). In fact, the six ILs mainly affect the gases diffusion in PSF by affecting the membrane microstructure. The effect of 3 imidazolium-based ILs ([Meim][Tf₂N], [Vim][TFSO₃], [Vim][Tf₂N]) on O_2 diffusion within

PSF is greater than that on N₂ owing to the gas molecule size (Table 1-5). However, O₂ diffusion behavior of PSF/[Meim][Tf₂N] is quite different from PSF/[Vim][Tf₂N] and PSF/[Vim][TFSO₃] due to the different membrane microstructure (Figure 3-5 and Figure 3-7). Both [Meim][TFSO₃] and alkanolamine-based ILs have more influence on N₂ diffusion as compared with that of O₂. This can be explained by a more pronounced effect of these ILs on membranes. These composite membranes with a certain amount IL loading (20 wt% of [Meim][TFSO₃], 10 wt% of alkanolamine-based ILs) present the highest N₂ diffusion. In addition, when the IL loading is higher, the N₂ diffusion decrease. The reason may be that ILs presence decreases the volume for the N₂ diffusion within composite membrane.

The CO₂/O₂, CO₂/N₂ and O₂/N₂ selectivities of pure PSF membrane was 4.5, 17.7 and 3.9, respectively (Table 3-7). The CO₂/N₂ and O₂/N₂ selectivity of PSF/ILs composite membranes decreased slightly. The CO₂/O₂ selectivity of PSF/10[Vim][TFSO₃], PSF/20[Vim][TFSO₃], PSF/10[Meim][Tf₂N] and PSF/20Li(DOBA)[Tf₂N] was enhanced by 4.5%, 8.9%, 8.9% and 2.2%, respectively, as compared to pure PSF. The CO₂/O₂ selectivity of PSF/30[Meim][TFSO₃] and PSF/20Li(HDA)[Tf₂N] was the same as that for pure PSF. In addition, the CO₂/O₂ selectivity of other composite membranes showed a slight decrease.

One can see that the CO₂/O₂ and CO₂/N₂ selectivities of PSF/20 alkanolamine-based ILs are slightly higher than those of PSF/10 alkanolamine-based ILs. Therefore, one can suppose that further increasing the alkanolamine-based ILs content (using suitable compatibilizer) could improve the membrane gas selectivity performance.

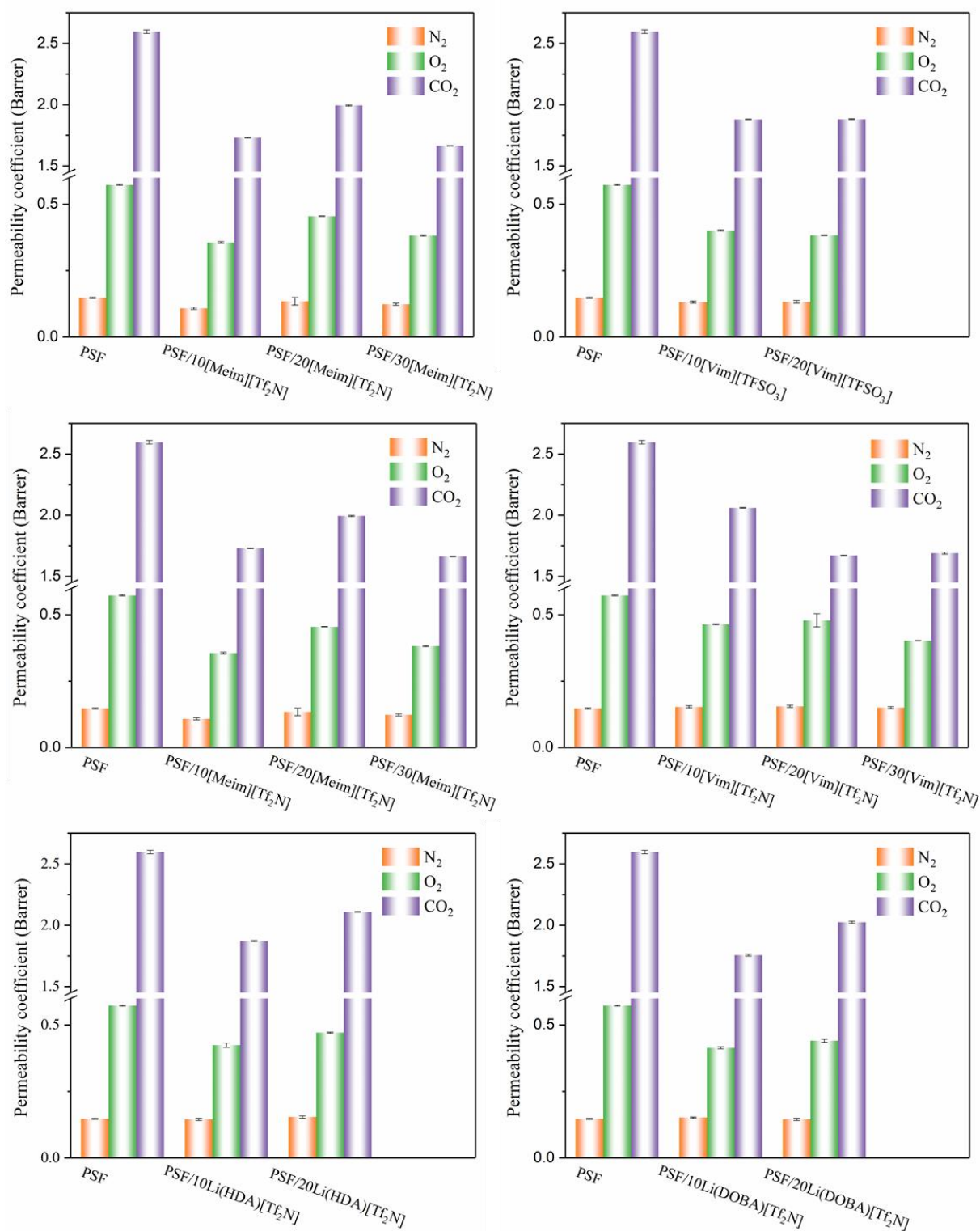


Figure 3-11 Permeability coefficients of PSF/IL-based membranes

Table 3-7 Gas selectivity of PSF/IL-based membranes

Sample	α		
	CO ₂ /O ₂	CO ₂ /N ₂	O ₂ /N ₂
PSF	4.5	17.7	3.9
PSF/10[Meim][TFSO ₃]	4.4	10.9	2.5
PSF/20[Meim][TFSO ₃]	4.0	8.2	2.0
PSF/30[Meim][TFSO ₃]	4.5	13.9	3.1
PSF/10[Vim][TFSO ₃]	4.7	14.3	3.1
PSF/20[Vim][TFSO ₃]	4.9	14.3	2.9
PSF/30[Vim][TFSO ₃]	-	-	1.0
PSF/10[Meim][Tf ₂ N]	4.9	16.0	3.4
PSF/20[Meim][Tf ₂ N]	4.4	14.9	3.4
PSF/30[Meim][Tf ₂ N]	4.4	13.5	3.1
PSF/10[Vim][Tf ₂ N]	4.4	13.5	3.0
PSF/20[Vim][Tf ₂ N]	3.5	10.8	3.1
PSF/30[Vim][Tf ₂ N]	4.2	11.3	2.7
PSF/10Li(DOBA)[Tf ₂ N]	4.2	11.6	2.7
PSF/20Li(DOBA)[Tf ₂ N]	4.6	13.9	3.0
PSF/10Li(HDA)[Tf ₂ N]	4.4	12.9	2.9
PSF/20Li(HDA)[Tf ₂ N]	4.5	13.7	3.1

The errors of all gas selectivities are less than 0.1

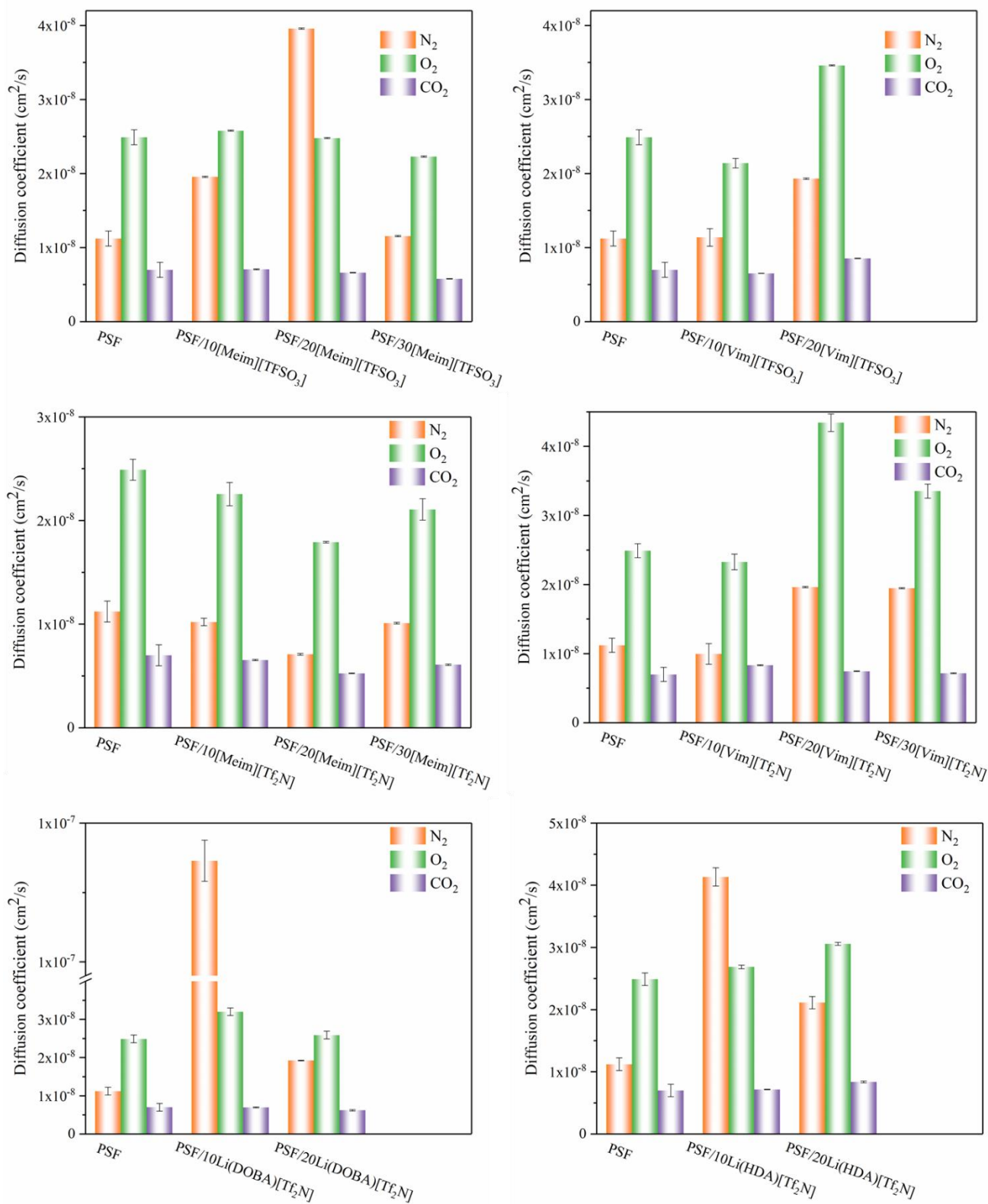


Figure 3-12 Diffusion coefficients of PSF/IL-based membranes

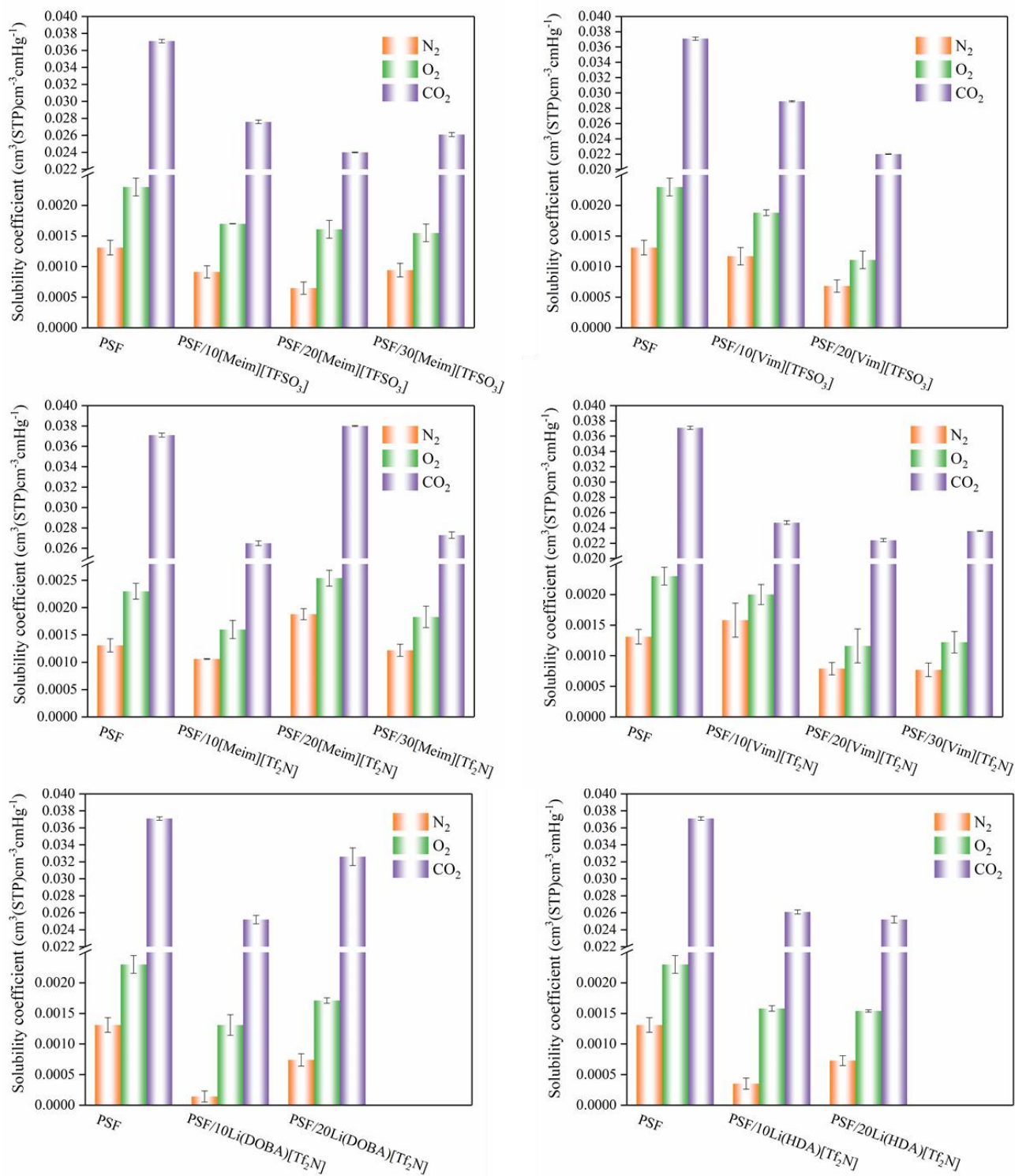


Figure 3-13 Solubility coefficients of PSF/IL-based membranes

3.4 Conclusion

The preparation process of PSF-based composite membranes containing six ILs ([Meim][TFSO₃], [Vim][TFSO₃], [Meim][Tf₂N], [Vim][Tf₂N], Li(DOBA)[Tf₂N] and Li(HDA)[Tf₂N]) was optimized, and PVA was utilized as a supporting material in membrane preparation process for the first time. SEM analysis demonstrated the successful formation of dense composite membranes, except in case of PSF/30[Vim][TFSO₃], PSF/30[Vim][TFSO₃], PSF/20[Vim][Tf₂N] and PSF/30[Vim][Tf₂N] owing to poor compatibility of [Vim]⁺-based ILs and PSF at high IL loading. FTIR analysis indicated that no new chemical bonds were formed, suggesting that the ILs and PSF were physically mixed. Additionally, F mapping revealed that the IL was homogeneously distributed within the PSF matrix. TGA tests demonstrated that both PSF and PSF-based composite membranes exhibited decomposition temperatures exceeding 300°C, confirming suitable thermal stability for gas permeation application. Surface energy measurements confirmed that the IL incorporation enhanced the surface polarity of PSF. DSC measurements revealed the lowering of the T_g value of PSF/IL composite membranes as compared with PSF, meaning ILs ability to plasticize the polymer matrix. Linear fits of T_g in case of composite membranes *via* Gordon-Taylor equation showed that [Meim][TFSO₃] (R² = 0.983), [Meim][Tf₂N] (R² = 0.990), [Vim][Tf₂N] (R² = 0.983), and Li(HDA)[Tf₂N] (R² = 0.981) dispersed within PSF matrix better than Li(DOBA)[Tf₂N] (R² = 0.959). Additionally, mechanical tests confirmed the plasticizing ability of ILs by the increasing strain at break and a slightly decreasing Young's modulus of PSF/IL composite membranes as compared with PSF.

In this study, all gases permeated membranes by solution-diffusion mechanism. Gas permeation results showed that the membrane gases permeability coefficients followed the next order: $P(N_2) < P(O_2) < P(CO_2)$ which was expected. Only the gases solubility coefficients of PSF/20[Meim][TFSO₃] membrane was slightly higher than that of pure PSF due to the influence of higher polarity and more free volume. Gas diffusion coefficients of PSF/IL composite membrane was affected by their microstructure and gases Van Der Waals volume. The composite membranes microstructure changed by [Meim][Tf₂N], [Vim][TFSO₃], [Vim][Tf₂N], which affected the O₂ diffusion. However, [Meim][TFSO₃], Li(DOBA)[Tf₂N] and Li(HDA)[Tf₂N] mainly influence the N₂ diffusion of PSF-based membrane. Further, only CO₂/O₂ selectivity of PSF/[Vim][TFSO₃] composite was enhanced with IL loading increasing, and PSF/20[Vim][TFSO₃] presented the highest CO₂/O₂ selectivity of 4.9.

References

- [1] L. Martínez-Izquierdo, C. Téllez, J. Coronas, Highly stable Pebax[®] Renew[®] thin-film nanocomposite membranes with metal organic framework ZIF-94 and ionic liquid [Bmim][BF₄] for CO₂ capture, *J. Mater. Chem. A* 10 (2022) 18822–18833.
- [2] M. Farrokhsara, F. Dorosti, New high permeable polysulfone/ionic liquid membrane for gas separation, *Chinese Journal of Chemical Engineering* 28 (2020) 2301–2311.
- [3] I.V.B. Maggay, H.N. Aini, M.M.G. Lagman, S.-H. Tang, R.R. Aquino, Y. Chang, A. Venault, A Biofouling Resistant Zwitterionic Polysulfone Membrane Prepared by a Dual-Bath Procedure, *Membranes* 12 (2022) 69.
- [4] R.M. Almuhtaseb, A. Awadallah-F, S.A. Al-Muhtaseb, M. Khraisheh, Influence of Casting Solvents on CO₂/CH₄ Separation Using Polysulfone Membranes, *Membranes* 11 (2021) 286.
- [5] A. Alkhouzaam, M. Khraisheh, M. Atilhan, S.A. Al-Muhtaseb, L. Qi, D. Rooney, High-pressure CO₂/N₂ and CO₂/CH₄ separation using dense polysulfone-supported ionic liquid membranes, *Journal of Natural Gas Science and Engineering* 36 (2016) 472–485.
- [6] S.-C. Lu, A.L. Khan, I.F.J. Vankelecom, Polysulfone-ionic liquid based membranes for CO₂/N₂ separation with tunable porous surface features, *Journal of Membrane Science* 518 (2016) 10–20.
- [7] I. Smallwood, *Handbook of Organic Solvent Properties*, Butterworth-Heinemann, 2012.
- [8] X. Dong, D. Lu, T.A.L. Harris, I.C. Escobar, Polymers and Solvents Used in Membrane Fabrication: A Review Focusing on Sustainable Membrane Development, *Membranes* 11 (2021) 309.
- [9] Q. Xu, R. Liu, H. Yang, Effect of acid and alkali solutions on micro-components of coal, *Journal of Molecular Liquids* 329 (2021) 115518.
- [10] G.C. Kapantaidakis, S.P. Kaldis, X.S. Dabou, G.P. Sakellaropoulos, Gas permeation through PSF-PI miscible blend membranes, *Journal of Membrane Science* 110 (1996) 239–247.
- [11] A. Dehghani Kiadehi, A. Rahimpour, M. Jahanshahi, A.A. Ghoreyshi, Novel carbon nano-fibers (CNF)/polysulfone (PSf) mixed matrix membranes for gas separation, *Journal of Industrial and Engineering Chemistry* 22 (2015) 199–207.
- [12] A. Sarihan, E. Eren, Novel high performed and fouling resistant PSf/ZnO membranes for water treatme, *Membrane and Water Treatment* 8 (2017) 563–574.
- [13] G. Kaur, H. Kumar, M. Singla, Diverse applications of ionic liquids: A comprehensive review, *Journal of Molecular Liquids* 351 (2022) 118556.
- [14] X. Liu, L. Lebrun, N. Desilles, Enhancing thermal and mechanical properties of pyridine-based polyester with isosorbide for high gas barrier applications, *European Polymer Journal* 202 (2024) 112629.
- [15] W. Brostow, R. Chiu, I.M. Kalogeras, A. Vassilikou-Dova, Prediction of glass transition temperatures: Binary blends and copolymers, *Materials Letters* 62 (2008) 3152–3155.
- [16] E. Penzel, J. Rieger, H.A. Schneider, The glass transition temperature of random copolymers: 1. Experimental data and the Gordon-Taylor equation, *Polymer* 38 (1997) 325–337.
- [17] L. De Lorenzo, E. Tocci, A. Gugliuzza, E. Drioli, Pure and Modified Co-Poly(amide-12-b-ethylene oxide) Membranes for Gas Separation Studied by Molecular Investigations,

Membranes 2 (2012) 346–366.

- [18] A.L. Ahmad, A.A. Abdulkarim, B.S. Ooi, S. Ismail, Recent development in additives modifications of polyethersulfone membrane for flux enhancement, *Chemical Engineering Journal* 223 (2013) 246–267.
- [19] M. Pasichnyk, P. Stanovsky, P. Polezhaev, B. Zach, M. Šyc, M. Bobák, J.C. Jansen, M. Přibyl, J.E. Bara, K. Friess, J. Havlica, D.L. Gin, R.D. Noble, P. Izák, Membrane technology for challenging separations: Removal of CO₂, SO₂ and NO_x from flue and waste gases, *Separation and Purification Technology* 323 (2023) 124436.
- [20] A. Bondi, van der Waals Volumes and Radii, *J. Phys. Chem.* 68 (1964) 441–451.
- [21] W. Shi, E.J. Maginn, Molecular Simulation and Regular Solution Theory Modeling of Pure and Mixed Gas Absorption in the Ionic Liquid 1-n-Hexyl-3-methylimidazolium Bis(Trifluoromethylsulfonyl)amide ([hmim][Tf₂N]), *J. Phys. Chem. B* 112 (2008) 16710–16720.

Chapter 4

Preparation and characterization of PES- based composite membranes

4.1 Introduction

Due to its excellent characteristics described in Chapter 1 (section 1.5), PES may be another candidate to fabricate CO₂ separation membranes and overcome the limitations of PSF-based membranes.

Rostami and Khodaei [1] synthesized the hybrid structure MIL-53(Al)@MWCNT membrane by combining MIL-53(Al) particles with -COOH functionalized MWCNT, which were incorporated into PES for CO₂/CH₄ and CO₂/N₂ separation. The MMMs consisting of 5 wt% of MIL-53(Al)@MWCNT had a higher CO₂/N₂ and CO₂/CH₄ ideal selectivity of 87 and 58.6, respectively, as compared to pure PES membrane (CO₂/N₂ - 12 and CO₂/CH₄ - 15). Additionally, the MMMs exhibited a CO₂ permeability of 183 Barrer, overcoming that of pure PES membrane (55 Barrer) and exceeding the Robeson upper bounds (Figure 1-2). The CO₂ absorption capacity of MIL-53(Al)@MWCNT was enhanced by both carboxylic groups and Al³⁺ metal sites, while the uptake of N₂ and CH₄ remained limited: the MMMs exhibited a strong CO₂ selectivity.

Mannan *et al* [2] combined 1-ethyl-3-methyl imidazolium bis(trifluoromethylsulfonyl)imide ([Emim][Tf₂N]) ionic liquid and PES to prepare dense composite membranes for CO₂ separation. The results indicated a substantial increase in the CO₂ permeability, with a rise from 2.42 Barrer for pure PES membrane to 298.84 Barrer for PES/[Emim][Tf₂N] (50 wt%), at 25°C and 25 bar, and the CO₂/CH₄ ideal selectivity was enhanced to 57.53 as compared to pure PES (15.91). Since [Emim][Tf₂N] has a high affinity with CO₂, the CO₂ solubility and its diffusion inside the composite membrane can be improved.

Mohshim *et al* [3] worked on CO₂ gas separation performance of PES-based mixed matrix membranes with [Emim][Tf₂N] and SAPO-34 obtained by casting method. PES/SAPO-34 (20 wt%)/[Emim][Tf₂N] (20 wt%) presented promising CO₂/CH₄ ideal selectivity (62.2) as compared to PES/SAPO-34 (20 wt%) (20.7) at room temperature and 30 bar. The CO₂ permeance of PES/SAPO-34 (20 wt%)/[Emim][Tf₂N] (20 wt%) increased by 253% (300 GPU) as compared to PES/SAPO-34 (20 wt%) (85.69 GPU), thanks to the large number of pores provided by SAPO-34. Also, [Emim][Tf₂N] attached to SAPO-34 can act as a fast absorber of CO₂ to facilitate the CO₂ permeation. In addition, [Emim][Tf₂N] improved the compatibility between PES and SAPO-34, resulting in an improvement of the interfacial adhesion between SAPO-34 and PES, and in obtaining defect-free membranes.

In this Chapter, six ILs ([Meim][TFSO₃], [Vim][TFSO₃], [Meim][Tf₂N], [Vim][Tf₂N], Li(DOBA)[Tf₂N] and Li(HDA)[Tf₂N]) were introduced into a PES matrix to fabricate dense

composite membranes. The influence of these different ILs and their loadings on the microstructure, thermal properties, chemical structure, mechanical properties, and gas permeation properties of PES/ILs composite membranes was investigated and discussed.

4.2 Membrane preparation

4.2.1 PES-based composite membranes

The PES membranes preparation procedure was the same as that of PSF-based membranes described in Chapter 3 (Section 3.2).

4.3 Membrane Characterization

4.3.1 Transparency

The optical images of PES and PES/ILs composite membranes are shown in Figure 4-1. The pure PES membrane demonstrated remarkable transparency and glossiness. Even if all PES/ILs composite membranes also were glossy, the addition of an IL into the PES matrix decreased transparency, especially at higher loading, probably due to a compatibility limit between PES and ILs. PES/ILs containing [Vim]⁺ showed the worst transparency.



Figure 4-1 Optical photos of PES and PES/ILs membranes

4.3.2 Chemical structure and microstructure of membranes

The incorporation of ILs inside the PES matrix was studied by FT-IR spectroscopy (Figure 4-2). The vibrational C=O peak, appeared at 1667 cm^{-1} in all membranes, was attributed to residual *N*-methyl-2-pyrrolidone, which was the solvent used for membrane preparation.

Concerning pure PES, the C=C stretching of the benzene rings was detected at 1576 cm^{-1} and 1483 cm^{-1} [4]. The sulfone (S=O) group exhibited symmetric and asymmetric vibrations at 1145 cm^{-1} and 1293 cm^{-1} , respectively [5]. The asymmetric stretching of the C-O bond in the ether was seen at 1233 cm^{-1} and 1100 cm^{-1} [6]. All these bands were observed at their distinctive places, as reported in the

literature, and were noted for every composite membrane.

In PES/[Meim][TFSO₃] and PES/[Vim][TFSO₃] composite membranes, the S=O band of [TFSO₃]⁻ appeared at 1031 cm⁻¹. The S=O bands of [Tf₂N]⁻ were seen at 1196 cm⁻¹ and 1352 cm⁻¹ in PES/[Meim][Tf₂N] and PES/[Vim][Tf₂N], and at 1199 cm⁻¹ and 1350 cm⁻¹ in PES/Li(DOBA)[Tf₂N] and PES/Li(HDA)[Tf₂N] composite membranes. According to the above analysis, the ILs were effectively incorporated inside the PES matrix.

The morphology of the composite membranes was observed using SEM on both surfaces (contacting air and contacting PVA) and cross-section and the results are gathered in Figure 4-3, Figure 4-4 and Figure 4-5. Uniform and smooth surfaces (close to air) were observed, in the case of composite membranes as well as for pure PES. However, there were numerous streaks on the surface close to PVA: probably due to the presence of hydrogen bonds between the F of the composite membrane and the OH of the PVA support, the composite membranes stuck with PVA during the membrane drying and generated these defects. The F-mapping of the composite membranes (Figure 4-3 and Figure 4-5) showed that the F distribution was uniform, suggesting that the ILs were well dispersed within the composite membranes.

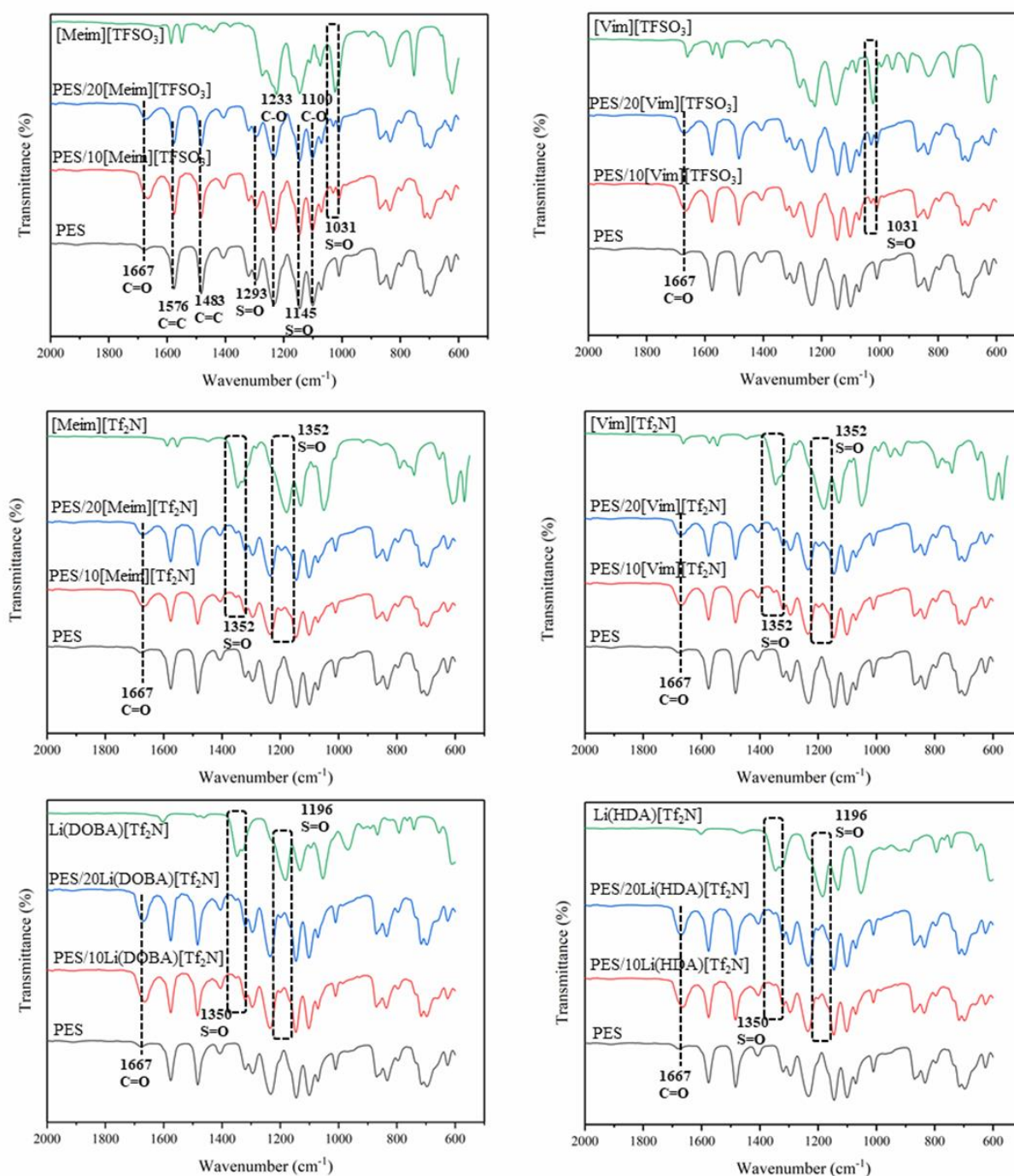


Figure 4-2 FT-IR spectra of PES and PES/ILs membranes

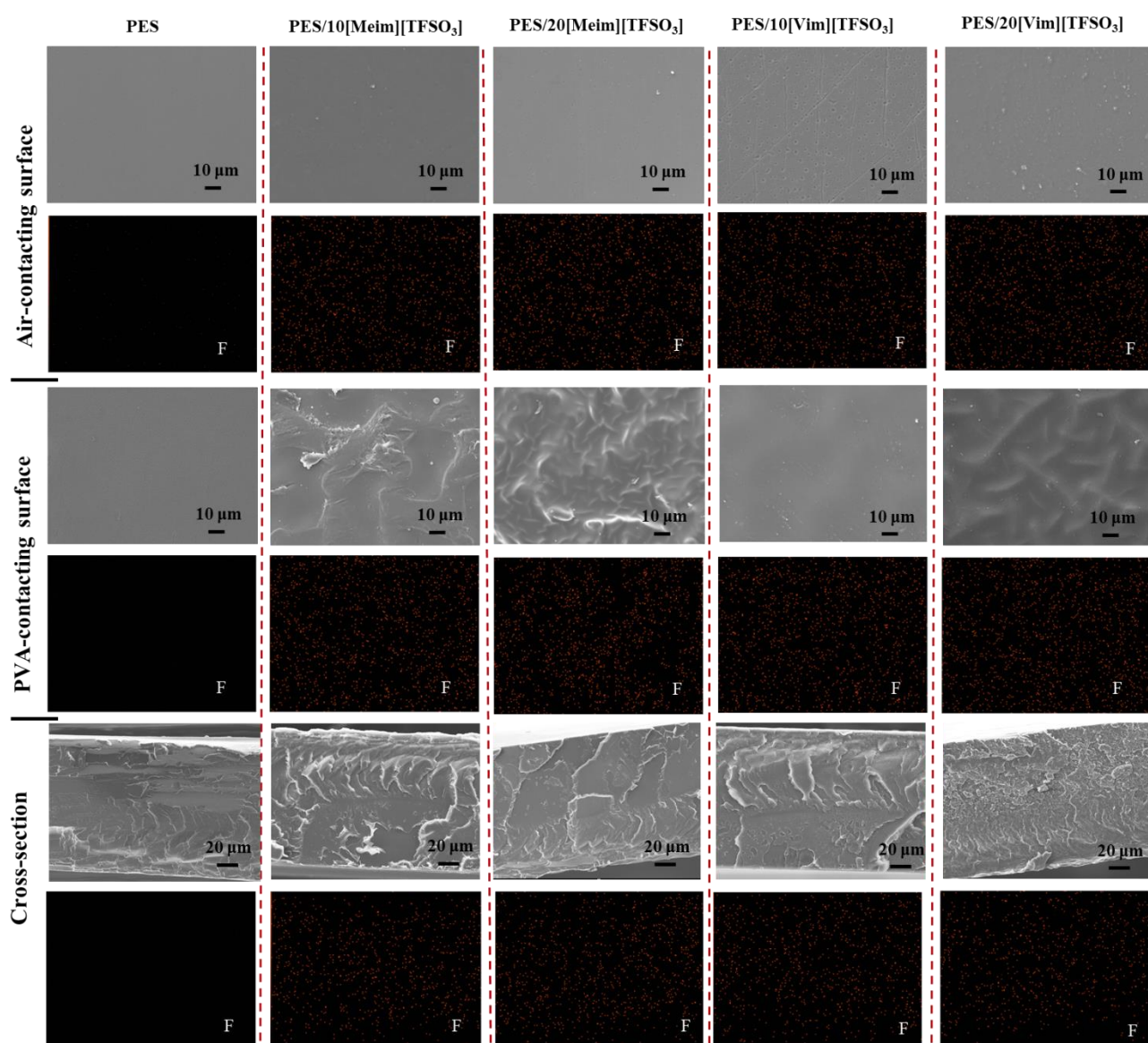


Figure 4-3 SEM images and F-mappings of PES, PES/[Meim][TFSO₃] and PES/[Vim][TFSO₃] membranes

The cross-sectional SEM images (Figure 4-3 and Figure 4-5) confirm the dense structure of PES and PES/ILs membranes, with a thickness of approximately 150 μm , and with uniform ILs distributions. The membranes with 20 wt% of [Vim][TFSO₃] or [Vim][Tf₂N] showed the presence of micropores in the cross-section, indicating a lower compatibility at this loading between the ILs containing [Vim]⁺ and PES. This result is consistent with the lower membrane transparency obtained for these ILs (Figure 4-1).

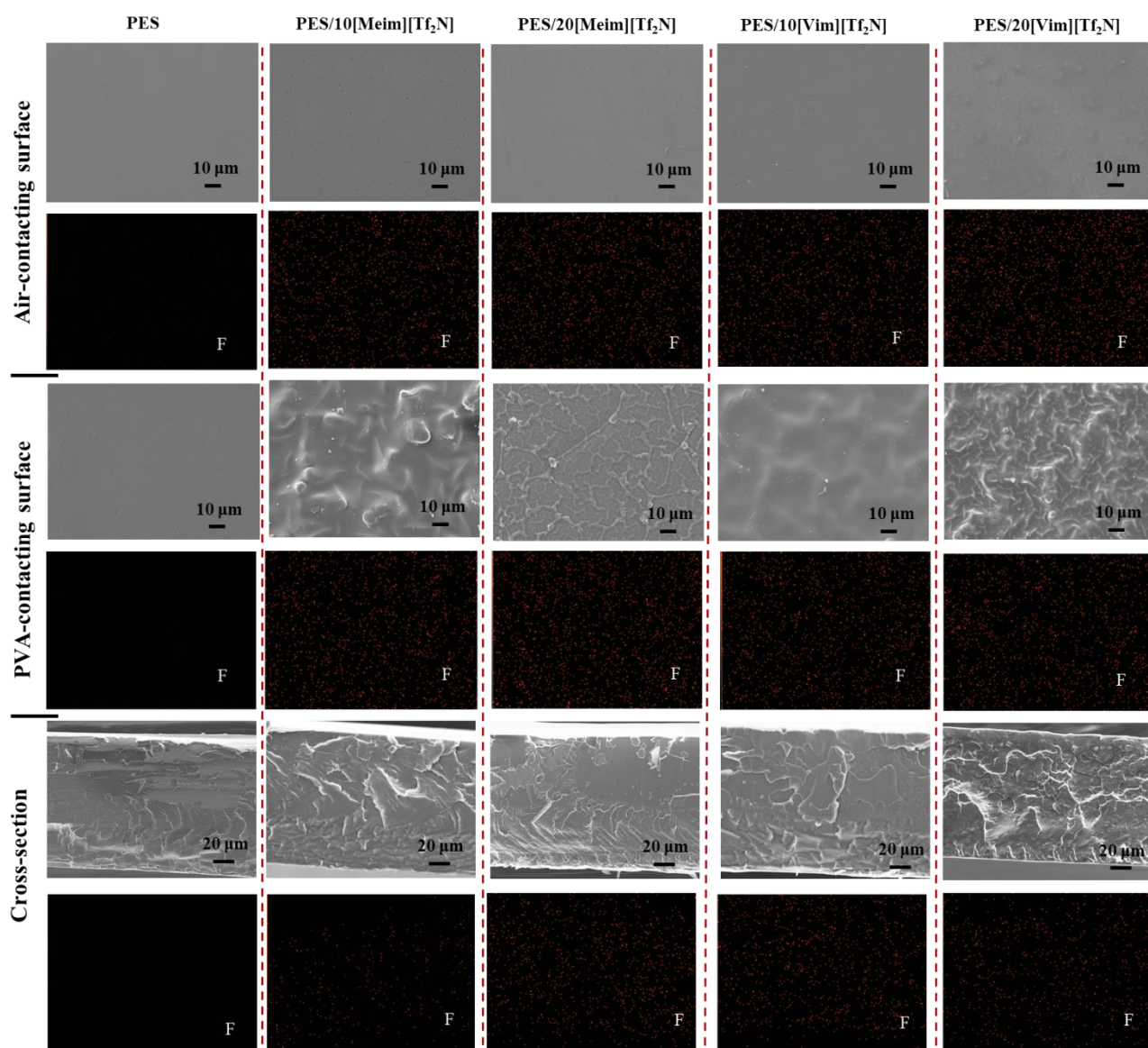


Figure 4-4 SEM images and F-mappings of PES, PES/[Meim][Tf₂N] and PES/[Vim][Tf₂N] membranes

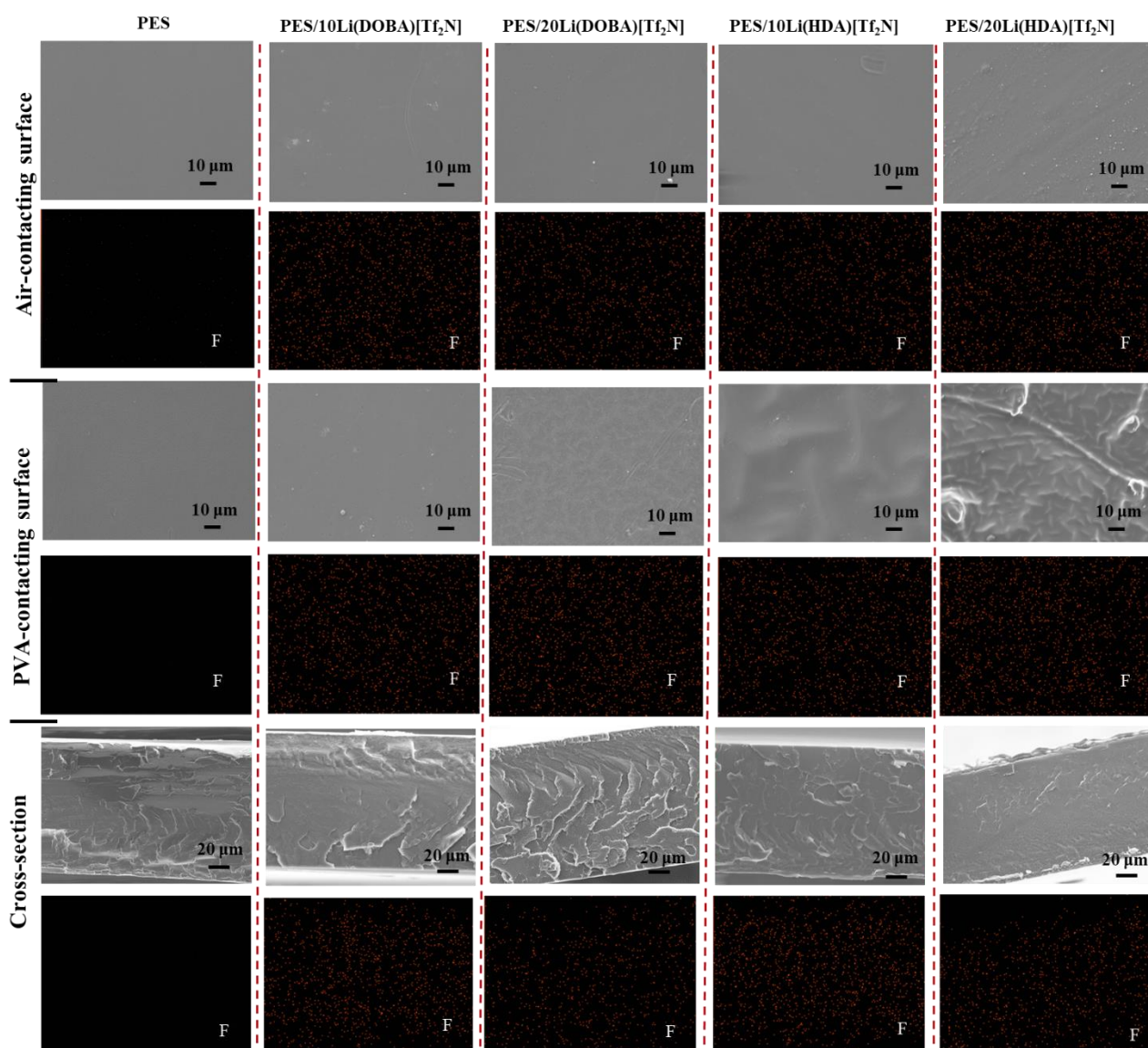


Figure 4-5 SEM images and F-mappings of PES, PES/Li(DOBA)[Tf₂N] and PES/Li(HDA)[Tf₂N] membranes

4.3.3 Thermal characterization

4.3.3.1 Thermal stability

The thermal stability curves of PES and PES/ILs membranes are shown in Figure 4-6. The TGA curves indicated a first weight loss, from 175°C to 250°C, corresponding to approximately 9%, owing to the presence of residual *N*-methyl-2-pyrrolidone as previously observed in FT-IR spectra (Figure 4-2). The next degradation step, observed between 400°C and 600°C, could be attributed to the simultaneous thermal degradation of both ILs and PES.

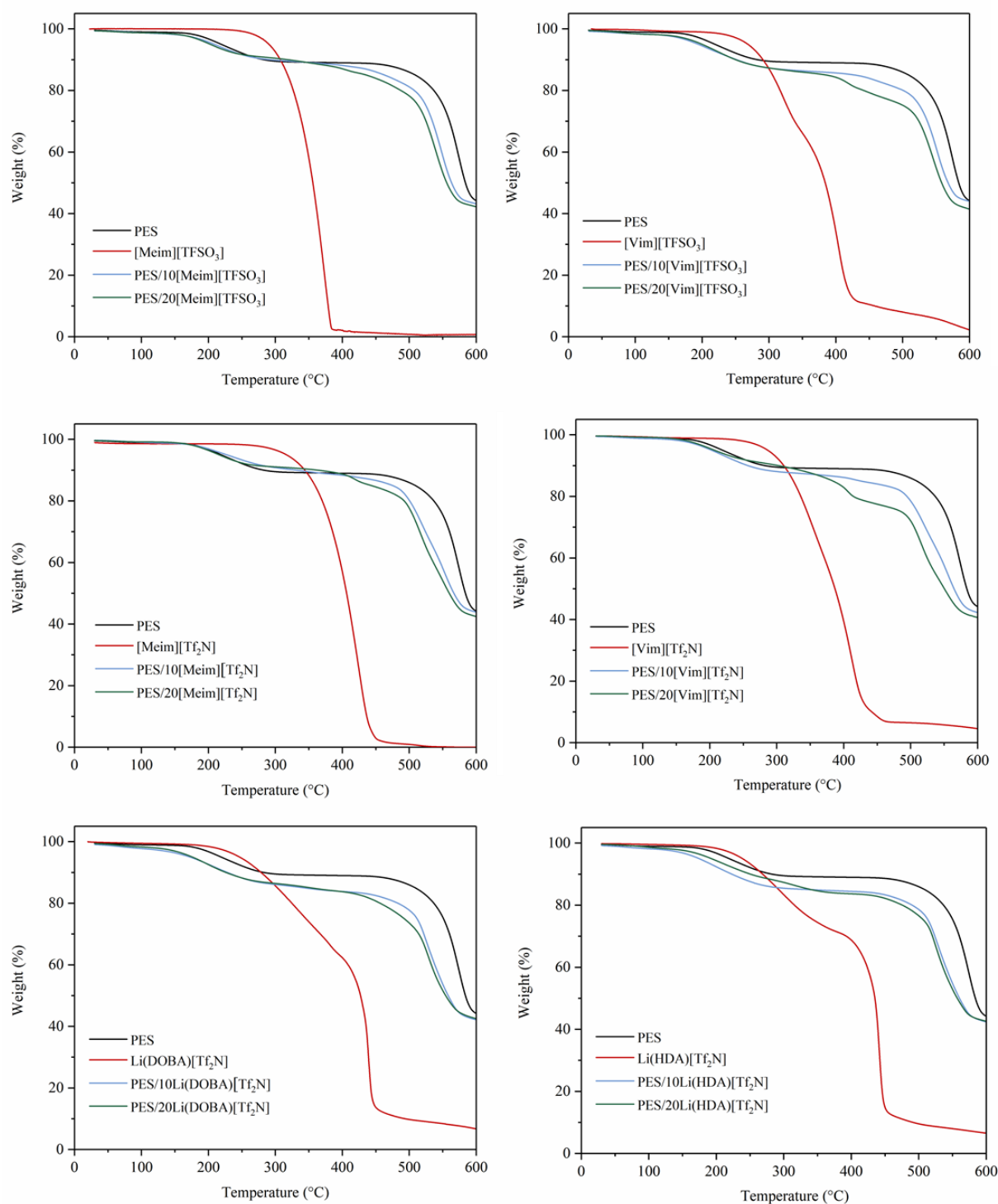


Figure 4-6 TGA curves of PES and PES/ILs membranes

The thermal stability of the composite membranes was decreased in comparison to pure PES membrane owing to the early degradation of ILs. However, the membrane degradation exceeded 400°C demonstrating the excellent thermal stability of composite membranes.

4.3.3.2 Differential scanning calorimetry (DSC)

DSC analysis was used to evaluate the impact on the T_g value of blending ILs in a PES matrix. The DSC curves and T_g value of membranes are shown in Annex 4 and Table 4-1, respectively. For pure PES, T_g was measured (from the second heating cycle) at 179°C, which was lower than the classical reported value of 231°C [7]. This plasticization effect could be attributed to the remaining solvent evidenced by TGA. The T_g value of all composite membranes (Table 4-1) was lower than the value of pure PES, as already mentioned in the literature [8], and decreased with increasing the IL loading. For example, T_g of PES/20[Meim][TFSO₃] was 89°C, which was lower than T_g of PES/10[Meim][TFSO₃] (97°C): IL acted as plasticizer, consequently resulting in the softening of the PES matrix. Since the plasticization of a polymer matrix has a notable impact on its mechanical characteristics and gas permeability properties [9,10], this effect will be further examined.

As for PES-based membranes, all PES-based composite membranes revealed calculated T_g values that were higher than those obtained experimentally (Table 4-1). Therefore, it can be concluded that Fox equation (Equation 3-1) is not suited for PES-based composite membranes.

Table 4-1 T_g of PES/ILs membranes

Sample	T_g (°C)/Experiment	T_g (°C)/Calculated (Fox) (Equation 3-1)
PES	179	-
PES/10[Meim][TFSO ₃]	97	137
PES/20[Meim][TFSO ₃]	89	107
PES/10[Vim][TFSO ₃]	104	nd
PES/20[Vim][TFSO ₃]	98	nd
PES/10[Meim][Tf ₂ N]	107	137
PES/20[Meim][Tf ₂ N]	94	108
PES/10[Vim][Tf ₂ N]	92	132
PES/20[Vim][Tf ₂ N]	89	99
PES/10Li(DOBA)[Tf ₂ N]	89	138
PES/20Li(DOBA)[Tf ₂ N]	84	109
PES/10Li(HDA)[Tf ₂ N]	90	141
PES/20Li(HDA)[Tf ₂ N]	69	114

nd – no data available

The fits of T_g by Gordon-Taylor equation (Equation 3-3) (Figure 4-7) were not linear (R^2 was less than 0.96), indicating that the ILs exhibited only a partial compatibility with PES, which is concordant with the reduced membrane transparency (Figure 4-1).

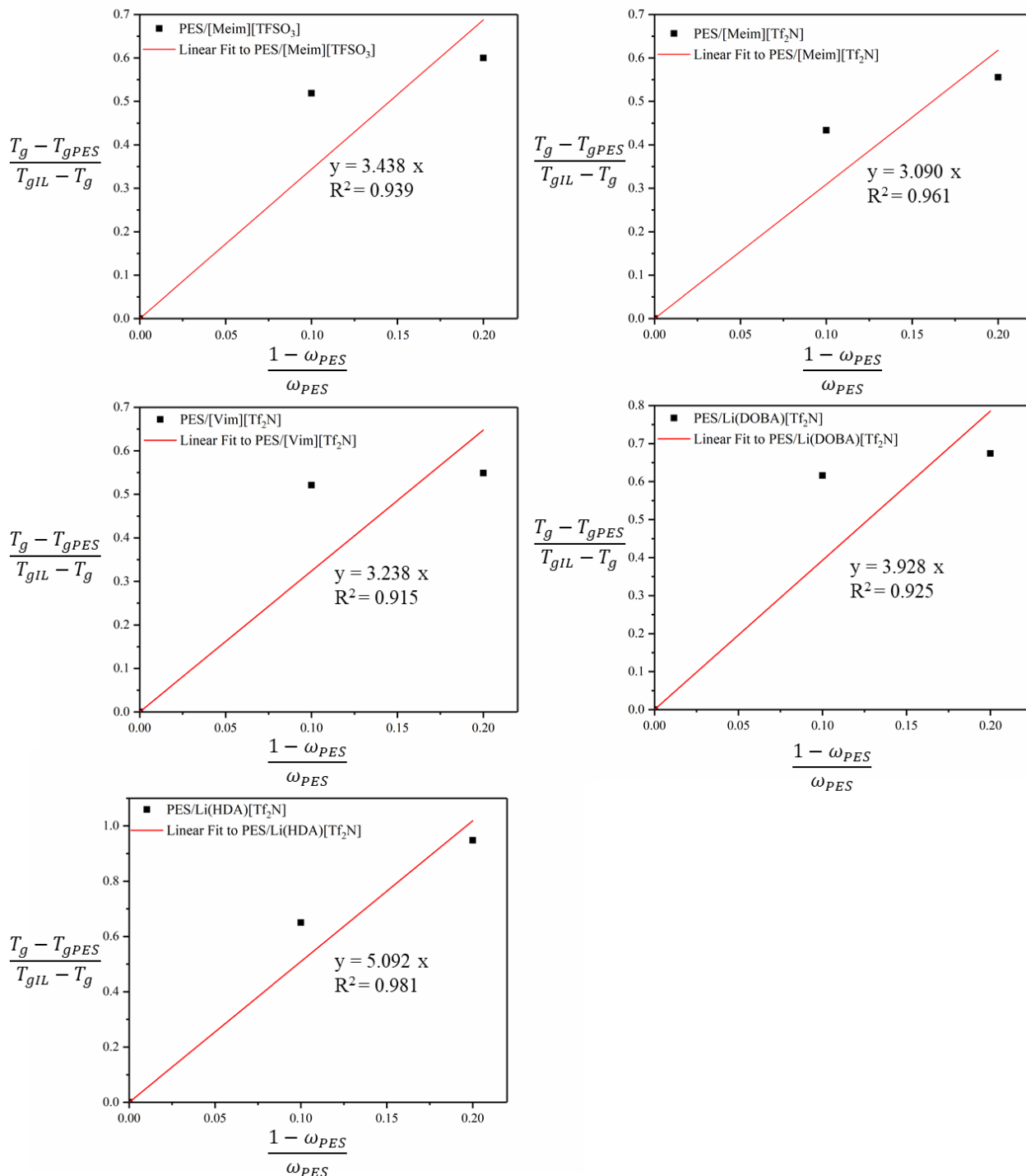


Figure 4-7 T_g linear fits by Gordon-Taylor equation (Equation 3-3) for PES/IL composite membranes

4.3.4 Surface energy

To investigate the impact of ILs on the surface energy of the composite membranes, contact angle measurements were conducted, and the surface energy (γ_s), with the dispersive (γ_s^d) and polar (γ_s^p) components, was determined using the Owens - Wendt method (Table 4-2). Since the rough membrane surface close to PVA seen by SEM (Figure 4-3 and Figure 4-5) could impact the contact angle measurements, the characterization was limited to the membrane surface close to air.

Table 4-2 Solvent contact angles and surface energy of PES and PES/ILs membranes

Sample	Contact angle (°)			γ_s	γ_s^d	γ_s^p
	Water	Diiodomethane	Glycerol			
PES	79.2 ± 0.6	30.0 ± 0.9	75.8 ± 0.3	42.0	39.6	2.5
PES/10[Meim][TFSO ₃]	73.0 ± 1.1	32.6 ± 0.2	65.1 ± 0.6	45.0	39.1	4.9
PES/20[Meim][TFSO ₃]	62.0 ± 1.9	50.1 ± 0.3	53.1 ± 0.3	45.8	32.7	13.1
PES/10[Vim][TFSO ₃]	69.8 ± 1.2	36.1 ± 0.6	69.7 ± 0.5	42.4	36.5	6.2
PES/20[Vim][TFSO ₃]	61.1 ± 0.3	50.7 ± 0.4	65.3 ± 0.5	42.7	29.4	13.0
PES/10[Meim][Tf ₂ N]	70.2 ± 0.4	34.0 ± 0.2	69.4 ± 0.8	43.5	37.7	5.8
PES/20[Meim][Tf ₂ N]	60.6 ± 1.0	47.2 ± 0.3	62.8 ± 0.4	44.1	31.6	12.6
PES/10[Vim][Tf ₂ N]	71.4 ± 1.8	32.2 ± 0.2	70.5 ± 0.4	43.2	37.9	5.3
PES/20[Vim][Tf ₂ N]	63.9 ± 0.4	43.7 ± 0.3	60.6 ± 1.6	44.8	34.4	10.4
PES/10Li(DOBA)[Tf ₂ N]	70.7 ± 0.8	36.3 ± 0.4	70.5 ± 0.5	42.4	36.6	5.9
PES/20Li(DOBA)[Tf ₂ N]	62.9 ± 0.3	47.9 ± 0.4	62.9 ± 0.3	43.3	31.7	11.6
PES/10Li(HDA)[Tf ₂ N]	72.6 ± 0.3	35.7 ± 0.2	69.2 ± 0.4	42.8	37.6	5.2
PES/20Li(HDA)[Tf ₂ N]	65.3 ± 0.6	48.2 ± 0.4	60.3 ± 0.5	43.3	32.7	10.6

The incorporation of ILs reduced the water and glycerol contact angles, and increased the contact angle of diiodomethane, resulting in an increase in γ_s and γ_s^p values and a decrease in γ_s^d . These changes, becoming more pronounced with higher ILs loadings, suggested that the ILs acted as polar additives.

The enhancing of membrane surface polarity can have a negative influence on CO₂, O₂ and N₂ solubility coefficients, as these gases are characterized by low polarity. However, membranes surface

with high surface polarity are more suitable for CO₂ solubility as explained in Chapter 3 (Section 3.3.4).

4.3.5 Mechanical properties

The membrane mechanical characteristics were examined using Young's modulus, strain at break, and tensile strength. The data and curves are shown in Table 4-3 and Figure 4-8, respectively.

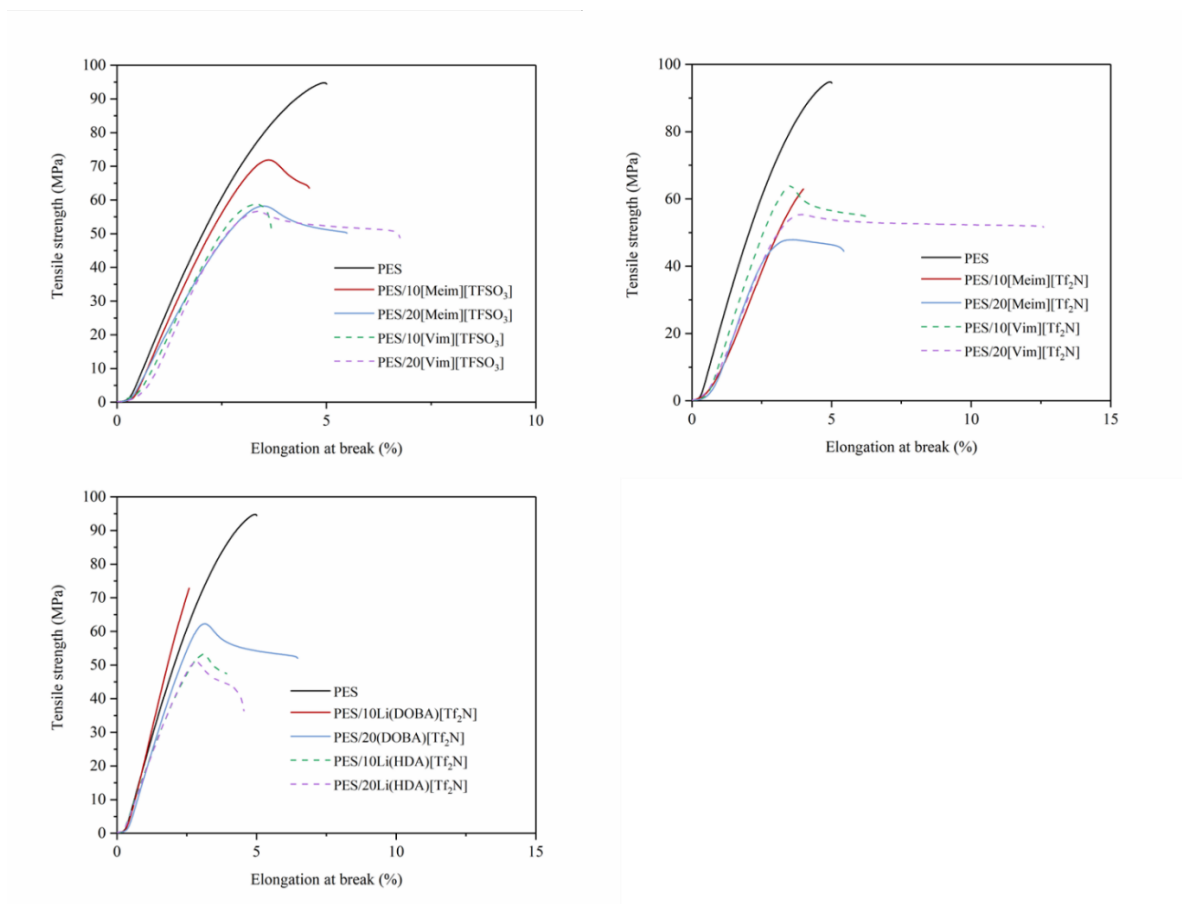


Figure 4-8 Stress - strain curves of PES and PES/ILs composite membranes

Table 4-3 Mechanical data of PES and PES/ILs membranes

Sample	Young's Modulus (MPa)	Tensile strength (MPa)	Strain at break (%)
PES	2390 ± 40	94.8 ± 5.0	4.9 ± 0.2
PES/10[Meim][TfSO ₃]	2210 ± 105	71.9 ± 4.0	4.5 ± 0.1
PES/20[Meim][TfSO ₃]	2140 ± 62	57.8 ± 0.5	5.0 ± 0.4
PES/10[Vim][TfSO ₃]	2160 ± 39	58.8 ± 2.6	3.5 ± 0.1
PES/20[Vim][TfSO ₃]	2110 ± 70	56.7 ± 1.3	6.2 ± 0.3
PES/10[Meim][Tf ₂ N]	1920 ± 56	62.9 ± 2.6	4.0 ± 0.4
PES/20[Meim][Tf ₂ N]	1911 ± 60	47.9 ± 0.6	5.2 ± 0.3
PES/10[Vim][Tf ₂ N]	2220 ± 71	63.9 ± 4.0	6.1 ± 0.2
PES/20[Vim][Tf ₂ N]	2050 ± 140	55.4 ± 5.3	12.5 ± 0.6
PES/10Li(DOBA)[Tf ₂ N]	2521 ± 120	70.5 ± 4.2	2.6 ± 0.3
PES/20Li(DOBA)[Tf ₂ N]	2268 ± 130	62.3 ± 5.0	6.4 ± 0.2
PES/10Li(HDA)[Tf ₂ N]	2170 ± 84	53.2 ± 3.9	3.9 ± 0.2
PES/20Li(HDA)[Tf ₂ N]	2159 ± 141	51.0 ± 2.1	4.5 ± 0.6

It could be seen that pure PES shows outstanding mechanical properties with a Young's modulus of 2390 MPa and a tensile strength of 94.8 MPa. The Young's modulus of all composite membranes was equivalent or slightly lower than that of pure PES, indicating that ILs had little or no effect on the stiffness of the composite membranes. The introduction of ILs had a more pronounced impact on the tensile strength: as the loading of ILs increased, the tensile strength of the membranes decreased. From the stress-strain curves (Figure 4-8), it was evident that the pure PES membrane exhibited brittle fracture. When adding a certain amount of IL, the composite membranes exhibited ductile fracture, accompanied by an increase in strain at break. It can be linked to the plasticizing effect of ILs on PES, in accordance with the results obtained by DSC measurements (Section 4.3.3.2).

4.3.6 Gas separation

The gases (CO_2 , N_2 and O_2) permeability and selectivity coefficients are shown in Figure 4-9 and Table 4-4, respectively. The corresponding diffusion and solubility coefficients are presented in Figure 4-10 and Figure 4-11, respectively. The gases (CO_2 , N_2 and O_2) solubility and permeability coefficients follow the expected order: $S(\text{CO}_2) > S(\text{O}_2) > S(\text{N}_2)$ and $P(\text{N}_2) < P(\text{O}_2) < P(\text{CO}_2)$, respectively, as already explained previously (Section 3.3.6). The gases diffusion coefficients of PES-based membranes follow the order: $D(\text{N}_2) > D(\text{O}_2) > D(\text{CO}_2)$ except for PES/10[Vim][Tf₂N] ($D(\text{O}_2) > D(\text{N}_2) > D(\text{CO}_2)$), which is different as compared with gases diffusion coefficients of PSF-based membranes ($D(\text{O}_2) > D(\text{N}_2) > D(\text{CO}_2)$). This can be explained by the fact that PES matrix structure is more suitable for N_2 diffusion. The studied IL loading only slightly increases the N_2 solubility coefficients (Figure 4-11) owing to the surface higher polarity and more available free volume.

The O_2 and CO_2 diffusion coefficients of PES/10[Vim][TFSO₃] and PES/20[Meim][TFSO₃] are higher than those of pure PES, that can be explained by numerous pathways presented in this membrane structure.

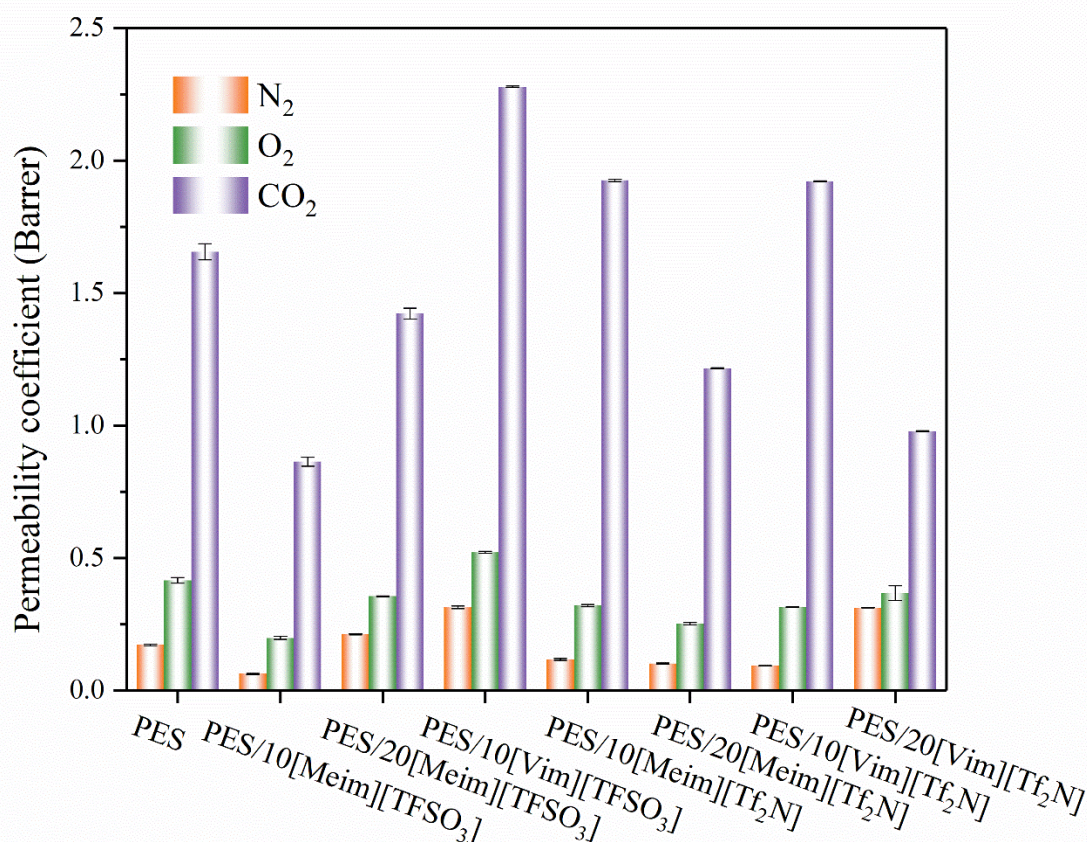


Figure 4-9 Permeability coefficients of PES/IL-based membranes

The gas permeability decreases in presence of imidazolium-based IL (not including 10 wt% of [Vim][TFSO₃] and 10 wt% [Vim][Tf₂N]), while increases when 10 wt% of [Vim][TFSO₃] is added, whatever the gas is. The PES/10[Meim][Tf₂N], PES/20[Meim][Tf₂N], PES/10[Meim][TFSO₃] and PES/10[Vim][Tf₂N] show the higher CO₂/O₂ and CO₂/N₂ selectivities than those of pure PES, indicating high affinity of these ILs with CO₂ within PES. In addition, PES/10[Vim][Tf₂N] presents higher CO₂ permeability coefficient (1.92 Barrer) than that of pure PES (1.66 Barrer), and best CO₂ separation performance with CO₂/O₂ selectivity (6.1) and CO₂/N₂ selectivity (20.4). However, PES/20[Vim][TFSO₃] and PES/20[Vim][Tf₂N] show lower gas selectivity than that of pure PES owing to the membranes' micromorphology (Figure 4-3 and Figure 4-4). PES/alkanolamine-based IL composite membranes are not selective owing to poor compatibility between PES and alkanolamine-based ILs.

Table 4-4 Gas selectivity data of PES and PES/ILs membranes

Sample	α		
	CO ₂ /O ₂	CO ₂ /N ₂	O ₂ /N ₂
PES	4.0	9.6	3.2
PES/10[Meim][TFSO ₃]	4.3	13.7	3.2
PES/20[Meim][TFSO ₃]	4.0	6.7	1.7
PES/10[Vim][TFSO ₃]	4.4	7.3	1.7
PES/20[Vim][TFSO ₃]	1.0	1.0	0.9
PES/10[Meim][Tf ₂ N]	6.0	16.3	2.7
PES/20[Meim][Tf ₂ N]	4.8	11.9	2.5
PES/10[Vim][Tf ₂ N]	6.1	20.4	3.4
PES/20[Vim][Tf ₂ N]	2.7	3.1	1.2
PES/10Li(DOBA)[Tf ₂ N]	0.9	1.0	0.9
PES/20Li(DOBA)[Tf ₂ N]	1.0	2.4	2.5
PES/10Li(HDA)[Tf ₂ N]	1.0	1.0	1.0
PES/20Li(HDA)[Tf ₂ N]	1.0	1.0	1.0

The errors of all gas selectivities are less than 0.1

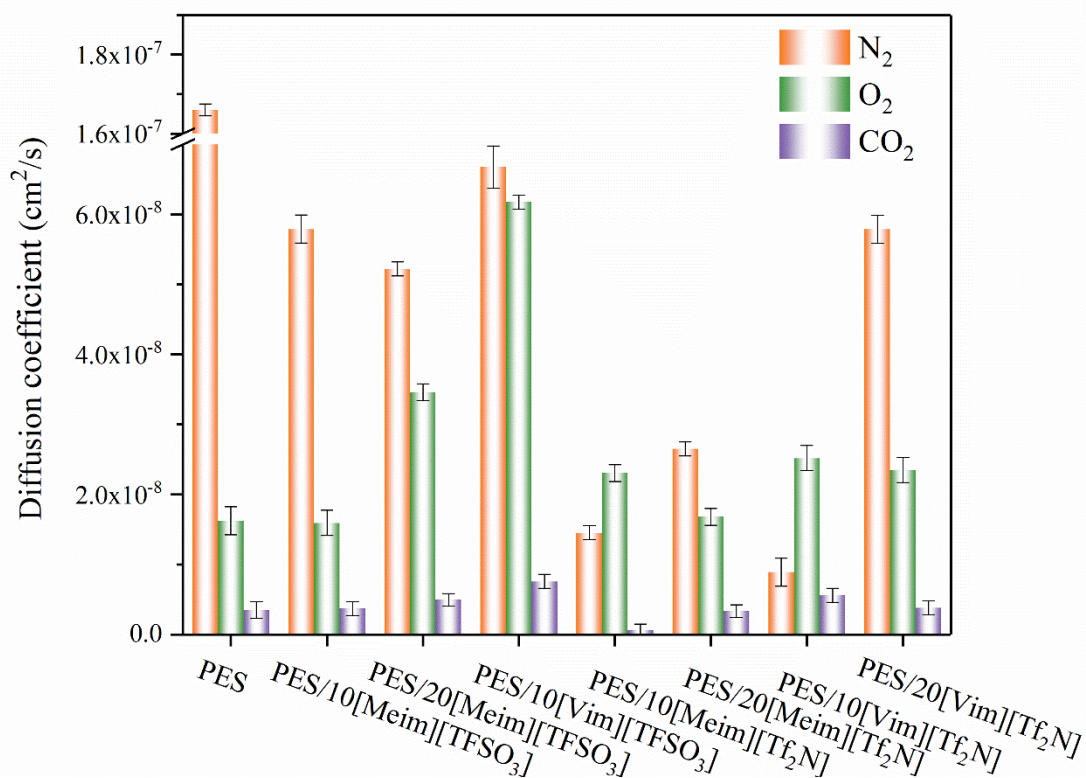


Figure 4-10 Diffusion coefficients of PES/IL-based membranes

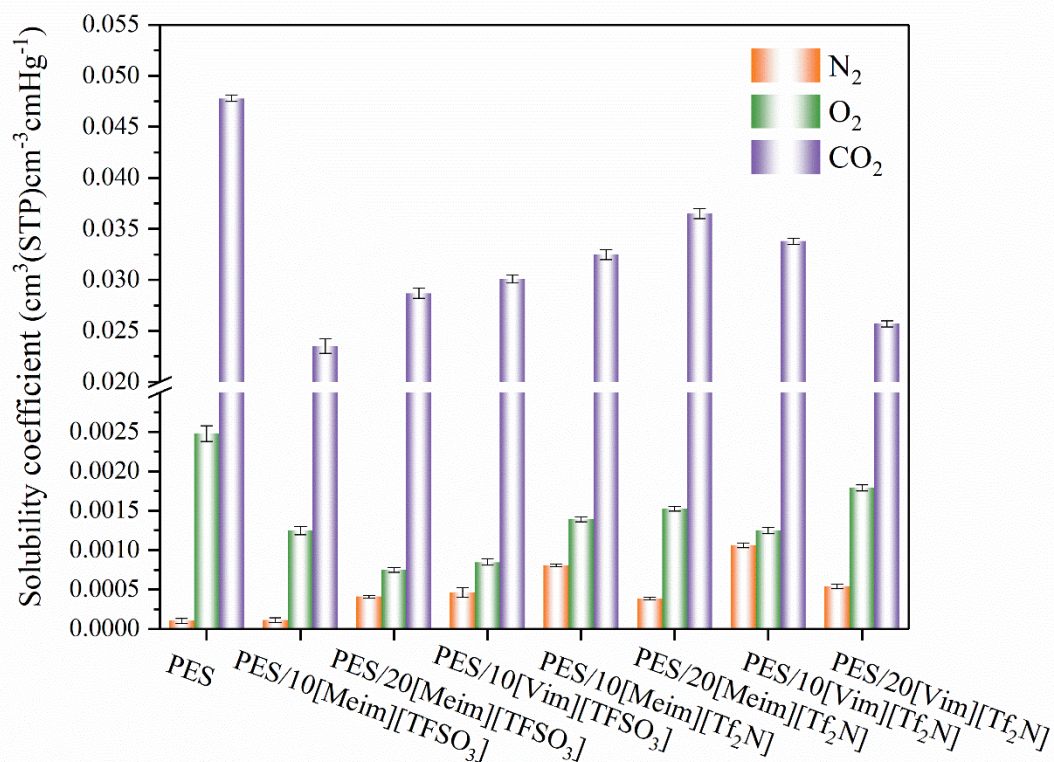


Figure 4-11 Solubility coefficients of PES/IL-based membranes

4.4 Conclusion

PES/ILs composite membranes were prepared successfully. Optical images of the composite membranes showed that the incorporation of ILs diminished the transparency of PES, with a more pronounced effect for [Vim]⁺ containing ILs. SEM confirmed that the PES-based membranes were dense, except PES/20[Vim][TFSO₃] and PES/20[Vim][Tf₂N] owing to poor compatibility between PES and [Vim]⁺ containing ILs at high loading. F-mapping revealed that ILs were neither agglomerated on the surface nor inside the composite membranes. No new chemical bonds were observed in the FT-IR spectra of composite membranes, suggesting physical blends between PES and ILs. The TGA results indicated 9% of the residual solvent in the composite membranes, and affirmed their thermal stability up to 350°C. DSC analysis revealed that the incorporation of ILs led to a reduction in the T_g value of PES, and this reduction was more pronounced with an increase of the IL loading. Modeling using Fox and Gordon-Taylor equations pointed a poor compatibility between IL and PES. Surface energy testing results indicated that the IL addition led to the PES surface energy increase. Mechanical tests indicated that the incorporation of ILs increased the PES strain at break, suggesting the IL plasticization effect. As one expected, the permeability coefficients of all membranes followed the order: $P(N_2) < P(O_2) < P(CO_2)$. PES/10[Vim][TFSO₃] presented higher gases permeability coefficients as compared to pure PES. Additionally, the CO₂/O₂ and CO₂/N₂ selectivities were enhanced by in the presence of 10 wt% of [Meim][TFSO₃], 10 wt% of [Meim][Tf₂N], 20 wt% of [Meim][Tf₂N] and 10 wt% [Vim][Tf₂N], as compared with the selectivity of pure PES membrane.

References

- [1] M. Saeid Rostami, M. Mehdi Khodaei, Effect of incorporated hybrid MIL-53(Al) and MWCNT into PES membrane for CO₂/CH₄ and CO₂/N₂ separation, *Fuel* 356 (2024) 129598.
- [2] H.A. Mannan, D.F. Mohshim, H. Mukhtar, T. Murugesan, Z. Man, M.A. Bustam, Synthesis, characterization, and CO₂ separation performance of polyether sulfone/[EMIM][Tf₂N] ionic liquid-polymeric membranes (ILPMs), *Journal of Industrial and Engineering Chemistry* 54 (2017) 98–106.
- [3] D.F. Mohshim, H. Mukhtar, Z. Man, The effect of incorporating ionic liquid into polyethersulfone-SAPO34 based mixed matrix membrane on CO₂ gas separation performance, *Separation and Purification Technology* 135 (2014) 252–258.
- [4] Y. Shin, M.F.N. Taufique, R. Devanathan, E.C. Cutsforth, J. Lee, W. Liu, L.S. Fifield, D.W. Gotthold, Highly selective supported graphene oxide membranes for water-ethanol separation, *Sci Rep* 9 (2019) 2251.
- [5] A. Mohamed, S. Yousef, A. Tonkonogovas, V. Makarevicius, A. Stankevičius, High performance of PES-GNs MMMs for gas separation and selectivity, *Arabian Journal of Chemistry* 15 (2022) 103565.
- [6] S. Yousef, J. Šereika, A. Tonkonogovas, T. Hashem, A. Mohamed, CO₂/CH₄, CO₂/N₂ and CO₂/H₂ selectivity performance of PES membranes under high pressure and temperature for biogas upgrading systems, *Environmental Technology & Innovation* 21 (2021) 101339.
- [7] X. Wen, C. He, Y. Hai, R. Ma, J. Sun, X. Yang, Y. Qi, H. Wei, J. Chen, Fabrication of an antifouling PES ultrafiltration membrane via blending SPSF, *RSC Advances* 12 (2022) 1460–1470.
- [8] D.M. Correia, L.C. Fernandes, P.M. Martins, C. García-Astrain, C.M. Costa, J. Reguera, S. Lanceros-Méndez, Ionic liquid–polymer composites: a new platform for multifunctional applications, *Advanced Functional Materials* 30 (2020) 1909736.
- [9] A. Bos, I.G.M. Pünt, M. Wessling, H. Strathmann, CO₂-induced plasticization phenomena in glassy polymers, *Journal of Membrane Science* 155 (1999) 67–78.
- [10] L. Wang, X. Guo, F. Zhang, N. Li, Blending and in situ thermally crosslinking of dual rigid polymers for anti-plasticized gas separation membranes, *Journal of Membrane Science* 638 (2021) 119668.

General Conclusion and Prospects

In this thesis, PSF/IL and PES/IL composite membranes for CO₂ separation application were fabricated and investigated in terms of morphological, thermal, chemical, mechanical, and gas (CO₂, O₂ and N₂) permeation properties.

Firstly, six ILs ([Meim][TFSO₃], [Vim][TFSO₃], [Meim][Tf₂N], [Vim][Tf₂N], Li(DOBA)[Tf₂N] and Li(HDA)[Tf₂N]) were synthesized successfully. Their chemical structure was confirmed by FT-IR and ¹H NMR analysis, and their thermal properties were analyzed by DSC and TGA. DSC results revealed that [Meim]⁺-based imidazolium ILs were polymorphic, and T_m of [TFSO₃]⁻-based imidazolium ILs was higher than that of [Tf₂N]⁻-based imidazolium ILs due to smaller size (stronger ionic bound). Furthermore, imidazolium-based ILs had stronger crystallization ability than alkanolamine-based ILs. The TGA results confirmed that all ILs were thermally stable enough for the preparation of PSF-based and PES-based membranes, and imidazolium-based ILs were more thermally stable than alkanolamine-based ILs.

Secondly, the preparation process of PSF-based dense composite membranes with different ILs ([Meim][TFSO₃], [Vim][TFSO₃], [Meim][Tf₂N], [Vim][Tf₂N], Li(DOBA)[Tf₂N] and Li(HDA)[Tf₂N]) was optimized. The composite membranes' chemical structure was characterized by FT-IR analysis, confirming the effective physical blending of ILs with PSF. The composite membranes' dense structure was revealed by SEM, except in the case of PSF with 20 wt% and 30 wt% of [Vim]⁺-based imidazolium ILs owing to poor compatibility between PSF and ILs at high concentration. Linear fits of composite membranes' T_g *via* Gordon-Taylor equation showed that [Meim][TFSO₃], [Meim][Tf₂N], [Vim][Tf₂N], and Li(HDA)[Tf₂N] dispersed within PSF matrix better than Li(DOBA)[Tf₂N], which was confirmed by F-mapping analysis. The IL role as plasticizer was noted through the T_g value decrease in case of composite membranes and the increase of strain at break as compared to neat PSF. Gas permeation measurement underlined the membrane gases permeability coefficients order ($P(N_2) < P(O_2) < P(CO_2)$) as expected in case of solution-diffusion mechanism. The membrane gases solubility coefficients were only slightly enhanced in the presence of 20 wt% of [Meim][TFSO₃] owing to higher polarity and more free volume. [Meim][Tf₂N], [Vim][TFSO₃] and [Vim][Tf₂N] mainly influenced the O₂ diffusion coefficients, while [Meim][TFSO₃], Li(DOBA)[Tf₂N] and Li(HDA)[Tf₂N] changed the N₂ diffusion coefficients of PSF-based membranes. PSF/20[Vim][TFSO₃] and PSF/10[Meim][Tf₂N] membranes were characterized by the highest CO₂/O₂ selectivity of 4.9.

Thirdly, the same ILs were introduced into PES matrix. SEM images showed dense structures, except for PES/20[Vim][TFSO₃] and PES/20[Vim][Tf₂N], which showed the worst transparency and

porous structures indicating poor compatibility between PES and 20 wt% of [Vim]⁺-based ILs. FT-IR spectra of composite membranes suggested physical blends between PES and ILs. T_g values were lower and strain at break were higher than those of pure PSF revealing the IL role as plasticizer to soften the PES matrix. The TGA analysis revealed that the composite membranes withstood temperatures up to 350°C without any thermal degradation. As one expected, the permeability coefficients of all membranes followed the order: $P(N_2) < P(O_2) < P(CO_2)$. The PES/20[Meim][Tf₂N], PES/10[Meim][TFSO₃] and PES/10[Vim][Tf₂N] showed higher CO₂/O₂ and CO₂/N₂ selectivities than those of pure PES, indicating high affinity of these ILs with CO₂ within PES, especially PES/10[Vim][Tf₂N] with CO₂/O₂ selectivity (6.1) and CO₂/N₂ selectivity (20.4).

The results obtained in this work gives a new insight to the knowledge about tailoring the membrane properties for CO₂ separation. Numerous prospects could be proposed for further study, some of them are listed below.

The imidazolium-based and alkanolamine-based ILs synthesized in this study have good thermal stability, and have strong CO₂ absorption capacity as reported in the literature. Therefore, they could be introduced into other polymer matrixes for CO₂ separation. In addition, their plasticizing effect could make them useful as plasticizers.

As the gas permeability coefficient of PSF/IL composite membranes was found to be lower than that of pure PSF, these membranes could be used as gas barriers. Besides, the CO₂/O₂ and CO₂/N₂ selectivities of PSF/20 alkanolamine-based ILs were found to be slightly higher than those of PSF/10 alkanolamine-based ILs. And the CO₂/O₂ and CO₂/N₂ selectivities of most PES/imidazolium-based IL composite membranes were enhanced as compared with pure PES: PES/IL membranes could be applied in gas separation field. Furthermore, if the IL loading could be increased with appropriate compatibilizers such as PEG, the gas selectivity performance may reach the desired level. Finally, in general, gas permeability can be enhanced with higher temperature and pressure. Therefore, the excellent thermal stability and mechanical properties of PSF and PES composite membranes could make them useful for gas separation at high temperature and pressure.

Last but not least, PES/10[Vim][Tf₂N] membrane gave the best gas separation performance, but incorporating 20 wt% IL gave worse results. Therefore, investigating the elaboration of PES composite membranes with lower [Vim][Tf₂N] loadings than 10 wt% would be of great interest.

Annexes

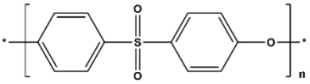
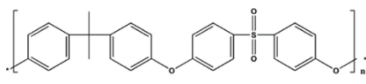
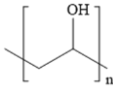
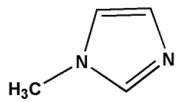
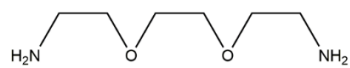
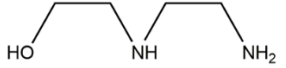
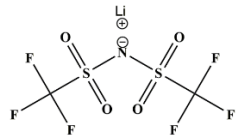
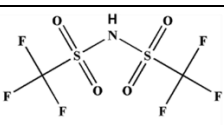
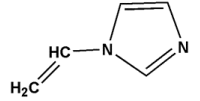
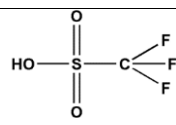
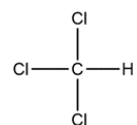
Annex 1 Reagents

Polysulfone ($M_n \sim 22\,000$ g/mol), polyether sulfone ($M_n \sim 58\,000$ g/mol), polyvinyl alcohol Mowiol[®] 8–88 ($M_w \sim 67\,000$ g/mol, degree of hydrolysis: 86.7–88.7 mol%), diiodomethane (>99%, stab), bis(trifluoromethane)sulfonimide lithium salt (99.95%) and 2,2'-(ethylenedioxy)bis(ethylamine) (98%) were supplied by Sigma-Aldrich (France). *N*-vinyl imidazole (99%), 1-methylimidazole (99%), *N*-methyl-2-pyrrolidinone (99.5%), diethyl ether (anhydrous, 99.5%), chloroform (>98%) and 2-hydroxyethylenediamine (99%) were provided by Fisher Scientific (France). Trifluoromethanesulfonic acid (>98%) and bis(trifluoromethanesulfonyl)imide (>99.0%) were bought from TCI (Belgium). Glycerol (>99%), dimethylformamide (>99%) and tetrahydrofuran (>99%) were obtained from VWR (France). Ultrapure water ($R = 18.2$ M Ω ·cm) was made by a Milli-Q system (Siemens, France). All chemicals were used as received.

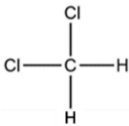
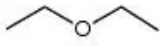
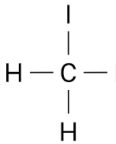
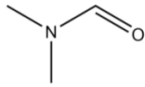
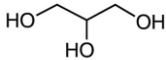
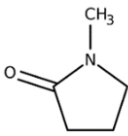

CO₂ (>99.99%), N₂ (>99.99%) and O₂ (>99.99%) were purchased from Linde (France) and used as received.

The abbreviation, chemical structure and CAS number of chemicals are shown in Table A1-1.

Table A1-1 Short name, chemical structure and CAS number of chemicals

Chemical	Abbreviation	Chemical structure	CAS
<i>Polymers</i>			
polyether sulfone	PES		SU306311
polysulfone	PSF		25135-51-7
polyvinyl alcohol	PVA		9002-89-5
<i>Raw chemicals of ionic liquid synthesis</i>			
1-methylimidazole	Meim		616-47-7
2,2'-(ethylenedioxy)bis(ethylamine)	DOBA		929-59-9
2-hydroxyethylenediamine	HDA		111-41-1
bis(trifluoromethane)sulfonimide lithium salt	Li[Tf ₂ N]		90076-65-6
bis(trifluoromethanesulfonyl)imide	H[Tf ₂ N]		82113-65-3
N-vinyl imidazole	Vim		1072-63-5
trifluoromethanesulfonic acid	H[TFSO ₃]		1493-13-6
<i>Solvents</i>			
chloroform	CHCl ₃		67-66-3

Annex 1

dichloromethane	CH ₂ Cl ₂		75-09-2
diethyl ether	DE		60-29-7
diiodomethane	CH ₂ I ₂		75-11-6
dimethylformamide	DMF		68-12-2
glycerol	GC		56-81-5
<i>N</i> -methyl-2-pyrrolidinone	NMP		872-50-4
tetrahydrofuran	THF		109-99-9

Annex 2 Characterizations

- ◆ Fourier transform infrared (FT-IR) spectroscopy

The spectra were obtained from 600 to 4000 cm^{-1} using 64 scans and a resolution of 4 cm^{-1} by a Spectrum Two spectrometer from PerkinElmer, equipped with an attenuated total reflection system with diamond (MKII Golden Gate from Specac), at 25°C.

- ◆ Nuclear magnetic resonance (^1H NMR) spectroscopy

The ILs chemical structures were determined by ^1H NMR (300 MHz Bruker spectrometer) at room temperature in DMSO- d_6 (99.8% D) or D_2O (99.9% D). Around 10 mg of ILs were dissolved in ~1.7 mL of deuterated solvent.

- ◆ Thermogravimetric analysis (TGA)

The thermal stability of ILs and membranes was investigated on a Q500 from TA Instruments, using a nitrogen atmosphere with a flow rate of 40 mL/min and 5.0-10.0 mg of sample, either in dynamic mode (temperature ranging from 30°C to 600°C at a heating rate of 10°C/min) or in isothermal mode (at 150°C for 800 min).

- ◆ Differential scanning calorimetry (DSC)

The thermal properties of ILs and membranes were studied on a Q2000 from TA Instruments. A sample of around 5 mg was heated from -90 (or -30) to 220°C at a heating rate of 10°C/min under N_2 atmosphere in closed hermetic aluminum pan, performing heating-cooling-heating cycle. The glass transition (T_g) and melting (T_m) temperatures were determined from the second heating at the midpoint and the maximum of the peak, respectively.

- ◆ Contact angle measurements

The static contact angle measurements (using water, diiodomethane and glycerol) of membranes were carried out using a goniometer Digidrop from GBX, with 3 μL droplets and 3 s photo time at room temperature (25°C) in air. The results were obtained from the average of ten drops and surface energy and its components were calculated with Windrop ++ Carrousel software by Owens - Wendt method.

- ◆ Scanning electron microscopy (SEM)

The membrane surfaces were coated with a thin gold layer by smart coater (DII-29030SCTR) in 2 min. The membrane morphology (surface and cross-section) was observed on a scanning electron microscope (JEOL) with an EDX apparatus under a voltage of 5 kV and using JCM-7000 software. The distribution of fluorine (elemental mapping) was analyzed by the same machine under a voltage of 15 kV.

- ◆ Mechanical properties

The mechanical properties (Young's modulus, tensile strength, strain at break) of pure and composite membranes were tested on a ZwickRoell Z010 test machine (Software TestXpert II-V3.5) with a stretching rate of 2 mm/min at room temperature (25°C) according to ISO 527-2:2014-04 standard. The distance between the grips was 21 mm. On each sample, 5 tests were conducted and the obtained values were averaged.

- ◆ Gas permeation measurements

The pure gas (CO₂, N₂ and O₂) permeation experiments were carried out with 4 bar feed gas pressure (absolute pressure) under 25°C based on time-lag method using home-made device (Figure A2-1). Firstly, a membrane sample was sealed between upstream and downstream compartments of the permeation module. Secondly, the high vacuum purge step was carried out during 15 hours. Thirdly, the stream of diffusing gas with an absolute pressure of 4 bar was injected into the upstream compartment. Due to the driving force resulting of the pressure difference between the upstream (4 bars) and downstream (~ 0 bar) compartments, the gas molecules diffuse through the membrane and the pressure increases in the downstream compartment. The pressure value was continuously measured over time with a pressure sensor (Druck, Effa AW-10-TA, Germany), until it reached a stationary state. For each membrane composition at least three measurements were performed for each gas and the averaged value is present.

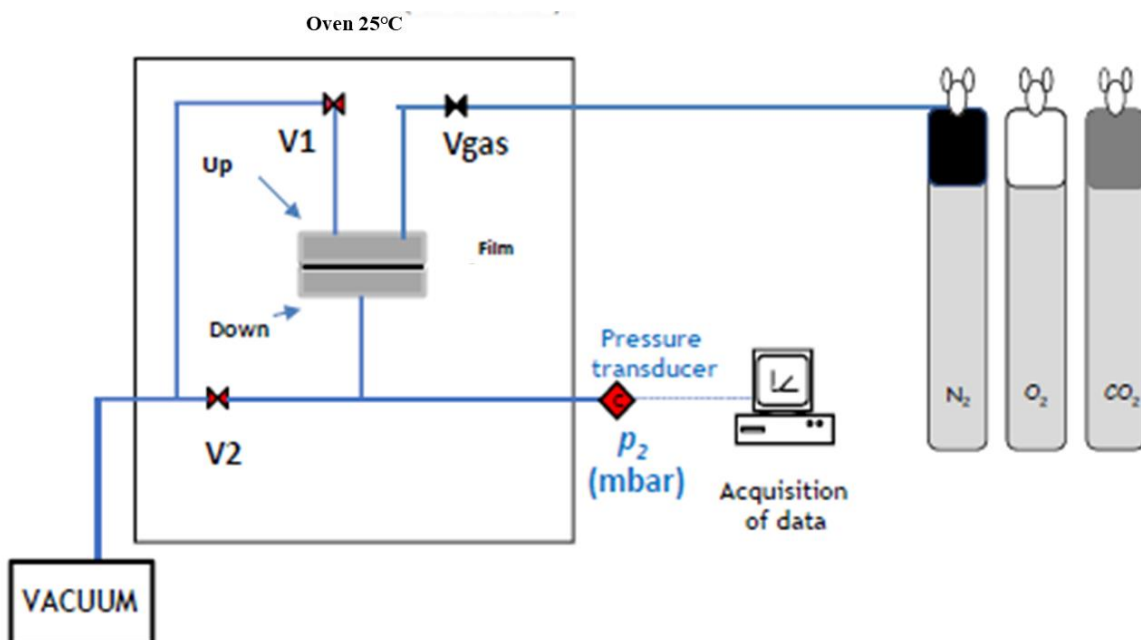
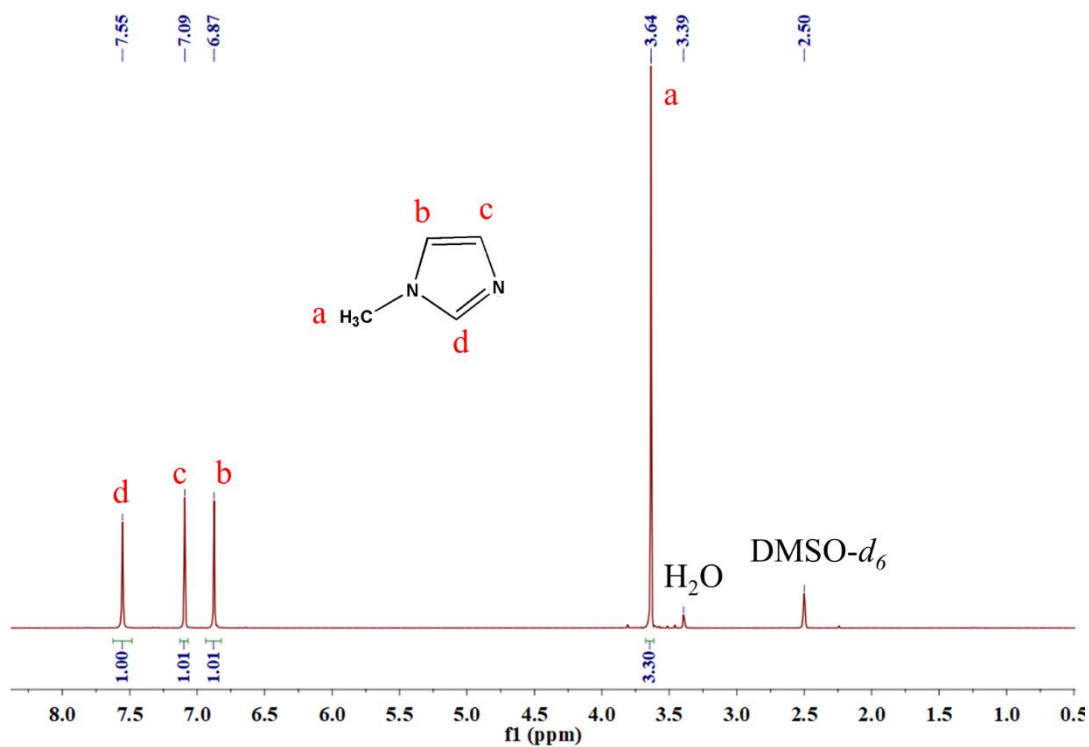
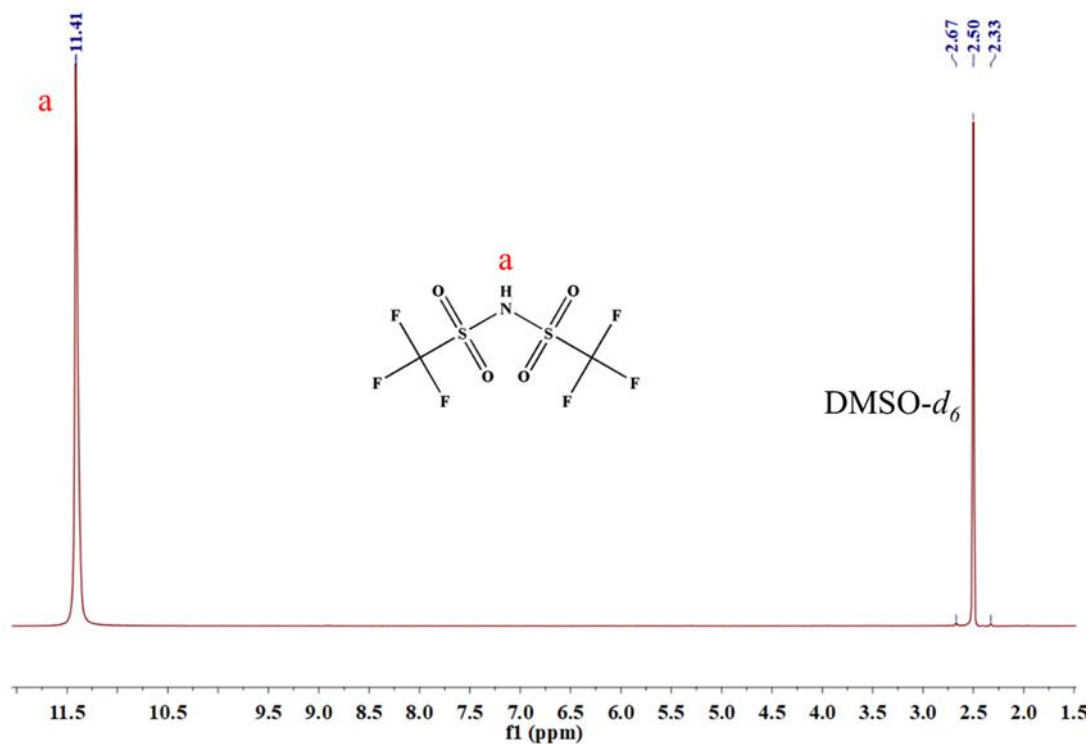
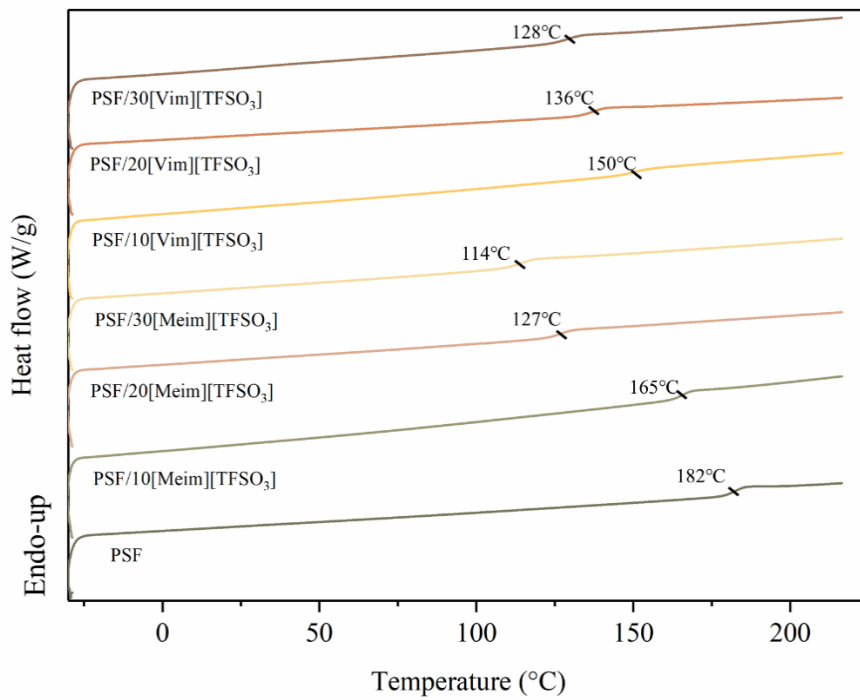
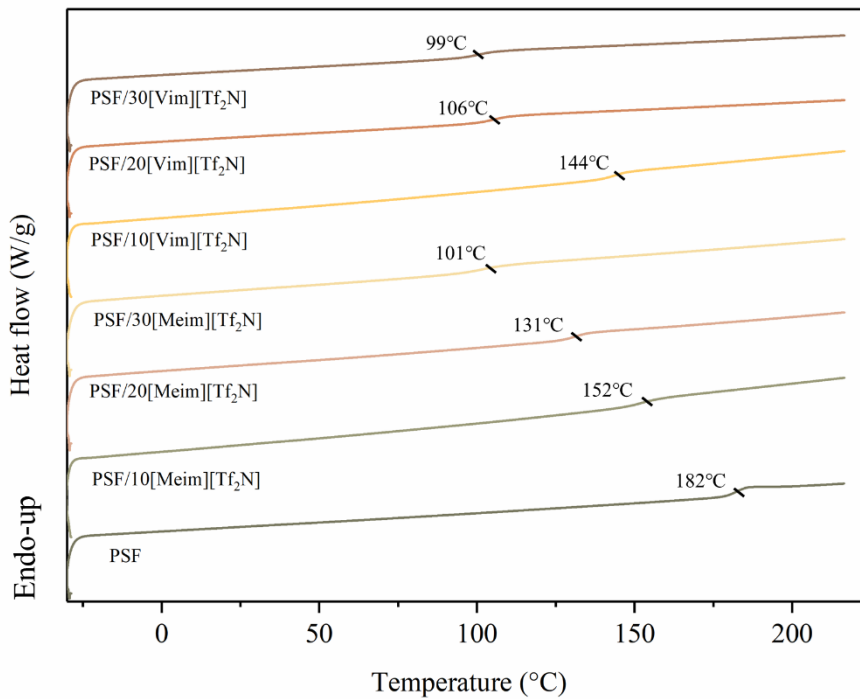
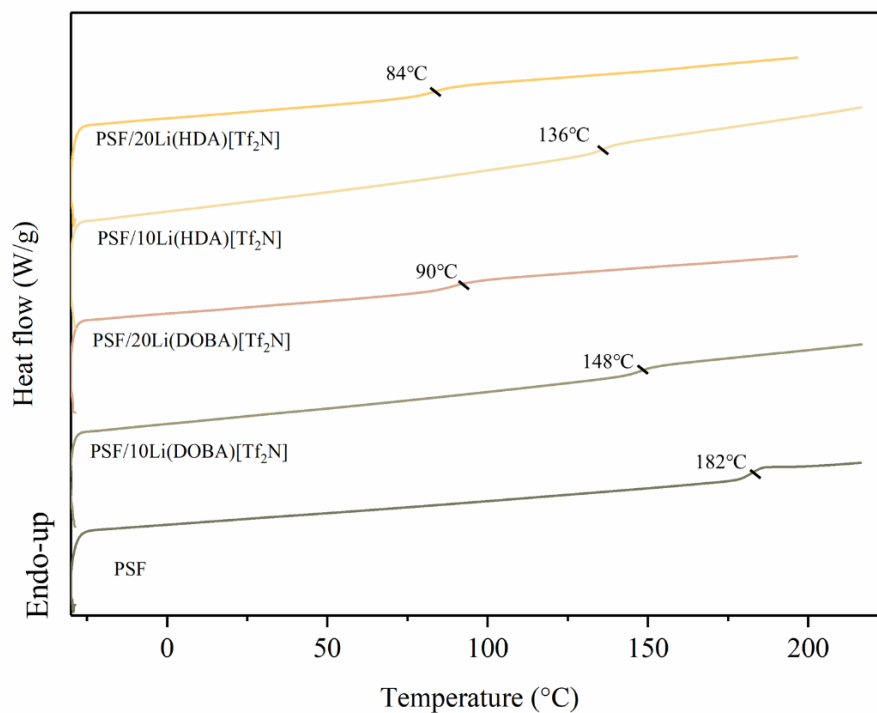
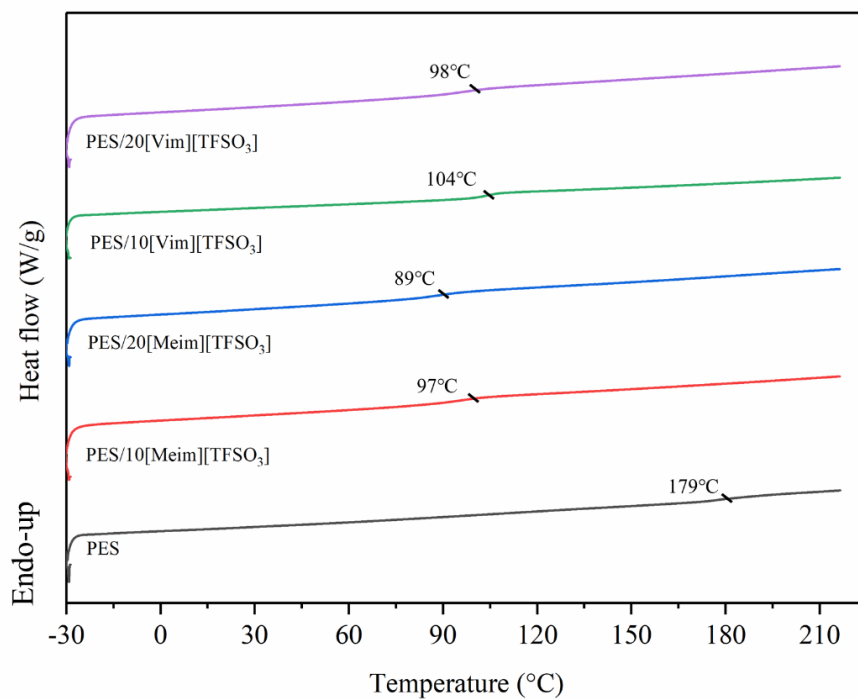
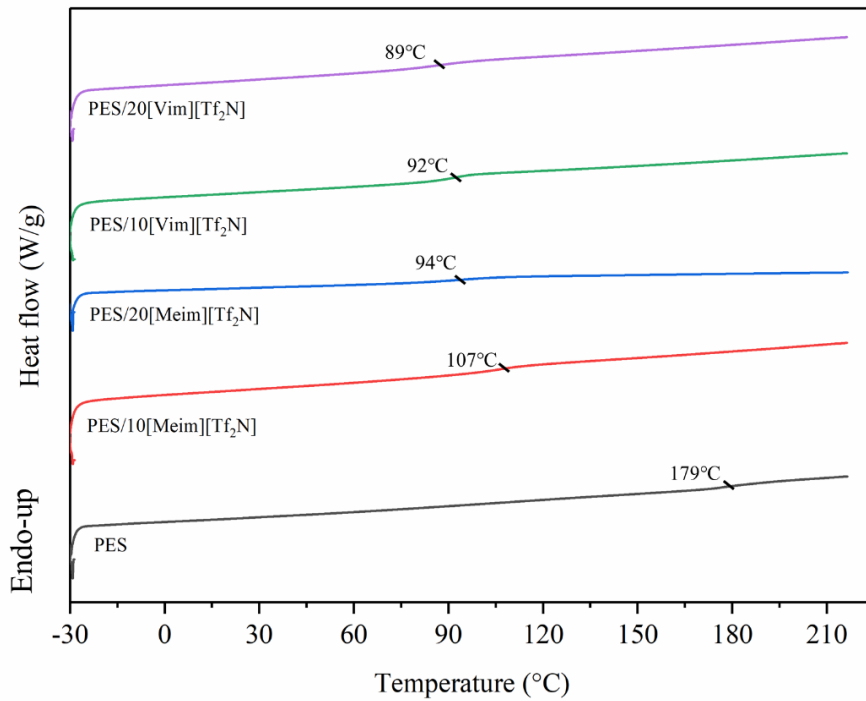
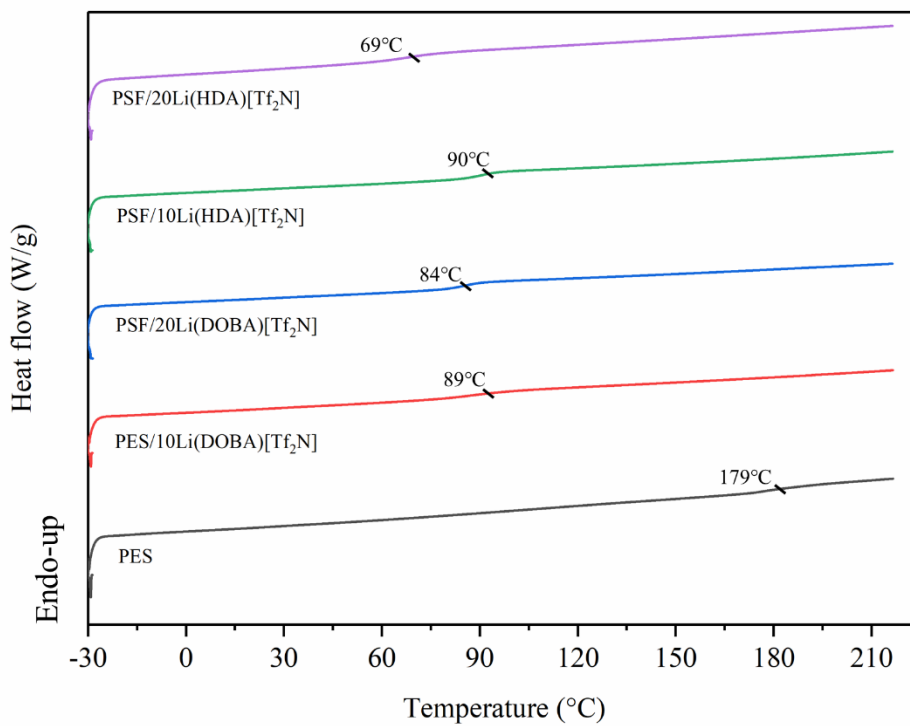


Figure A2-1 Set-up for gas permeation

Annex 3 ^1H NMR analysisFigure A3-1 ^1H NMR spectrum of *N*-vinylimidazole (Vim)Figure A3-2 ^1H NMR spectrum of bis(trifluoromethanesulfonyl)imide (Tf₂N)

Annex 4 DSC thermogramsFigure A4-1 DSC curves of PSF, PSF/[Meim][TFSO₃] and PSF/[Vim][TFSO₃] membranesFigure A4-2 DSC curves of PSF, PSF/[Meim][Tf₂N] and PSF/[Vim][Tf₂N] membranes

Figure A4-3 DSC curves of PSF, PSF/Li(DOBA)[Tf₂N] and PSF/Li(HDA)[Tf₂N] membranesFigure A4-4 DSC curves of PES, PES/[Meim][TFSO₃] and PES/[Vim][TFSO₃] membranes

Figure A4-5 DSC curves of PES, PES/[Meim][Tf₂N] and PES/[Vim][Tf₂N] membranesFigure A4-6 DSC curves of PES, PES/Li(DOBA)[Tf₂N] and PES/Li(HDA)[Tf₂N] membranes

Innovative composite polymer materials for CO₂ separation

Currently, the emission of CO₂, which is the primary contributor to global warming, is increasing at an alarming rate. Consequently, there is a growing global need for cutting-edge technologies that can effectively separate and capture CO₂. In the present work, a series of PSF/IL and PES/IL composite membranes for CO₂ separation were investigated. Six ILs ([Meim][TFSO₃], [Vim][TFSO₃], [Meim][Tf₂N], [Vim][Tf₂N], Li(DOBA)[Tf₂N] and Li(HDA)[Tf₂N]) were synthesized successfully and characterized by FT-IR, ¹H NMR, TGA and DSC. Composite membranes with different IL loadings were fabricated by solution casting method and exhaustively studied by FT-IR, TGA, DSC, SEM, F-mapping, surface energy, tensile tests, and gas permeation (CO₂, N₂ and O₂). Under 25°C and 4 bar, PES/10[Vim][Tf₂N] membrane showed a CO₂ permeability of 1.92 Barrer with improved CO₂/N₂ and CO₂/O₂ selectivities of 20.4 and 6.1, respectively.

Keywords: polysulfone (PSF), polyethersulfone (PES), ionic liquid (IL), composite membrane, CO₂ separation

Actuellement, les émissions de CO₂, principal responsable du réchauffement climatique, augmentent à un rythme alarmant. Par conséquent, il existe un besoin mondial croissant de technologies de pointe capables de séparer et de capturer efficacement le CO₂. Dans ce travail, une série de membranes composites PSF/IL et PES/IL pour la séparation du CO₂ ont été étudiées. Six IL ([Meim][TFSO₃], [Vim][TFSO₃], [Meim][Tf₂N], [Vim][Tf₂N], Li(DOBA)[Tf₂N] et Li(HDA)[Tf₂N]) ont été synthétisés avec succès et caractérisés par FT-IR, ¹H RMN, TGA et DSC. Des membranes composites avec différentes quantités d'IL ont été fabriquées par évaporation de solvant puis étudiées par FT-IR, TGA, DSC, MEB, cartographie du F, énergie de surface, essais de traction et perméation aux gaz (CO₂, N₂ et O₂). A 25°C et 4 bar, la membrane PES/10[Vim][Tf₂N] présente une perméabilité au CO₂ de 1,92 Barrer avec des sélectivités CO₂/N₂ et CO₂/O₂ améliorées de 20,4 et 6,1, respectivement.

Mots-clés : polysulfone (PSF), polyéthersulfone (PES), liquide ionique (IL), membrane composite, séparation du CO₂